Marine and Petroleum Geology 121 (2020) 104598

Contents lists available at ScienceDirect

Marine and Petroleum Geology

journal homepage: www.elsevier.com/locate/marpetgeo

Research paper

Structural analysis of the Smeaheia fault block, a potential CO_2 storage site, northern Horda Platform, North Sea

Mark Joseph Mulrooney [a,*], Johnathon Lee Osmond [a], Elin Skurtveit [a,b], Jan Inge Faleide [a], Alvar Braathen [a]

[a] Department of Geosciences, University of Oslo (UiO), PO Box 1047, Blindern, 0316, Oslo, Norway
[b] Norwegian Geotechnical Institute (NGI), PO Box 3930, Ullevål Stadion, 0806, Oslo, Norway

ARTICLE INFO

Keywords:
Smeaheia
CCS
Horda platform
North sea rift
Vette fault zone
Øygarden fault complex
Troll field
3D seismic

ABSTRACT

Smeaheia, a prominent fault block located on the Horda Platform, northern North Sea is identified as a potential subsurface CO_2 storage site. We utilise the GN1101 3D seismic survey to generate a high-resolution subsurface geomodel to inform the structural style and evolution of the fault block, to investigate geological controls on proposed CO_2 storage and provide a geometric framework as a basis for future analyses. Two basement-involved (first-order) north-south trending fault systems, the Vette Fault Zone (VFZ) and the Øygarden Fault Complex (ØFC), bound the 15 km-wide fault block. The VFZ bifurcates down-section where it is hard-linked with two separate basement structures, a phenomenon we term as "dual rooted". Apart from activity during the Permo-Triassic (Rift Phase 1) and the Late Jurassic–Early Cretaceous (Rift Phase 2), we present evidence that rifting in this part of the North Sea continued into the Late Cretaceous with minor reactivation in the Palaeocene–Eocene. Two segments of the VFZ interacted and linked at a relay ramp during Rift Phase 2. Second-order (thin-skinned) faults show basement affinity and developed during Rift Phase 2 in two distinct pulses. A population of polygonal faults intersects the overburden and developed during the Eocene to middle Miocene. We have revised the areal extent of two structural closures that define the Smeaheia fault block, Alpha (VFZ footwall) and Beta (ØFC hanging wall) which consist of Upper Jurassic Viking Group target formations. Simplified cross-fault juxtaposition analysis of the VFZ and second-order intra-block faults are presented and inform pressure communication pathways between the Smeaheia and Tusse fault block, as well as reservoir integrity and compartmentalisation. The geomodel further identifies important geological controls on CO_2 storage in the fault block including a thinning caprock above the Alpha structure, and identification of hard-linkage between deep tectonic faults and shallow polygonal faults.

1. Introduction

In an effort to combat climate change (Intergovernmental Panel on Climate Change Special Report, 2005; 2007, 2014), the European Commission has outlined an ambitious target to reduce anthropogenic emission of greenhouse gasses by 80–95% by 2050 (including 500 Gt of CO_2) with respect to 1990 levels (E.U. Commission, 2018). Carbon capture and storage (CCS) presents one of several technologies that can contribute to meeting this target. In CCS, CO_2 is captured at point sources e.g., CO_2-emitting industrial plants, transported to suitable injection sites by pipelines or ships and sequestered within subsurface storage formations, e.g., saline aquifers and depleted hydrocarbon fields (Intergovernmental Panel on Climate Change Special Report, 2005; Bachu, 2008; Benson and Cole, 2008; Gibbins and Chalmers, 2008). The technical feasibility of CCS has been successfully demonstrated offshore Norway both in the North Sea, i.e., the Sleipner CO_2 sequestration project (Torp and Gale, 2004; Arts et al., 2008), and in the Barents Sea, i.e., the Snøhvit CO_2 storage project (Eiken et al., 2011). Current EU-wide facilities, however, will fall short of the estimated 12 Gt of CO_2 storage required to meet the 2050 targets (International Energy Agency, 2013). As such additional sequestration projects are necessary.

The Smeaheia site (Statoil, 2016; Kaufmann et al., 2018; Lauritsen et al., 2018; Lothe et al., 2019), formerly Troll Kystnær (Statoil, 2016), is situated in the Norwegian sector of the northern North Sea (Fig. 1A), partly covering 9 exploration blocks (Fig. 1B).The site lies approximately 20 km east and 40 km northwest of the Troll A platform (Troll

* Corresponding author.
E-mail address: mark.mulrooney@geo.uio.no (M.J. Mulrooney).

https://doi.org/10.1016/j.marpetgeo.2020.104598
Received 22 March 2020; Received in revised form 14 July 2020; Accepted 15 July 2020
Available online 29 July 2020

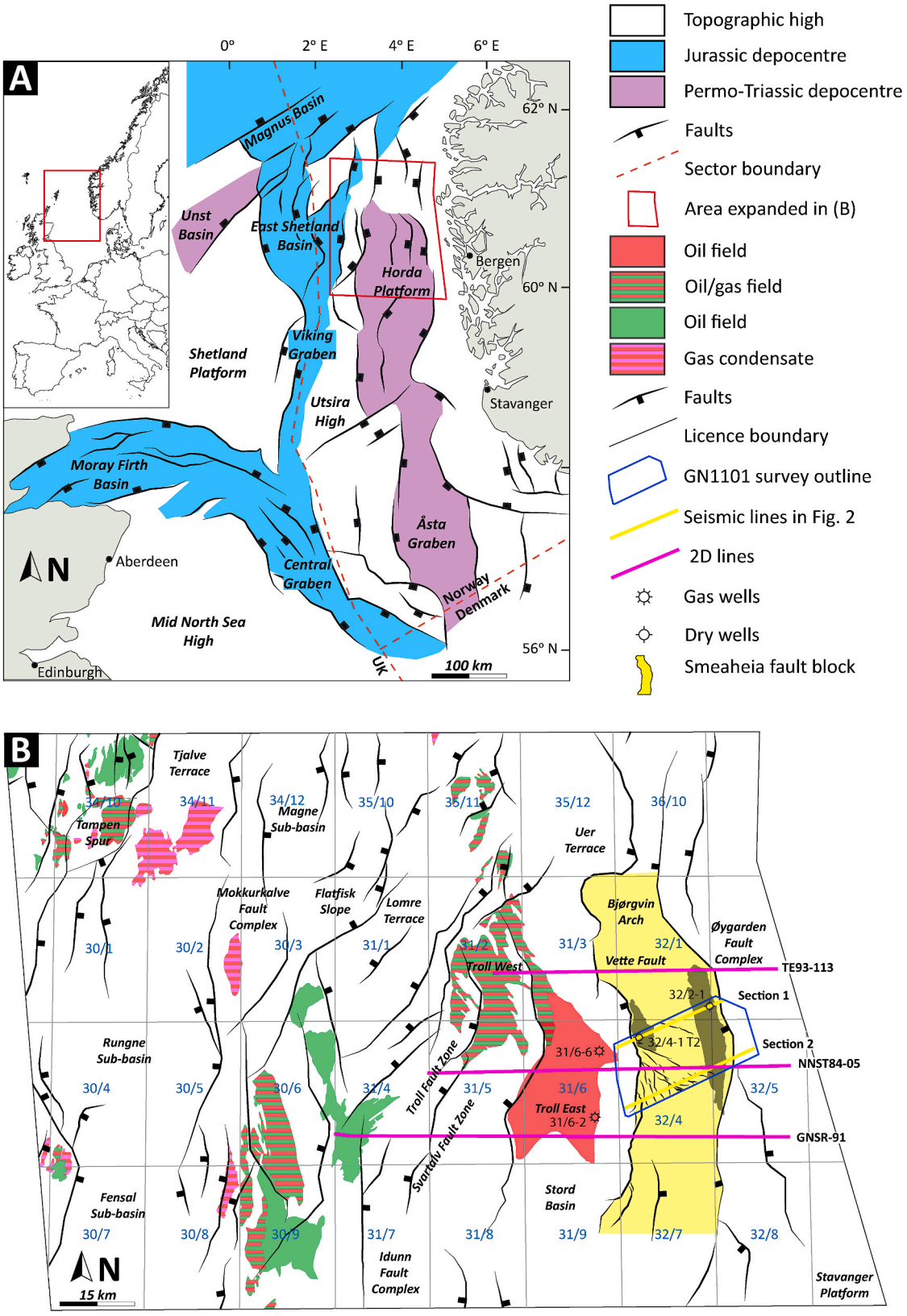

Fig. 1. A) Primary structural elements map of the North Sea (faults, basins, and structural highs) emphasising the trilete rift system and dominantly Permo-Triassic and Jurassic depocentres. Sector boundaries shown with red stippled line. Compiled from Roberts et al. (1995), Færseth et al. (1995) and Domínguez (2007). Inset: Simplified outline of Western Europe showing geographical location of the North Sea rift system. B) Structural elements and oil/gas accumulations of the northern Horda Platform in the Norwegian sector of the northern North Sea. Redrafted from the Norwegian Petroleum Directorate Fact Maps (http://npd.no/en/Maps/Fact-maps). The regional 2D seismic transects are shown in Appendix 3 (TE93-113), Appendix 4 (NNST84-05) and Appendix 5 (GNSR-91). (For interpretation of the references to colour in this figure legend, the reader is referred to the Web version of this article.)

East) and the Kollsnes processing plant, respectively. Target aquifers consist of the Middle–Upper Jurassic coastal-shallow marine sandstones of the Viking Group (Sognefjord and Fensfjord formations; Dreyer et al., 2005; Holgate et al., 2013; Furre et al., 2019). Two first-order (basement-involved) north-south trending faults, the Vette Fault Zone (VFZ) and the Øygarden Fault Complex (ØFC) bound an east tilting fault block characteristic of the Horda Platform (Fig. 1B). Here, two storage prospects have been identified, Alpha and Beta (Fig. 2), which are formed by footwall and hanging wall three-way structural closures, respectively, and are capped by Upper Jurassic marine claystones of the Draupne Formation (Skurtveit et al., 2012). The Alpha and Beta prospects were drilled previously in 1996 and 2008, respectively, primarily exploring the Sognefjord, Fensfjord and Krossfjord formations for commercial hydrocarbon accumulations (32/4-1 T2 Final Well report, 1997; 32/2-1 Final Well End of well report, 2008). Possible hydrocarbon migration scenarios (e.g., Goldsmith, 2000) from the neighbouring Troll East were invalidated as neither well indicated hydrocarbon shows.

The Smeaheia fault block has been proposed as a potential CO_2 storage site due to sufficient estimated structural storage capacity, excellent reservoir quality, and its adjacency to the coastline and existing subsea infrastructure (Statoil, 2016; Kaufmann et al., 2018; Lauritsen et al., 2018). After injection into Alpha, CO_2 is envisaged to migrate up-dip via a spill point and accumulate in Beta. The future success of the Smeaheia fault block as a storage site will depend on maturation of the geological understanding of the area. Fundamentally, both the Alpha and Beta prospects require the sealing capacity of the caprock to tolerate the buoyancy forces of the projected CO_2 columns to prevent injected fluids being lost to the surface (e.g., Ingram and Urai, 1999; Egermann et al., 2006; Busch et al., 2010; Kaldi et al., 2013). Further, both prospects require juxtaposition (Allan, 1989) or capillary (membrane) seals (e.g. Yielding et al., 1997, 1998) in order to restrict fluid flow across the VFZ and the ØFC that bound them, respectively. Similar to top seal failure, cross-fault leakage occurs when buoyancy forces of a hydrocarbon or CO_2 column exceed the capillary threshold pressure of the juxtaposed formation, or the fault rock itself (Knipe et al., 1997, 1998; Yielding et al., 1997, 2010; Fisher and Knipe, 1998). The capillary threshold pressure along both the VFZ and the ØFC must therefore be sufficient to accommodate the expected CO_2 columns in Alpha and Beta. Similarly, smaller second-order faults that intersects the prospects may also support minor CO_2 columns, i.e., baffle CO_2 injection and increase storage formation pressure (e.g., Bretan et al., 2011). The possibility of cross-fault pressure communication between the Smeaheia fault block and the Tusse fault block (where the Troll East field is situated) presents another significant uncertainty (Orsini et al., 2020). Depletion is possible within the Smeaheia fault block owing to over 20 years of hydrocarbon production from the Troll fields and may have consequences for storage capacity. Fault juxtaposition across a relay ramp along the VFZ and adjacent to the depleting Troll East field (Tusse fault block) can provide insight into the likelihood of this scenario prior to drilling of the prospects. An additional uncertainty is associated with fault reactivation owing to increasing storage formation pressure over the course of CO_2 injection operations.

Seismic data is often used to image and monitor CO_2 injection changes in the subsurface over time in ongoing sequestration projects (i.e., 4D seismic monitoring; Chadwick et al., 2005; Lumley, 2010; Ivanova et al., 2012). More fundamentally, seismic data can be used to assess the suitability of, and risks associated with subsurface CO_2 sites, i.e., identify the presence and continuity of caprocks, traps and storage formations as well as potential leakage sites (e.g., Chadwick et al., 2004; Sundal et al., 2016; Roelofse et al., 2019). This contribution aims to increase our knowledge of the Smeaheia fault block by establishing a tectonic framework in order to reduce uncertainties associated with storage of CO_2. We present a detailed description of the structural architecture and geological evolution of the Smeaheia fault block which includes novel findings regarding the timing of the second rift phase in the northern North Sea. A high-resolution (50 × 50 m) geomodel is presented and forms the basis for revising the areal extent of the structural closures and identifying faults that intersect the storage formation and caprock. As such, the work focuses on the Viking Group. The geomodel also informs cross-fault lithological juxtaposition of the Alpha-bounding VFZ, the VFZ relay ramp and intra-block second-order faults.

2. Geological setting

The Horda Platform (Hospers and Ediriweera, 1991; Faerseth and Ravnås, 1998; Roberts et al., 1995; Færseth, 1996; Odinsen et al., 2000a, b; Bell et al., 2014; Whipp et al., 2014; Duffy et al., 2015; Phillips et al., 2019) forms an approximately 300 km north–south elongated, 100 km wide structural high along the eastern margin of the northern North Sea. The platform is bounded by the northern part of the Viking Graben to the west which is a failed arm of the Arctic-North Atlantic rift system (Ziegler, 1990; Bartholomew et al., 1993; Glennie, 1995), and the Øygarden Fault Complex (Faerseth et al., 1995) to the east. The latter delineates a major change in crustal thickness (onshore-offshore Norwegian transition) and has done so since the Permian (Christiansson et al., 2000). The Horda Platform (Fig. 1) is characterised by a series of west-dipping half-grabens bound by north–south striking basement-involved faults that exhibit throws in the 4–5 km range, spacing between 15 and 20 km and rotations of approximately 8–12° (Færseth, 1996; Bell et al., 2014; Whipp et al., 2014; Duffy et al., 2015). Depth to the crystalline basement ranges from 3 to 5 km across the platform (Bell et al., 2014; Fazlikhani et al., 2017). Fig. 3 correlates chronostratigraphy, seismic ties and main tectonic events that characterise the Horda Platform.

The crystalline basement underlying the Horda Platform is comprised of a series of terrains accreted during the Caledonian (460–400Ma) and Variscan (400–300Ma) orogenies (Ziegler, 1975, 1982; Frost et al., 1981; Gee et al., 2008) as well as Devonian low-grade metasediments (Fossen, 1992; Faerseth et al., 1995; Færseth, 1996; Fossen and Hurich, 2005; Osmundsen et al., 2000; Osmundsen and Andersen, 2001; Sturt and Braathen, 2001). Basement rheology is primarily identified on the basis of seismic facies from deep reflection seismic (e.g., Christiansson et al., 2000; Gabrielsen et al., 2015; Fazlikhani et al., 2017; Wrona et al., 2018). Basement composition and structural grain are highly heterogeneous, the latter of which primarily reflect Caledonian lineaments (Faerseth et al., 1995). While the Iapetus suture has been interpreted from deep reflection seismic to run in a NNE-SSW trend aligned along the Sogn and Viking grabens (Matthews and Cheadle, 1986; Gibbs, 1987; Freeman et al., 1988; Odinsen et al., 2000a,b), onshore Norway, northeast–southwest and north–south Caledonian trends have also been recognised in the southwest (e.g., Karmøy and Stavanger shear zones) and south central (e.g., Mandal-Ustaoset fault) parts of the country (e.g., Ramberg et al., 1977; Sigmond, 1985; Faerseth et al., 1995; Gabrielsen et al., 2002; Braathen et al., 2004; Gabrielsen et al., 2019).

Following the culmination of the Caledonian orogeny, regionally distributed gravitational collapse during the Devonian exploited contractional Caledonian structures and resulted in a series of low-angle shear zone-controlled intermontane basins that outcrop in western Norway where they dip towards the south, ESE, and WNW (e.g., Norton, 1986; Fossen,1992; Wennberg, 1996; Osmundsen et al., 2000; Osmundsen and Andersen, 2001; Braathen et al., 2004; Fossen and Hurich, 2005; Vetti and Fossen, 2012; Fossen et al., 2017). Underlying the Horda Platform, Devonian shear zones that dip less than 40° towards the east-southeast and west-northwest and associated metasediments have been mapped by Fazlikhani et al. (2017) and manifest as high amplitude dipping and low angle, low frequency reflectors, respectively. Fazlikhani et al. (2017) suggest that the northern extent of the VFZ studied herein links at depth with one such low-angle normal basement shear zone, which supports the concept that Mesozoic rift events (Permo-Triassic and Jurassic-Cretaceous) reactivated basement structures (Faerseth et al., 1995; Phillips et al., 2019).

The rift block architecture of the Horda Platform primarily evolved

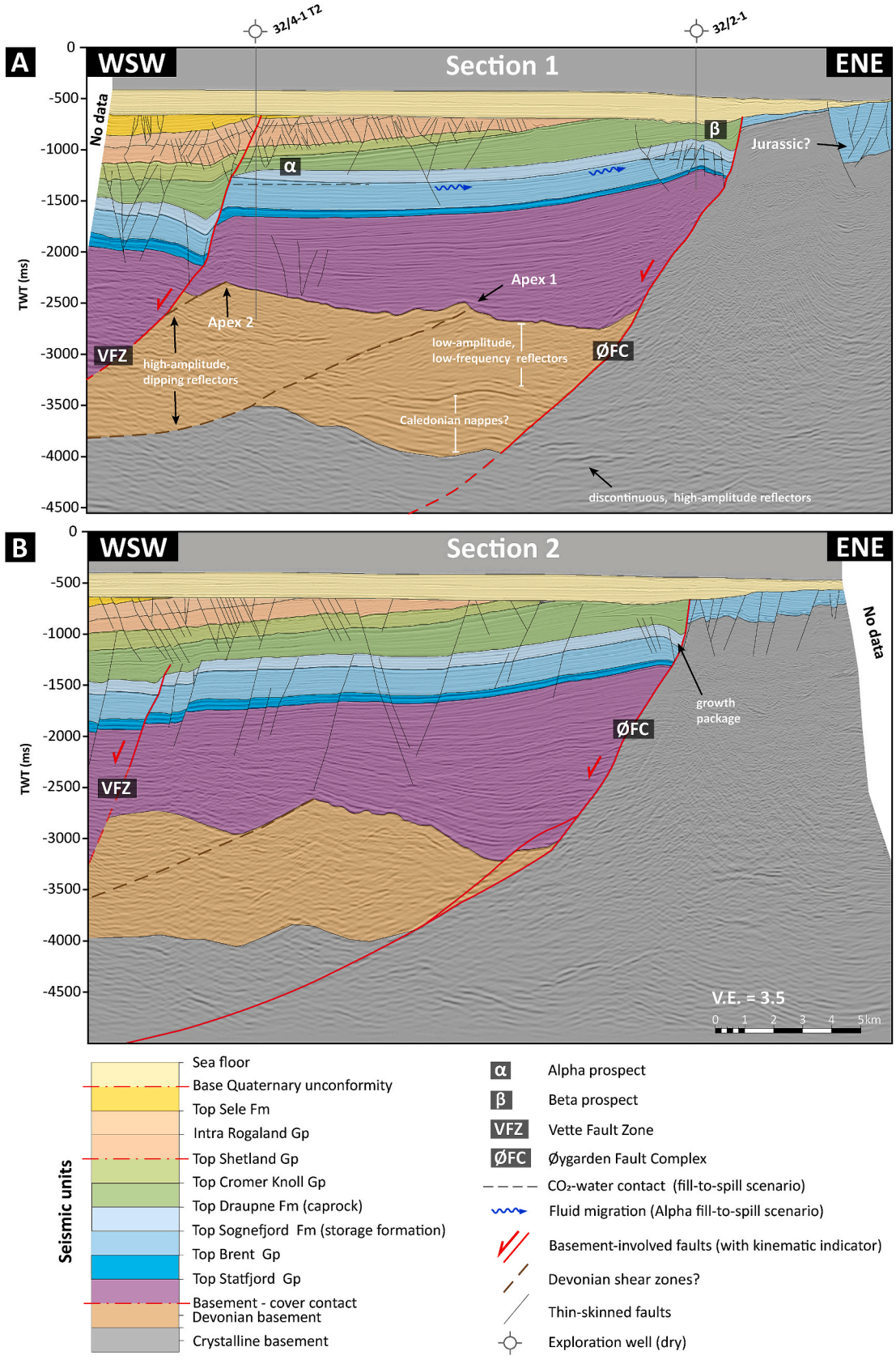

(caption on next page)

Fig. 2. Two interpreted WSW-ENE trending seismic transects through the GN1101 3D survey. Location shown in Fig. 1B. Section 1 intersects both historical exploration wells 31/4-1 T2 and 32/2–1 that targeted the Alpha and Beta prospects, respectively. Section 2 is situated south of the potential prospects. Both sections show that the target storage formation and caprock units are bound by two basement-involved (first-order) faults, the Vette Fault Zone and the Øygarden Fault Complex which delineate the Smeaheia fault block. Prospective CO_2-water formation contacts are shown for a fill-to-spill scenario in section 1. Migration of CO_2 from a filled-to-spill Alpha prospect is depicted by blue arrows. Thin-skinned, intra-block faults can be seen to intersect the formation and caprock, but are more prevalent in section 2 as they branch towards the south. The Beta prospect is intensely faulted. Note, the large population of closely spaced, low-displacement normal faults that affect the Upper Cretaceous to lower Cenozoic but do not occur above the base Quaternary unconformity. A narrow graben with possible Jurassic infill (no local well constraints) is interpreted in the footwall of the Øygarden Fault Complex. At depth, high-amplitude basement reflectors that likely represent Devonian and Caledonian structures and metasediments are highlighted. Age, chronostratigraphy and tectonic events with respect to the seismic horizons can be seen in Fig. 3. Uninterpreted versions of section 1 and 2 are shown in Appendix 2. (For interpretation of the references to colour in this figure legend, the reader is referred to the Web version of this article.)

during the Late Permian to Early Triassic during which an east–west phase of extension, likely related to the breakup of the Pangean supercontinent, took place and lasted between 25 and 37 Myrs (Ziegler, 1982, 1990; Ter Voorde et al., 2000). Rifting during the Permo-Triassic was widespread throughout the northern North Sea, however, the largest magnitude of fault activity (throws up to 5 km) took place on the western side of the Horda Platform (Faerseth et al., 1995; Færseth, 1996; Ter Voorde et al., 2000; Duffy et al., 2015; Phillips et al., 2019). Permo-Triassic rifting exhibited slip rates of 0.1–1.5 mm/yr (Bell et al., 2014) and a mean Beta factor of 1.33 (Odinsen et al., 2000a,b) on the Horda platform.

The dominant north–south trend of Permo-Triassic faults is discordant to that of Caledonian and Devonian structures, and may represent reactivation of a Precambrian grain (Faerseth et al., 1995; Phillips et al., 2019). Changes in polarity, however, occur when north–south striking faults interact with structures of the aforementioned ages, e.g., the Bergen Arcs which is a Caledonian feature and the Nordfjord-Sogn Detachment, which represents a Devonian shear zone (Faerseth et al., 1995). East–west extension is supported by the dominance of north–south striking faults as well as the presence of contemporaneous alkaline dykes that strike between north–south and NNW-SSE onshore Norway (Blystad et al., 1995; Faerseth et al., 1995). Up to 3 km of syn-rift stratigraphy (Duffy et al., 2015; Phillips et al., 2019) is associated with Permo-Triassic rifting which is dominated by the Scythian to Rhaetian Hegre Group and comprised of continental sandstones and mudstones deposited in large fluvial systems (Lervik et al., 1989; Lervik, 2006). The Early to Middle Jurassic represents a 70 Myr period of relative tectonic quiescence and post-rift thermal subsidence during which continental and fluvio-deltaic to shallow-marine sediments of the Statfjord, Dunlin and Brent groups were deposited (Deegan and Scull, 1977; Helland-Hansen et al., 1992).

Renewed rifting took place in the Late Jurassic to Early Cretaceous (Badley et al., 1988; Underhill and Partington, 1993; Roberts et al., 1995; Færseth & Ravnås, 1998; Coward et al., 2003; Cowie et al., 2005; Bell et al., 2014; Duffy et al., 2015; Phillips et al., 2019) associated with Early Jurassic rise and Middle to Late Jurassic deflation of the central North Sea dome, as well as far field stress related to North Atlantic rifting (Ravnås and Steel, 1997; Doré et al., 1997, 1999; Davies et al., 2001; Torsvik et al., 2002; Nøttvedt et al., 2008; Whipp et al., 2014) and resulting in a trilete rift system in the North Sea (Davies et al., 2001).

Jurassic to Cretaceous rifting in the northern North Sea is characterised by large-scale reactivation of north–south striking Permo-Triassic faults resulting in rapid accrual of fault length up-section and was followed by a phase dominated by displacement accrual of up to 300 m (Faerseth et al., 1995; Deng et al., 2017). Rifting was slower and less intense than in the Permo-Triassic with slip rates of 0.01 mm/yr (Bell et al., 2014) and a mean Beta value of 1.08 (Odinsen et al., 2000a, b).

As well as reactivation, a new population of smaller, northwest-southeast striking, 2–10 km long faults facilitated strain where pre-existing structures were not preferentially orientated (Færseth, 1996; Færseth & Ravnås, 1998; Tomasso et al., 2008). Strike deviation from Permo-Triassic faults is consistent with an anticlockwise rotation of the extension axis between events from east-west to northeast–southwest (e.g., Deng et al., 2017 and supported herein), however, non-rotation and northwest-southeast directions have been postulated by previous workers (Badley et al., 1988; Roberts et al., 1990, 1993; Ziegler, 1990; Stewart et al., 1992; Bartholomew et al., 1993; Brun and Tron, 1993; Færseth, 1996; Doréet al., 1997; Faerseth and Ravnås, 1998). These northwest-southeast striking faults show close spacing (0.5–5 km), are thin skinned—only affecting post-Upper Triassic stratigraphy, and generally exhibit throws of less than 100 m. Individual faults remained active for 10–40 Myrs (Cowie et al., 2005), with strain localisation onto larger north-south trending faults during the later phases of activity (Odinsen et al., 2000a,b). Where both populations interact, complicated displacement, cross-cutting and branching relationships have been identified (e.g., Bell et al., 2014; Duffy et al., 2015; Deng et al., 2017). Whereas Permo-Triassic rifting was broad and distributed across the North Sea, Jurassic-Cretaceous rifting was diachronous with strain localisation in the Viking Graben area credited to modification of the lithosphere during the earlier rift phase (Phillips et al., 2019). Migration of fault activity eastwards took place over a 30 My period (Bell et al., 2014) as the North Atlantic Ocean opening extensional stress became dominant (Phillips et al., 2019). The ØFC marks the eastern extent of major activity (Bell et al., 2014).

Middle Jurassic–Early Cretaceous syn-rift is represented by the fully marine Viking Group which is comprised of three stacked, shallow marine clastic sequences; the Krossfjord, Fensfjord and Sognefjord formations, all of which interfinger basinward with shelfal deposits of the Heather Formation (Steel, 1993; Nøttvedt et al., 1995; Ravnås and Bondevik, 1997; Ravnås and Steel, 1998; Ravnås et al., 2000; Dreyer et al., 2005). Late Kimmeridgian–Late Berriasian marine flooding of the North Sea basin resulted in deposition of the deep marine, organic-rich mudstones of the Draupne Formation.

The Northern North Sea Unconformity Complex (Kyrkjebø et al., 2004),also referred to as the Base Cretaceous or Late Cimmerian unconformity (e.g., Fyfe et al., 1981; Rawson and Riley, 1982), generally divides syn-and post-rift in the North Sea, above which, deep-water clastics and carbonates of the Cromer Knoll and Shetland groups (e.g., Deegan and Scull, 1977; Ziegler, 1990; Roberts et al., 1993; Lepercq and Gaulier, 1996; Gabrielsen et al., 2001; Gradstein et al., 2016) were deposited in a thermally subsiding basin. Minor Cretaceous reactivation, however, caused vertical movements on some large faults (Gabrielsen, 1989).

Early Cenozoic sedimentation on the Horda Platform is characterised by marine deposition of silty claystones of the Rogaland and Hordaland groups in a rapidly and thermally subsiding basin (Faleide et al., 2002; Anell et al., 2012). Early–middle Miocene contractional inversion is linked to erosion and non -deposition of large parts of the Hordaland Group on the Horda platform (Rundberg et al., 1995; Nøttvedt et al., 1995; Jordt et al., 1995, 2000). Polygonal faults have been described affecting a <1000 m succession of ppper Eocene–middle Miocene Hordaland Group mudstones in the northern North Sea (Clausen et al., 1999; Wrona et al., 2017), and are envisaged to have nucleated in the Eocene to Early Oligocene and with possible reactivation in the late Oligocene to middle Miocene. A high density of pockmarks and associated carbonate build-ups have been mapped locally on the sea floor (Nordland Gp) of the Horda Platform in the Troll East area (Fig. 1) by Forsberg et al.

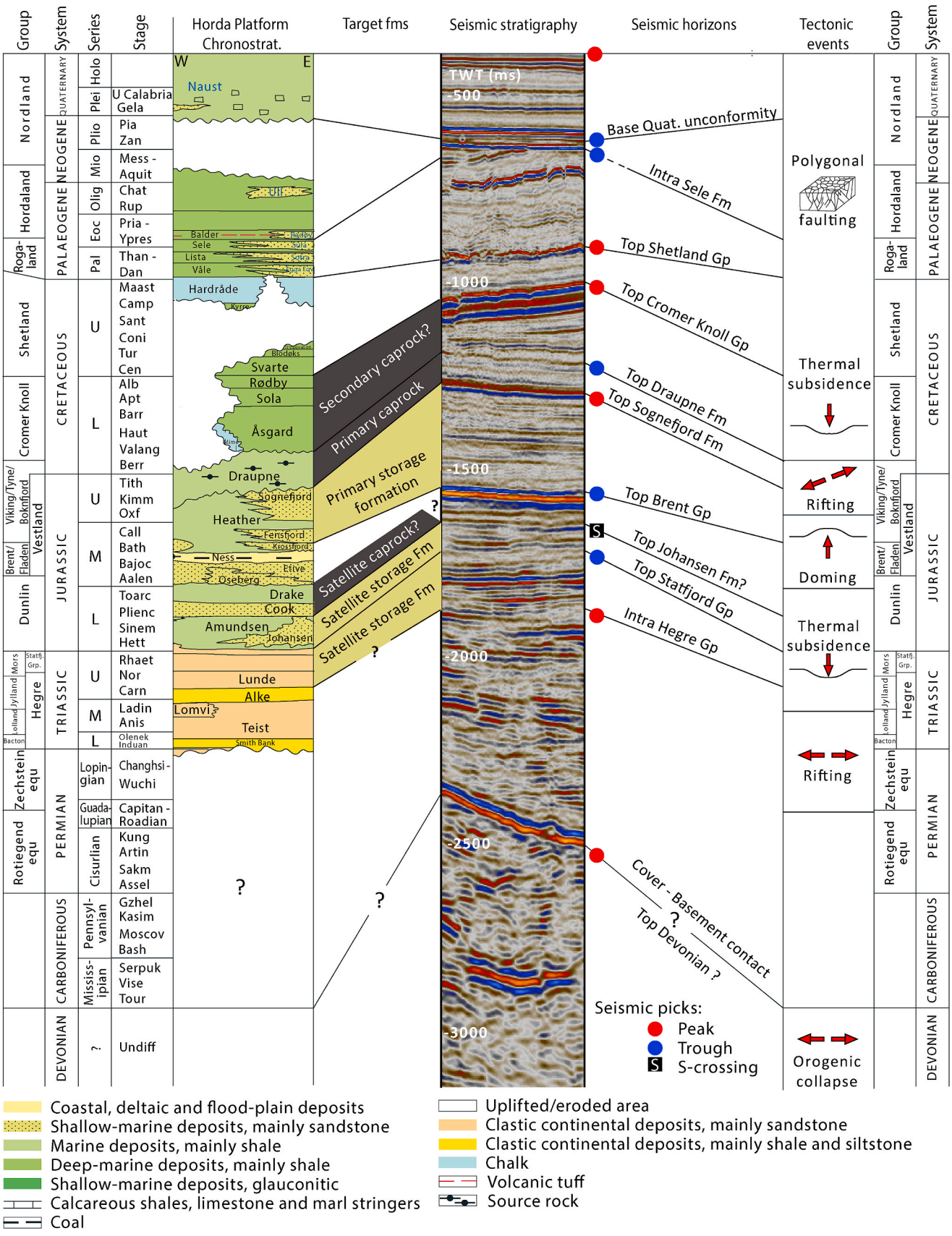

Fig. 3. West-east chronostratigraphic chart of the Horda Platform sourced from NPD (https://npd.no/en/facts/geology/lithostratigraphy/). Potential storage and caprock formations for CO_2 containment in Smeaheia are highlighted. Sample of seismic imagery from the GN1101 3D seismic survey is presented showing stratigraphic correlation to the chronostratigraphic chart and seismic horizons picked in this study. Timing of tectonic events is compiled from Færseth (1996), Odinsen et al. (2000a,b), Bell et al. (2014), Duffy et al. (2015) and Wrona et al. (2017).

(2007) and Mazzini et al. (2016). Geochemical and radiocarbon dating of associated carbonates suggest these features formed due to rapid dissociation and leakage of gas hydrates (biogenic methane) due to warming following the Younger Dryas 9.59 ± 1.38 Ka, and are not observed to be currently active (Mazzini et al., 2017).

3. Data and methodology

3.1. Seismic data

The fundament of this study is interpretation of the GN1101 3D seismic survey which images a 442.25 km^2 area of the Smeaheia fault block and bounding faults, including the majority of the proposed Alpha and Beta CO_2 storage closures (Fig. 1B).The survey was acquired in 2011 by Gassnova SF and has inline and crossline spacing of 12.5 and 25 m, respectively. The maximum resolved depth of the survey is 5000 ms TWT. The survey has normal polarity and a zero-phase wavelet. Seismic processing focused on resolving the Jurassic interval, and as such, imagery from that depth is excellent. Faults with throws as low as 5 ms TWT (approximately 15 m) can be resolved down to this interval. The survey azimuths are 065–245° (inlines) and 155-335° (cross-lines), where inlines strike approximately perpendicular to the VFZ and the ØFC, but oblique to smaller intra-block second-order faults.

3.2. Well control

Seismic interpretation has been tied to four legacy exploration wells, 31/6-6, 31/6–2, 32/4-1 T2, and 32/2–1, the locations of which are shown in Fig. 1B; seismic picks are shown in Fig. 3 and are similar to those made by Whipp et al. (2014), as well as by operators in the area according to the Norwegian Petroleum Directorate Fact Pages database (NPD; https://factpages.npd.no/). Well 31/6-6 (1984) is located on the hanging wall side of the VFZ, and penetrates the Triassic Hegre Group at 2250 m. Wells 32/4-1 T2 (1996), and 32/2–1 (2008) intersect the Alpha and Beta prospects, respectively. Well 32/4-1 T2 was drilled into basement with a total depth of 3186 m, whereas well 32/2–1 penetrates the Triassic Lunde Formation at a total depth of 1300 m. When needed, lithological information was constrained by well logs and operator reports sourced from NPD (https://factpages.npd.no).

3.3. Methodology

A high-resolution geomodel of the Smeaheia subsurface was interpreted from the GN1101 3D seismic survey utilising the Petrel E&P Software Platform, and constrained by regional 2D seismic and well control. Fault and horizon interpretation were conducted with an inline and crossline density of every 2 and 4 lines respectively, giving a geomodel with a 50 m grid resolution. All fault interpretation was conducted manually. Horizon interpretation was conducted utilising 2D seeded auto-tracking where possible. Seismic variance attribute maps were created for prominent seismic horizons. The variance attribute measures the similarity of waveforms or traces adjacent over a given lateral and/or vertical window (e.g., Pigott et al., 2013; Koson et al., 2014) and as such can be used to image discontinuity of seismic data related to faulting or stratigraphy.

The geomodel was imported into the Fault Analysis application of the PETEX Move suite where horizon–fault intersection lines (i.e., cut-offs) were interpreted. Each horizon was interpreted as close to its termination against a fault as possible (<50 m). Cut-offs were then mapped manually along the horizon edges at each fault, and the resulting 3D polylines were subsequently projected horizontally and perpendicularly to the fault strike. This method was used, as opposed to automatic cut-off generation by the software, in order to best honour fold geometries along the fault and reduce error where horizon dip angles are over 45° or cut-off geometry is erratic. This is particularly important when considering in-situ juxtaposition. Fault cut-offs were used to generate throw vs distance (T-d) plots and 3D visualisations of throw which were colour draped on 3D visualisations of fault surfaces. Similarly, cross-fault lithological juxtaposition was also generated, and the nature of juxtaposition, e.g., sandstone-on-sandstone, was ascribed a colour legend for visualization of cross-fault relationships. The high resolution geomodel facilitated high Sampling Interval/Fault Length Ratios (Ze and Alves, 2019) with the sampling intervals ranging between 0.7 and 1.25% of total fault lengths. This limits loss of information when calculating fault throw attributes.

Throw-depth profiles (T-z) and expansion index (E.I.) plots were constructed in order to constrain the depth of fault nucleation and to determine the growth history of seismically imaged normal faults (e.g., Tearpock and Bischke, 2002; Bischke, 1994; Cartwright and Mansfield, 1998; Hongxing and Anderson, 2007; Baudon and Cartwright, 2008; Jackson and Rotevatn, 2013; Tvedt et al., 2013; Osagiede et al., 2014). For an ideal blind fault, the site of fault nucleation usually correlates to the point of maximum throw on T-z plots (e.g., Cartwright and Mansfield, 1998; Hongxing and Anderson, 2007), with throw dissipating towards the upper and lower tips. Multiple throw spikes can signify more than one phase of fault activity, i.e., reactivation, or reflect the vertical linkage of a previously segmented fault (e.g., Cartwright et al., 1998; Baudon and Cartwright, 2008; Alves, 2012; Omosanya and Alves, 2014).

E.I. plots (Thorsen, 1963; Cartwright and Mansfield, 1998; Pochat et al., 2009) are generated by dividing the hanging-wall thickness of a stratal unit by its corresponding footwall thickness, and plotting these data directly against geological age or time depth. E.I. values greater than 1.0 indicate the fault intersected the free surface while growing, and created greater accommodation in the hanging wall for sediments to accumulate, i.e., syn-kinematic sedimentation. Synthesis of T-d, T-z and E.I. plots provide compelling evidence for fault timing, segmentation history and syn-kinematic sedimentation.

4. Structural description

4.1. The Smeaheia Fault Block

The Smeaheia fault block is located within the north-south striking Horda Platform (Fig. 1A), which is a primary structural element located along the eastern margin of the northern North Sea. Smeaheia (Fig. 1B) refers to the easternmost of the fault blocks that comprise the Horda Platform and is delineated by the ØFC to the east, and the VFZ to the west (North Sea Blocks 32/4 and 32/1). The Smeaheia Fault Block also coincides with parts of the Bjørgvin Arch and the Stord Basin to the south. The northern and southern extent of the Smeaheia block has not been previously defined, specifically, although Goldsmith (2000) provided some descriptions about the geology within the area of expired 205 and 369 production licenses used to drill wells 32/4-1 T2 and 32/2–1, respectively. In this contribution, we define the northern extent as the location of a sharp eastward jog in the trace of the VFZ where the Uer Terrace and the Bjorvin Arch bound each other. The southern extent is defined as the point where the VFZ tips out. Considering this definition, Smeaheia extends over 70 km north-south. The main structural elements of the Smeaheia fault block imaged by the GN1101 seismic survey are described herein. Attributes of 34 faults that were mapped in this study and that intersect the reservoir-caprock succession are summarised in Appendix 1.

4.2. First-order faults

The Smeaheia bounding fault systems (Figs. 1B and 2), the VFZ and the ØFC are defined as first-order faults, i.e., faults that are thick-skinned (basement-involved), and offset the basement-cover contact in Smeaheia by approximately −1500 and −1600 ms TWT, respectively. The basement-cover contact is undulating with reliefs of up to 300 ms TWT (Figs. 2 and 4A). East of the ØFC, the seismic character of the basement rock is continuously chaotic. A strong seismic reflector apparently

delineates the ØFC which exhibits a gentle listric geometry. Between the VFZ and the ØFC, the seismic character of the basement is irregular. A high amplitude, shallow dipping reflector is seen to the north of the GN1101 seismic survey and coincides with a positive undulation or promontory in the basement-cover contact. We term tsuch features "basement apexes" herein. This particular feature is annotated "Apex 1" in Figs. 2A and 4A. Below the basement-cover contact, an approximately 150 ms thick (but highly variable) interval of low amplitude, low frequency seismic reflectors are seen to dip gently to the west and lie on top of a series of high amplitude sub-horizontal, but undulating seismic reflectors that fan or wedge towards the ØFC. Infrequent, discontinuous, horizontal high-amplitude reflectors are observed in the basement footwall of the ØFC. An additional basement-cover contact apex (Apex 2 in Figs. 2 and 4) and underlying high amplitude, shallow-dipping reflectors can be seen directly underlying the cover expression of the VFZ. In the northern part of the GN1101 seismic survey Apex 2 (Fig. 4), the underlying low-angle reflector, and the VFZ are apparently hard-linked. Towards the south of the study area, however, the apex and the

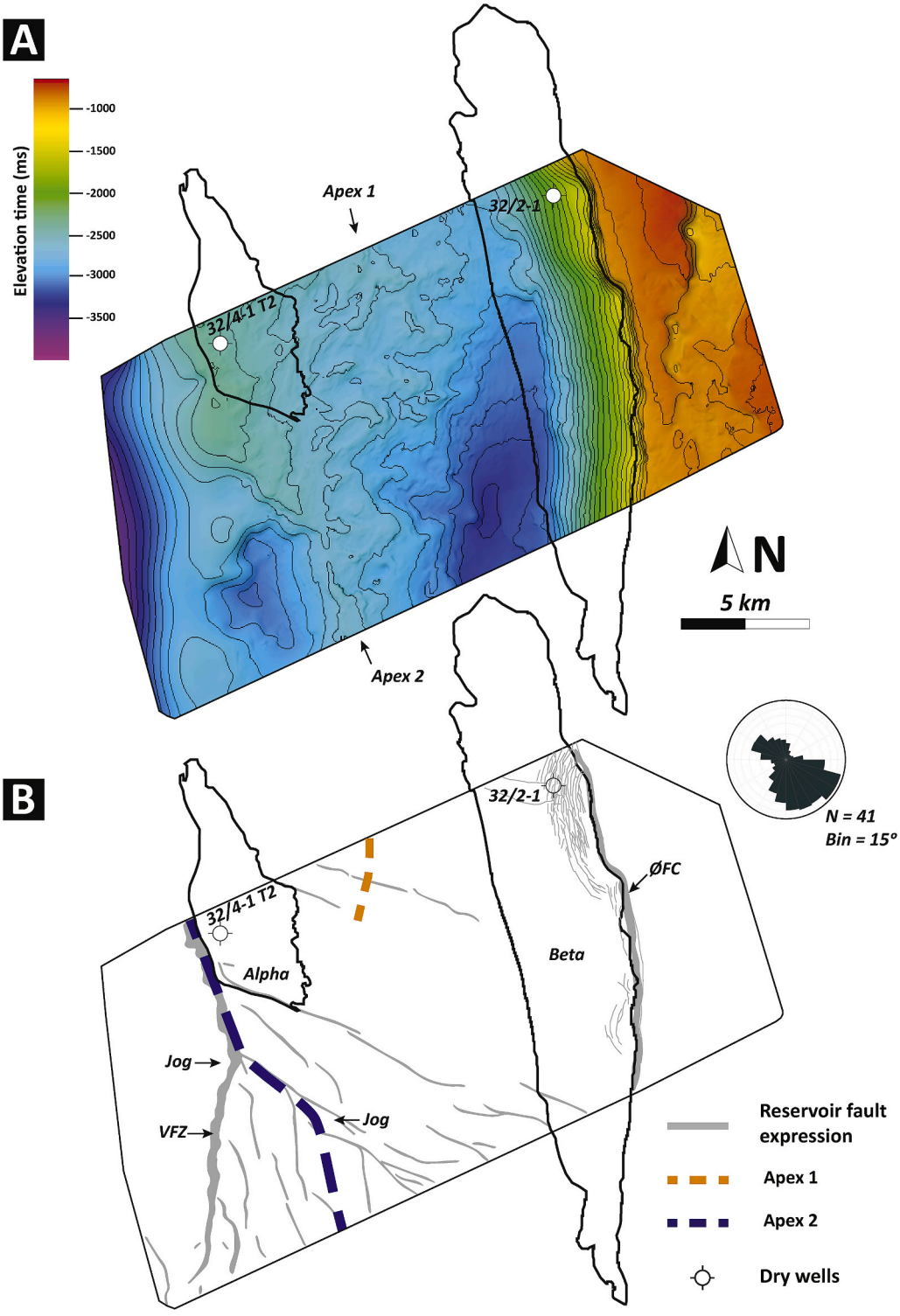

Fig. 4. A) Time structure map of the basement-cover contact showing a contour spacing of 100 ms. Two apexes, i.e., positive undulations or promontories, are labelled. Apex 1 is local and only recognised in the northern central extent of the GN1101 seismic survey. Apex 2 is more prominent, and continues throughout the entire survey. B) Map trace of Apex 2 (stippled blue line) that exhibits two distinct kinks in strike direction. The figure also shows a fault heave map (grey) for the top Sognefjord Formation (storage formation-caprock interface), the rose diagram shows fault strike for this horizon. The VFZ is hard-linked to Apex 2 and a low angle, high amplitude basement reflector towards the north of the GN1101 seismic survey. Towards the south, the VFZ undergoes a jog towards the west, while Apex 2 deviates towards the east, before resuming a NNW-SSE strike towards the southern extent of the GN1101 seismic survey. Note, the intra-block (second-order) faults that intersect the storage formation branch laterally towards the south coincident with the divergence of the thin- and thick-skinned structures. Alpha (west) and Beta (east) closures for fill-to-spill scenarios are also shown. (For interpretation of the references to colour in this figure legend, the reader is referred to the Web version of this article.)

underlying low-angle reflector, diverge from the VFZ (Fig. 4). This divergence of thin- and thick-skinned features coincides with a westward jog in the trace of the VFZ (Figs. 4 and 5) where the fault zone undergoes a change from a NNW-SSE strike in the north, to a NNE-SSW strike in the south. The basement apex also shows a marked geometric change from mimicking the VFZ in the north (NNW-SSE) before changing towards a northwest-southeast strike from the same point as the VFZ deviates, before resuming a NNW-SSE strike to the southern extent of the GN1101 seismic survey. Further, this divergence of thin- and thick-skinned structures coincides with a southward branching of thin-skinned normal faulting (second-order; described below) that primarily intersect the Jurassic—Cretaceous successions (Fig. 4B).

The up-section extents of the VFZ and the ØFC are observed in seismic variance attribute maps (Fig. 5), which have been interpreted in fault heave maps (Fig. 6). The map trace of the ØFC shows the structure is comprised of a single through-going fault throughout the GN1101 survey. Further, the ØFC structure shows an undulating strike (corrugations with wavelengths of 1–2 km) and an overall concave-up curvature (scoop-shaped). These corrugations persist vertically along the fault surface. In cross-section (Fig. 2) a modestly defined fault-flat is observed between −1250 and −1600 ms TWT that coincides with the Upper Triassic interval and underlies the prominent hanging wall anticline that defines the Beta closure. From −2500 ms to −700 ms TWT the Permo-Triassic to Cretaceous succession in the hanging wall of the ØFC is juxtaposed with basement rock in the footwall of the fault complex. Above −700 ms TWT, the ØFC does not appear to intersect strata above the base Quaternary unconformity (Fig. 7) also known as the upper regional unconformity, i.e. Ottesen et al. (2018). In the footwall of the ØFC, no Permo-Triassic succession appears to be preserved, but may be present further south (Phillips et al., 2019). There is, however, a relatively thin package of presumably Mesozoic strata that onlaps crystalline basement and thickens to the east where it infills a narrow graben. Towards the south of the study area this graben diverges into a series of smaller horsts, grabens and half-grabens (Fig. 5B, C, G) similar to those mapped by Fossen et al. (1997). Our 2D seismic mapping of reflectors extended from the study area constrained by well data on the ØFC

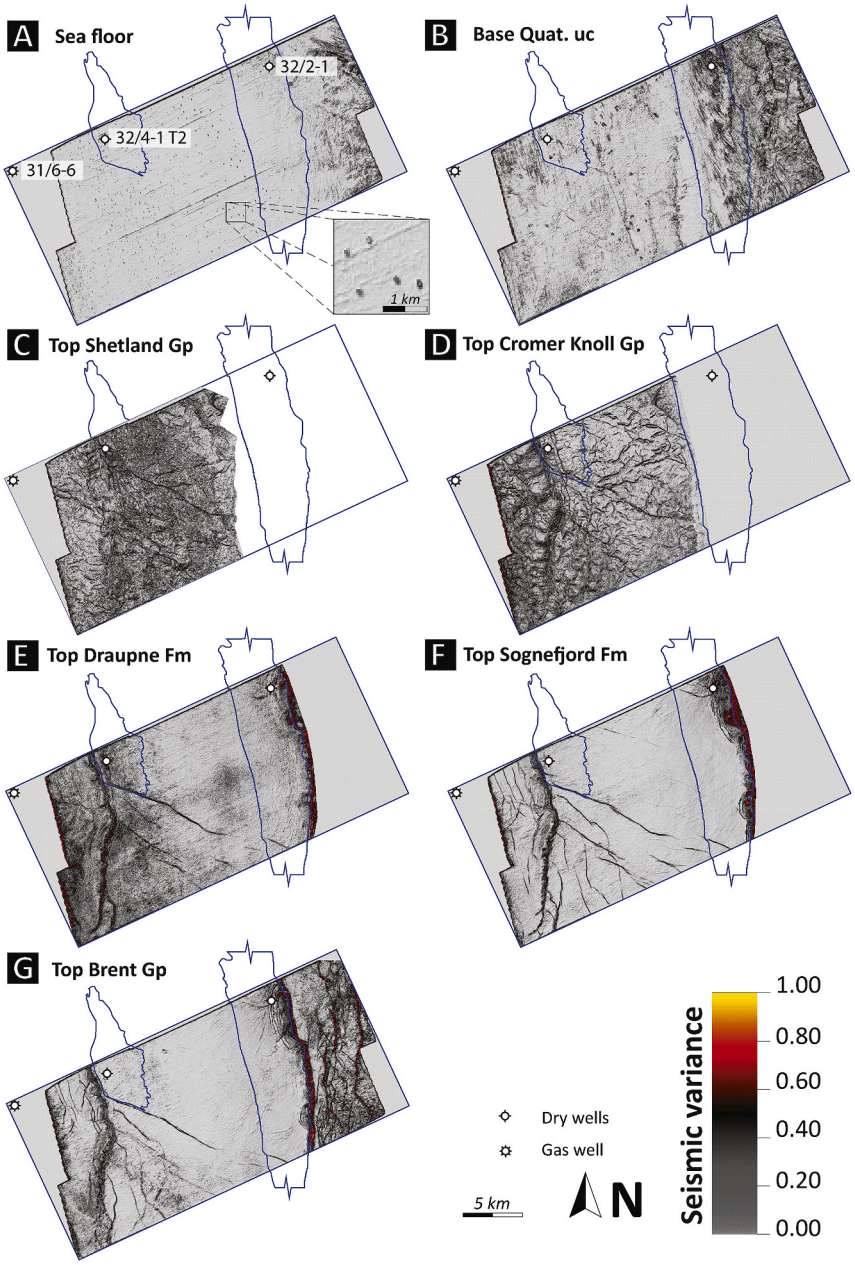

Fig. 5. Seismic variance attribute maps for seven horizons from the GN1101 3D seismic survey. A) Sea floor. Inset shows expanded view of pockmarks B) Base Quaternary unconformity, C) Top Shetland Group, D) Top Cromer Knoll Group, E) Top Draupne Formation, F) Top Sognefjord Formation, G) Top Brent Group. Blue outlines represent the Alpha (left) and Beta (right) closures. Key fault interpretation and nomenclature can be seen in Fig. 6. (For interpretation of the references to colour in this figure legend, the reader is referred to the Web version of this article.)

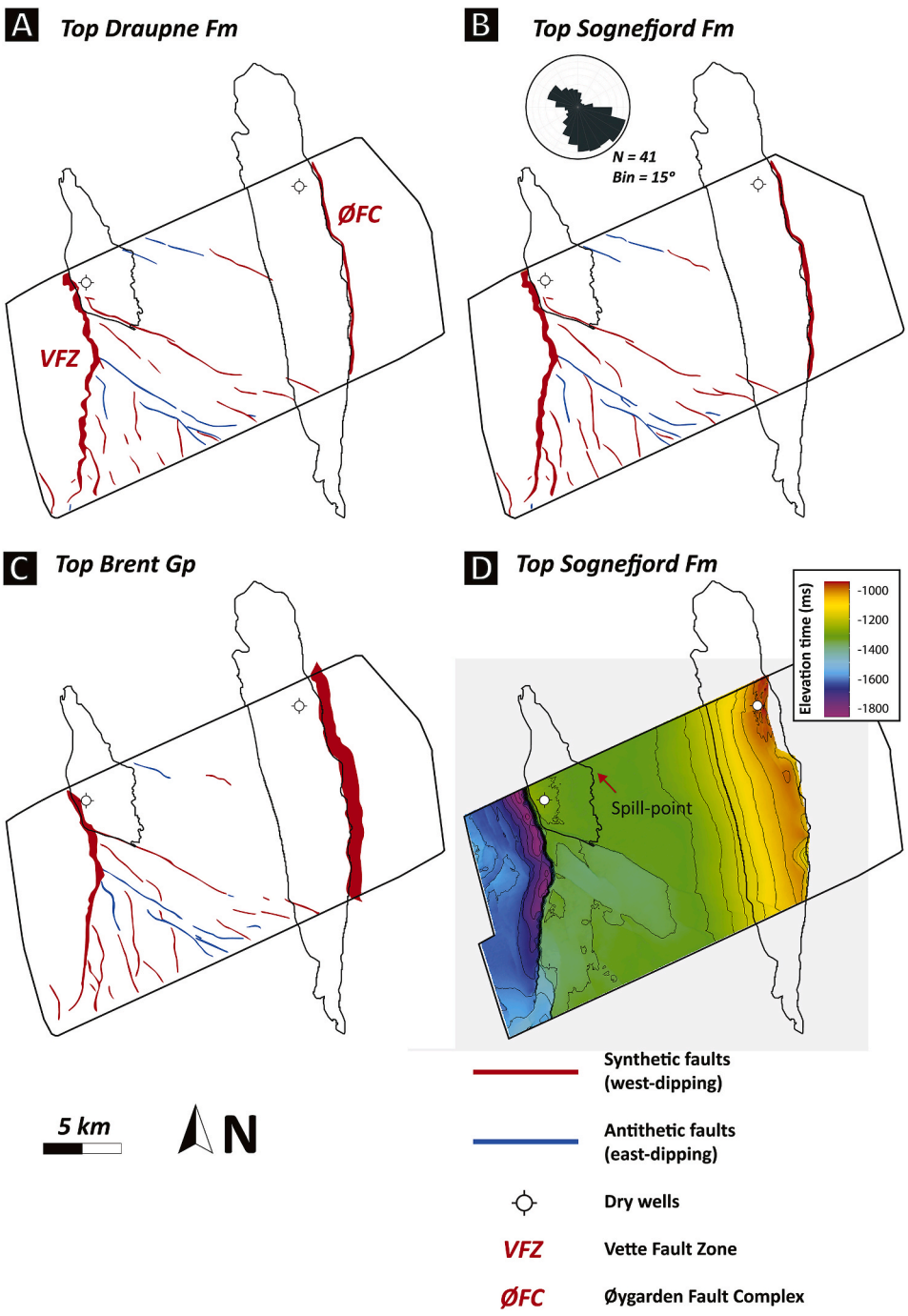

Fig. 6. Fault heave maps for three stratigraphic surfaces with fault dip direction indicated by colour, A) Top Draupne Formation, B) Top Sognefjord Formation and C) Top Brent Group. A rose diagram showing fault strike for the Top Sognefjord Formation is also shown in (B). The Smeaheia fault block-bounding Vette Fault Zone and the Øygarden Fault Complex trend north-south and dip towards the west. Subsidiary faults strike northwest-southeast and are predominantly synthetic to the fault block bounding faults, although a small population of antithetic (east-dipping) faults also exist. Note, a high population of low-displacement faults that intersect the Jurassic succession in the Beta prospect are not expressed on fault heave maps, but can be seen in variance attribute maps in Fig. 5. D) Time structure map of the top Sognefjord Formation. Contour spacing is 50 ms TWT. Outlines of Alpha and Beta closures for fill-to-spill scenarios are shown in all figures. (For interpretation of the references to colour in this figure legend, the reader is referred to the Web version of this article.)

hanging wall indicates that this package correlates primarily with Upper Jurassic or older sediments which is in accordance to previous interpretations by Rokoengen and Sørensen (1990), Fossen et al. (1997), Bell et al. (2014), Bjerkeli (2019) and Phillips et al. (2019). In the hanging wall of the ØFC, the Permo-Triassic succession thickens towards the fault whereas the Jurassic interval thins modestly. The upper-most of the Permo-Triassic succession and the entire Jurassic to Lower Cretaceous succession are both deformed by the anticlinal structure that defines the Beta closure. On the eastern flank of the anticline, the Sognefjord and Draupne formations, as well as the Cromer Knoll Group, show severe normal drag adjacent to the fault which created considerable accommodation for Cretaceous sedimentation. Quaternary strata, while not truncated by faulting, show an apparent sag geometry corresponding to the hanging wall of the underlying fault, amplifying the erosion from large-scale glacial scours.

As previously stated, in map view (Fig. 6), the VFZ shows a considerable strike deviation (jog) from NNW-SSE in the northern extent of the GN1101 seismic survey to NNE-SSW in the south. Superimposed on this trend, the VFZ also shows 1–2 km wavelength undulations (corrugations) in fault strike. These undulations persist vertically along the fault plane. In section view (Fig. 2A), from the top of the Jurassic succession (footwall) and up (−1300 ms TWT), the fault has a shallow dip (approximately 50°), but a steeper dip (approximately 60°) for the entire Upper Permo-Triassic–Jurassic successions (−1300 to −2100 ms TWT) before gradually shallowing with depth within the Permo-Triassic interval and basement beneath. As with the ØFC, the VFZ does not appear to cut up-section through the Quaternary strata (Fig. 7), which is flat-lying and of relatively uniform thickness in this area. The Permo-

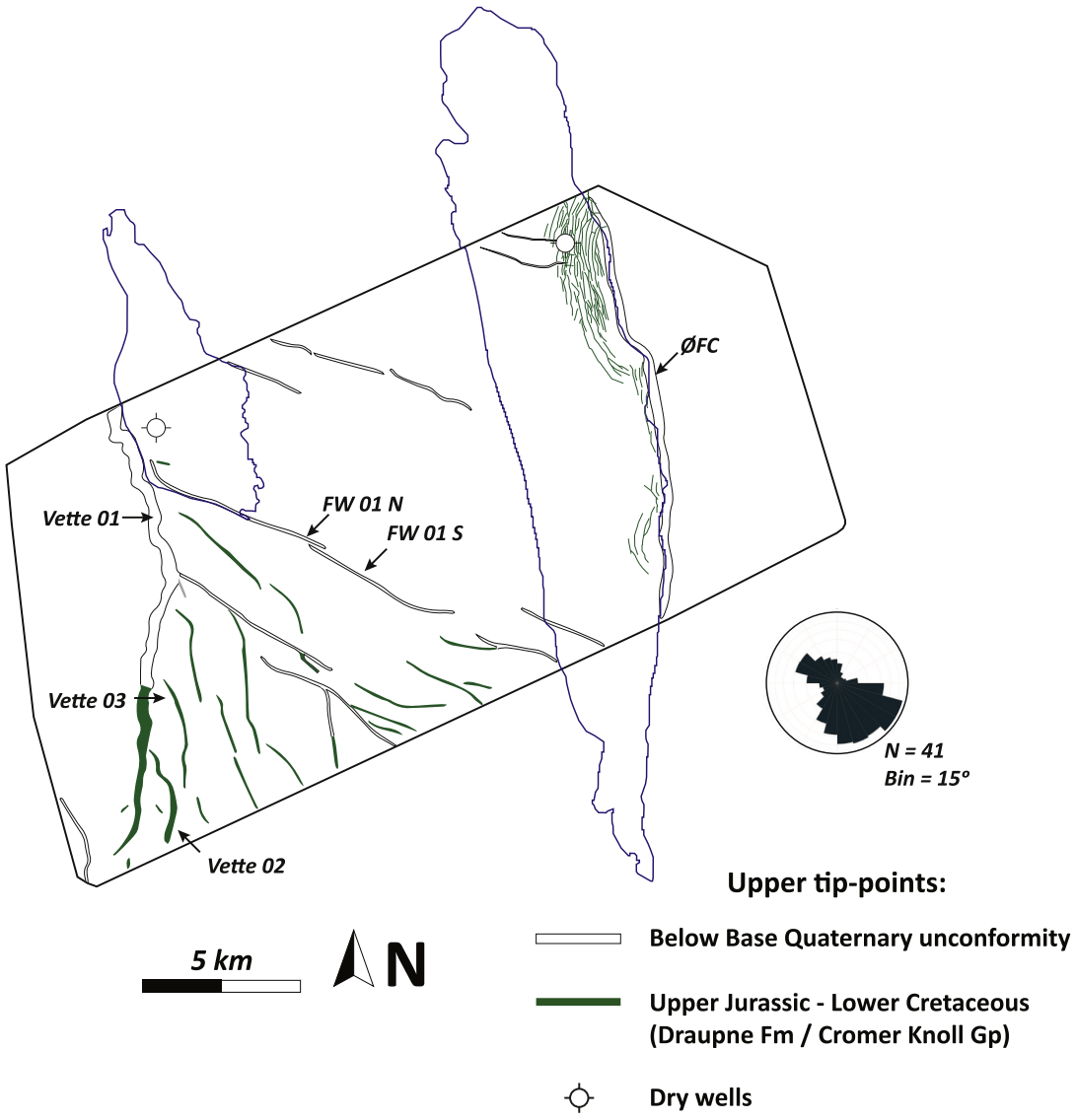

Fig. 7. Fault heave map for the top Sognefjord Formation (storage formation-caprock interface) colour coded by the up-section extent of each fault that intersects the prospective storage formation. The rose diagram shows fault strike for this horizon. Faults tip-out up-section within two broad intervals, i) within the Upper Jurassic to Lower Cretaceous intervals, i.e., the Draupne Formation and the Cromer Knoll Group (green faults), and ii) higher up in the section just below the base Quaternary unconformity (white faults). Individual fault segments of the Vette Fault Zone and the second-order faults analysed in Figs. 8 and 10–12 are annotated. Alpha (west) and Beta (east) closures for fill-to-spill scenarios are also shown. (For interpretation of the references to colour in this figure legend, the reader is referred to the Web version of this article.)

Triassic succession shows a large wavelength (5–6 km) roll-over fold within the hanging wall of the VFZ and considerable thickening towards the fault, whereas the equivalent footwall strata thins and gently dips towards the fault. The Jurassic hanging wall succession also shows roll-over, thins towards the fault and displays severe normal drag. The footwall expression of the succession dips synthetically towards the fault and thickens away. Large thickening in the hanging wall of the Cretaceous successions towards the fault is apparent. The Cenozoic successions below the base Quaternary unconformity show minimal offset, but still possess thicker hanging wall packages. Further, the Cretaceous to the lower-most of the Cenozoic packages dip towards the west and are truncated by the base Quaternary unconformity (Fig. 7). The base Quaternary unconformity dips gently to the east in the hanging wall of the ØFC and to the west in the footwall. Correspondingly, the deepest point is located 2.5 km to the west of the ØFC where Quaternary sediments are at their thickest. The entire Quaternary unit thins rapidly towards the east where it overlies the ØFC footwall. The sea floor dips gently to the east of the area imaged by the GN1101 seismic survey where it exhibits a northwest-southeast orientated depression.

The persistent listric nature of the ØFC throughout the GN1101 seismic survey (Fig. 2) is consistent with continued reactivation of a single basement-involved structure that propagated up-section throughout Mesozoic rift events in the northern North Sea. A similar interpretation can be made for the northern extent of the VFZ imaged by the GN1101 seismic survey, however, the trend change of the VFZ away from the underlying basement apex structure (Apex 2, Fig. 4) shows the VFZ is hard-linked with at least two different older basement structures (dual-rooted); the basement apex to the east (Fig. 4) and an additional structure below the imaged depths of the GN1101 seismic survey. A northern North Sea-wide basement seismic facies study by Fazlikhani et al. (2017) further corroborates these observations. The dual-rooted nature of the shallow parts of the VFZ probably resulted from basement structures being imperfectly orientated for reactivation during later Mesozoic rift events. It is envisaged that reactivated thick-skinned faults propagated up-section and became hard-linked with younger shallower faults, the strikes of which are more systematically orientated

to the causal stresses. Consequentially, the deviation of the VFZ from the basement structure towards the south of the study area (Fig. 4) appears to result in a zone of diffuse strain during the Jurassic–Cretaceous rift event where northwest-southeast thin-skinned second-order faults branch towards the southeast at either side of the underlying basement apex. Phillips et al. (2019) have noted that a larger jog towards the north of the VFZ (Fig. 1B) corresponds to a "domain boundary" of Fossen et al. (2017) and further correlates with the subcrop of the Lomre Shear Zone mapped by Fazlikhani et al. (2017). As such the style of basement-younger fault interactions in the Horda Platform are variable.

The persistent chaotic seismic facies below the top basement reflector are interpreted as Devonian metasediments and Caledonian basement (Fig. 2). The high-amplitude, shallow dipping reflectors (brown in Fig. 2) that underlie the basement-cover contact apex are interpreted as Devonian shear zones. The interval of low-amplitude, low-frequency, gently dipping seismic reflectors that lie directly below the basement-cover contact (down to −3200 ms TWT) are interpreted as Devonian clastic metasediments, an interpretation that is corroborated by Well 32/4-1 T2 (*PL 205 Licence Group Well 32/4-1-T2 Final Well report,* 1997) which penetrated this interval (Fig. 2). The underlying series of high amplitude sub-horizontal, but undulating seismic reflectors (−3200 to −3900 ms TWT) that appear to fan or wedge towards the ØFC may represent pre-Caledonian metasediments and layered Caledonian nappes and/or Devonian clastic metasediments (see Fazlikhani et al., 2017). The less-frequent, discontinuous, horizontal high amplitude reflectors observed in the basement footwall of the ØFC (−3500 ms TWT to −4000 ms TWT) may again represent Caledonian nappes or discrete mafic igneous sills which are potentially of Permian age (e.g., Heeremans and Faleide, 2004).

The vertically persistent corrugations that characterise both of the Smeaheia block-bounding faults are commonplace in large normal fault systems and likely represent the positions of former fault segments that coalesced laterally as the faults evolved towards large through-going structures (e.g., Lee and Bruhn, 1996; Ferrill et al., 1999; Lohr et al., 2008; Mulrooney et al., 2017, 2018b). The lower-angle, upper portion of the VFZ (Fig. 2) in comparison with the ØFZ is probably lithologicaly controlled, where the argillaceous nature of the Cretaceous and Cenozoic strata favours lower-angle faults (e.g., Peacock and Xing, 1994). The footwall of the ØFC, on the other hand, is comprised of uplifted crystalline basement (Bertram and Milton, 1988; Nadin et al., 1995, 1997). Both faults show steep dips associated with the more sand-prone Jurassic succession. Shallowing with depth and overall listric geometries are common for deep-seated basement involved faults (Bally et al., 1981; Shelton, 1984; Williams and Vann, 1987). The lack of apparent thickening of the Jurassic succession in the hanging walls of the VFZ and indeed the fact that it thins towards the ØFC is anomalous as previous works describe the succession as dominantly syn-rift further west (Færseth, 1996; Bell et al., 2014; Whipp et al., 2014; Deng et al., 2017), north (Zhong and Escalona, 2020), and south (e.g., Osagiede et al., 2020). The diachronous nature, however, of the Jurassic–Cretaceous rift phase (Kyrkjebø et al., 2004; Bell et al., 2014; Whipp et al., 2014; Duffy et al., 2015), and the presence of a thick Cretaceous hanging wall wedge (Phillips et al., 2019 and supported herein) indicate that movement on the VFZ took place quite late in this rift phase. Further, the deeper-buried nature of the VFZ hanging wall strata (500 ms TWT deeper) may mask thickness variations in time migrated seismic data. Clear thickness increases in the Permo-Triassic and Cretaceous successions in the hanging walls of both faults is in accordance with large displacement accrual during deposition.

The Quaternary package is interpreted as post-rift where differential compaction (e.g., Jackson et al., 2008) is primarily attributed to the sag geometry in the hanging wall of the ØFC. Conversely, no such localised sag is evident in the hanging wall of the VFZ where the Quaternary succession is generally flat-lying. The thinning of the Quaternary successions to the east of the study area likely reflects the aforementioned differential compaction in addition to tectonic rejuvenation of Norway (e.g., Fjeldskaar et al., 2000).

The roll-over geometries expressed in the hanging walls of both the VFZ and the ØFC (Fig. 2) are credited to the listric and ramp-flat-ramp natures of the respective faults (e.g., Dula Jr., 1991; McClay and Scott, 1991; Xiao and Suppe, 1992). For both faults, the well-developed normal drag (Fig. 2) observed in hanging wall packages of the Jurassic–Cretaceous are consistent with breach of extensional monoclines that formed ahead of faults as they propagated up section (e.g., Sharp et al., 2000; Jackson et al., 2006; Braathen et al., 2011; Maher and Braathen, 2011; Mulrooney et al., 2017). The gently westward-dipping nature of footwall sediments in both structures also corresponds to breach of extensional monoclines where the majority of the propagation folding is preserved in the hanging wall (Jackson et al., 2006). The higher westward-dip angle of the top Draupne Formation horizon is credited to erosion.

4.3. The Vette relay zone

Seismic variance attribute maps of the southwestern extent of the GN1101 survey exhibit a relay zone in the VFZ comprising of three main synthetic segments (Vette 01, 02 and 03) as well as three smaller segments that splay from the larger structures (Figs. 5 and 8). The northern extent of both Vette 03 and Vette 02 curve towards and are hard-linked with Vette 01. South of the linkage points, Vette 02 and 03 are laterally separated from Vette 01 by 1100 and 1300 m, respectively. The Vette 01, apart from the southern 5 km of the segment, continues up-section to the base Quaternary unconformity. The southern 5 km of Vette 01, Vette 02 and Vette 3 exhibit a more limited vertical extent, tipping out up-section within the Upper Jurassic to Lower Cretaceous Draupne Formation and the lower part of the Cromer Knoll Group. Vette 02 continues for 25 km to the south as another major segment of the VFZ (Fig. 1B).

Throw vs distance (T-d), Throw vs depth (T-z) and Expansion Index (E.I.) plots are presented in Fig. 9 for Vette 01 and Vette 02. Vette 01 shows established displacement (up to 1000 ms TWT) within basement rocks which decreases throughout the Permo-Triassic succession to 500 ms TWT, a spike in displacement within the Jurassic succession (600 ms TWT), a dramatic curtailment of displacement through the Cretaceous strata, followed by a gradual dissipation of displacement within the lower Cenozoic (Fig. 9A). No offset of the Quaternary succession is observed. The fault exhibits a saw-tooth T-d profile (Fig. 9A) where 6 local displacement minima which represent sudden decreases in throw (>50 ms TWT) over a short interval are seen. Expansion of hanging wall strata (in relation to footwall strata thickness of the same package) is observed within the Triassic (E.I. of 1.5), Upper Jurassic (E.I. of 1.5), Lower Cretaceous (E.I. of 2.7) and again within the upper Palaeocene Sele Formation (E.I. of 1.6).

To the south, Vette 02 (Fig. 9B) shows no established displacement within the basement, a gradual increase throughout the Permo-Triassic, which reaches a maximum within the Jurassic succession (175 ms TWT), before decreasing throughout the Lower Cretaceous Cromer Knoll Group. No displacement is observed within the Shetland Group or above. T-d plots (Fig. 9B) show 3 marked displacement minima. A dramatic decrease in throw is observed where the fault approaches the Vette 01 segment to the north. In addition, displacement of the Draupne Fm dissipates to zero 2.5 km south of the northernmost extent of the fault segment. Expansion of hanging wall strata is only observed in the Late Jurassic (E.I. of 1.125) and Early Cretaceous successions (E.I. of 1.165).

Figs. 10 and 11 show hanging wall and footwall horizon-fault intersections (cut-offs), lithological cross-fault juxtaposition (for generalised lithologies) and computed throw values for Vette 01 and Vette 02, respectively. Within the footwall of Vette 01, the thickness of the Draupne Formation, the prospective caprock, thins considerably towards the north of the fault segment compared to other mapped horizons. The prospective storage formation, here considered the entire

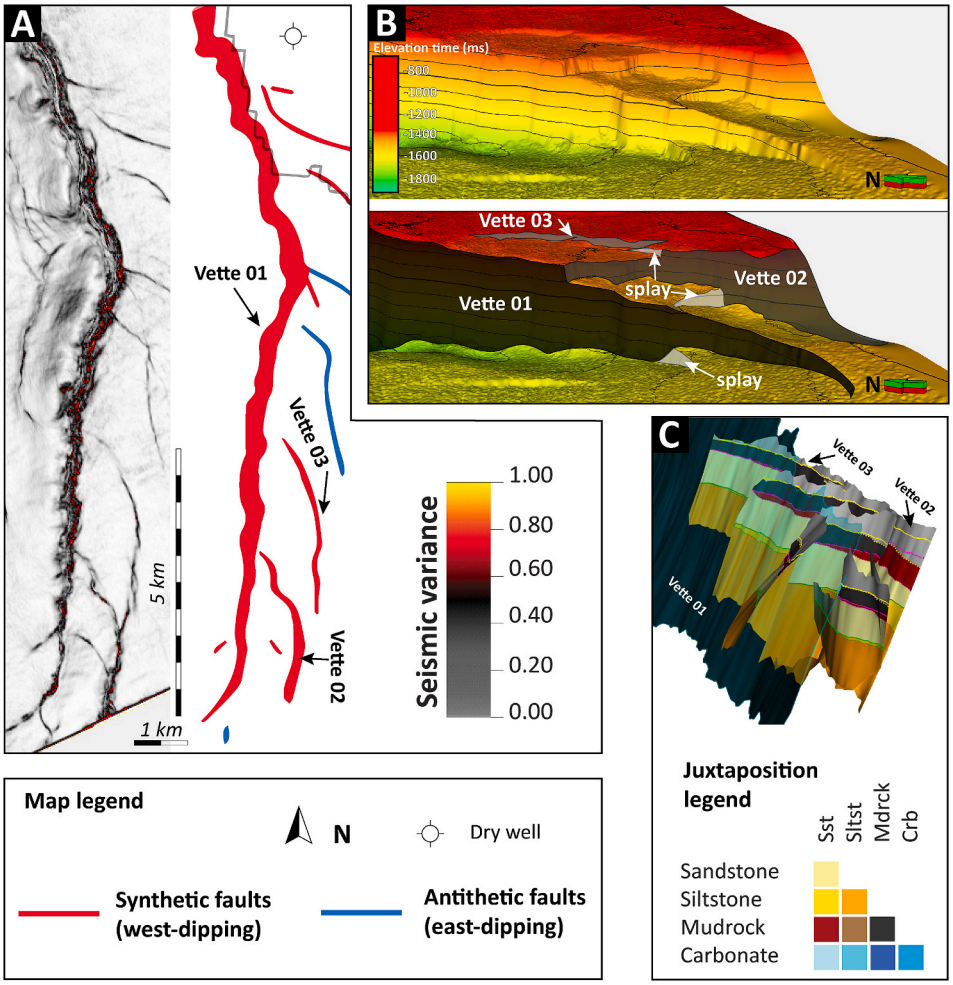

Fig. 8. A) Variance attribute map of the Vette Fault Zone (left) and interpretation (right) for the Top Sognefjord Formation. Red faults dip towards the west whereas blue faults dip towards the east. Note, the fault zone continues both north and south beyond the coverage of the GN1101 3D seismic survey. Three primary segments of the fault zone that form a relay zone are labelled (Vette 01, 02 and 03). B) A 3D perspective view of the relay zone as expressed at the Top Sognefjord Formation (top) with interpretation (bottom) of the primary fault segments and smaller splays. C) Simplified juxtaposition diagram (3D perspective) of faults in the vicinity of the relay zone. See Fig. 10 and 11 for more fault attributes of the Vette 01 and 02 faults and for the juxtaposition colour legend. (For interpretation of the references to colour in this figure legend, the reader is referred to the Web version of this article.)

interval from the top of the Brent Group to the top of the Sognefjord, i.e., the Viking Group sandstones, is dominantly self-separated across the VFZ (Fig. 10). Here the reservoir in the footwall is primarily juxtaposed against the Cromer Knoll Group (lightest blue colour; Fig. 10B). Towards the south of the Vette 01 fault segment, displacement dissipates (Fig. 10C) and the footwall reservoir is progressively juxtaposed against the caprock in the hanging wall, and finally self-juxtaposed (lightest yellow colour; Fig. 10B).

Given the lower measurable displacement on Vette 02 to the south (Fig. 11C) compared to Vette 01, the upper part of the footwall storage formation is juxtaposed against the Draupne Formation caprock in the hanging wall. The remaining majority of the footwall storage formation is self-juxtaposed across the fault. Towards the south of the imaged portion of Vette 02 (Figs. 9B and 11 C), throw increases significantly coincident with dramatic reduction on Vette 01 (Figs. 9A and 10C).

The Vette 01 segment developed during Permo-Triassic rifting and was reactivated during the Late Jurassic–Early Cretaceous. Displacement minima in Fig. 9A may represent sites where earlier fault segments linked (e.g., Lohr et al., 2008). The relay zone only shows evidence of activity during the Late Jurassic–Early Cretaceous (Fig. 9; see Discussion) where it formed by overlap of the Vette 01 and 02 segments. The rapid displacement drop-off on the Vette 02 segment towards the north likely reflects interaction with the larger Vette 01 segment (e.g., Duffy et al., 2015). The reduction in the trace length (tip-line retreat) of the Vette 02 segment up section (in the Draupne Fm) is also indicative of overlap of the fault strain field with that of the neighbouring Vette 01 segment (e.g., Childs et al., 2002). Vette 03 exhibits a much smaller displacement, and is interpreted as a minor structure that locally accommodates strain. Whereas the relay zone only shows evidence of activity during the Late Cretaceous to the Early Jurassic rift phase, the majority of the Vette 01 segment has continued to accrue displacement into the Cenozoic. The small splay faults (Fig. 8) likely result from localised stress variation in the shadows of the larger structures (e.g., Maerten et al., 2002). The nature of juxtaposition across the Vette 01 fault is favourable for CO_2 containment within the Alpha structure, whereas the juxtaposition across the relay zone (Fig. 8) probably promotes pressure communication between the Smeaheia fault block and the neighbouring Tusse fault block.

4.4. Second-order faults

A population of intra-block subsidiary faults with northwest-southeast strikes intersect the Smeaheia fault block (Figs. 5 and 6). These faults exhibit maximum trace lengths of approximately 7 km, spacing in the range of 1–3 km and maximum throws between 5 and 60 ms TWT (approx. 15–90 m). The faults are thin-skinned and tip out down section within the lower-most Jurassic or upper-most Permo-Triassic (Fig. 2B). Up section, the faults tip out within the Upper Jurassic–Lower Cretaceous Draupne Formation and Cromer Knoll Group (Fig. 7). The majority of the faults dip towards the southwest, i.e., synthetic to the VFZ (Fig. 6). A clear branching from a change in polarity on the Vette 01 and towards the southwest is observed. This results in a triangular region of diffuse strain with an area of approximately 110 km^2 that probably extends southwards of the GN1101 seismic survey. Several of the northwest-southeast striking faults intersect the reservoir-caprock succession of the Alpha closure in the area covered by the

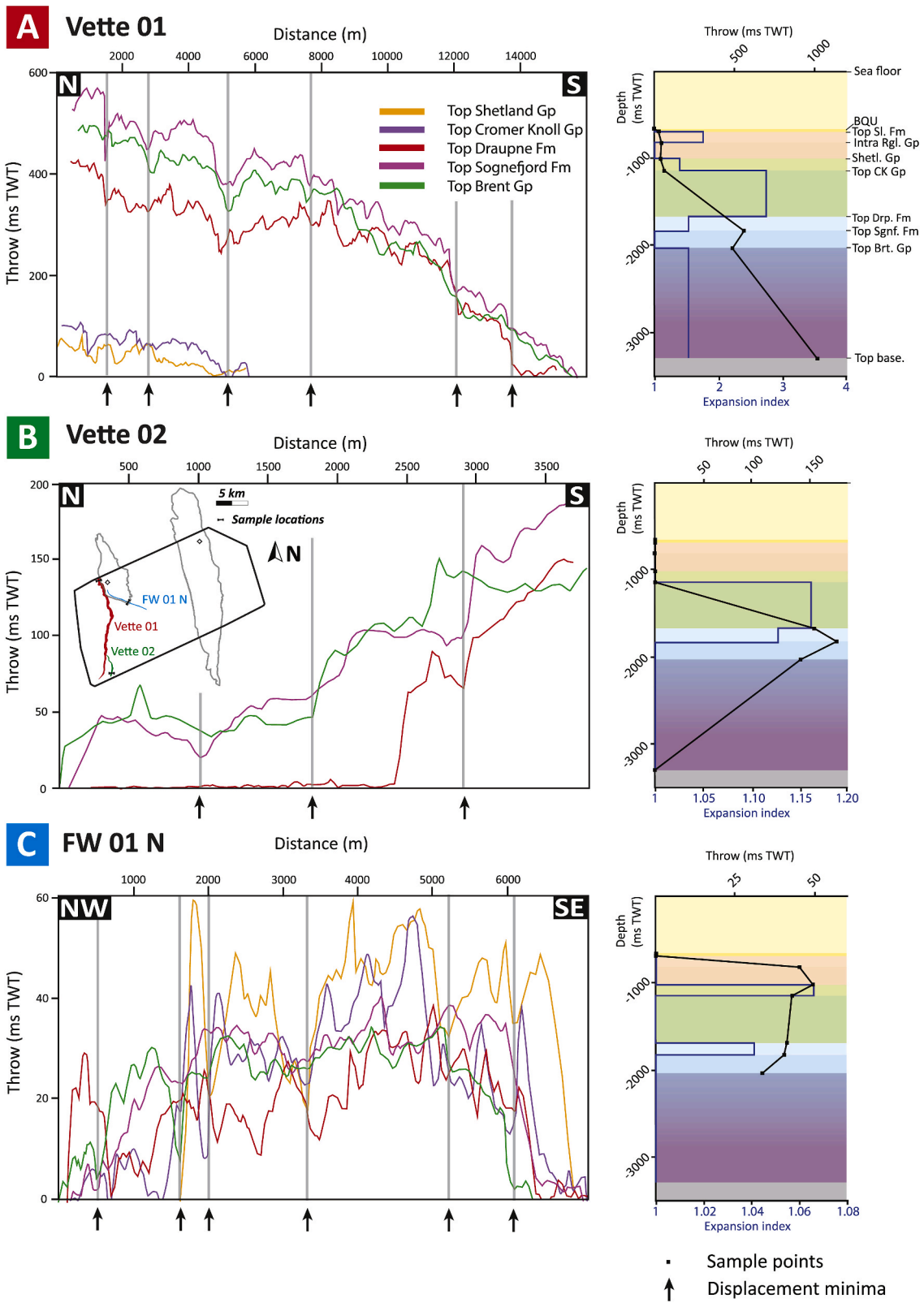

Fig. 9. (Left) Throw 'vs' distance (T-d) plots and (right) throw 'vs' depth (T-z)/Expansion Index (E.I.) for (A) the main northern Vette Fault Zone segment (Vette 01), (B) the main southern Vette Fault Zone segment (Vette 02) and (C) the synthetic second-order fault FW 01 N. Local displacement minima are highlighted in T-d plots. The inset map in (B) shows points of maximum throw where T-z and E.I were measured. Abbreviations: BQU = Base Quaternary unconformity, Sl. Fm = Sele Formation, Intra Rgl. Gp = Intra Rogaland Group, Shtl. Gp = Shetland Group, CK Gp = Cromer Knoll Group, Drp. Fm = Draupne Formation, Sgnf. Fm = Sognefjord Formation, Brt. Gp = Brent Group, Base. = Basement. Vette 01 is a thick-skinned (basement-involved) fault that shows evidence of activity in the Permo-Triassic, Late Jurassic–Late Cretaceous and Palaeocene–Eocene. Vette 02, while likely thick-skinned to the south, shows no evidence of activity before the Late Jurassic in the area covered by the GN1101 seismic survey. Activity continued into the Early Cretaceous. FW01 tips out down-section within the Permo-Triassic succession and shows pulses of activity during the Late Jurassic and the Late Cretaceous.

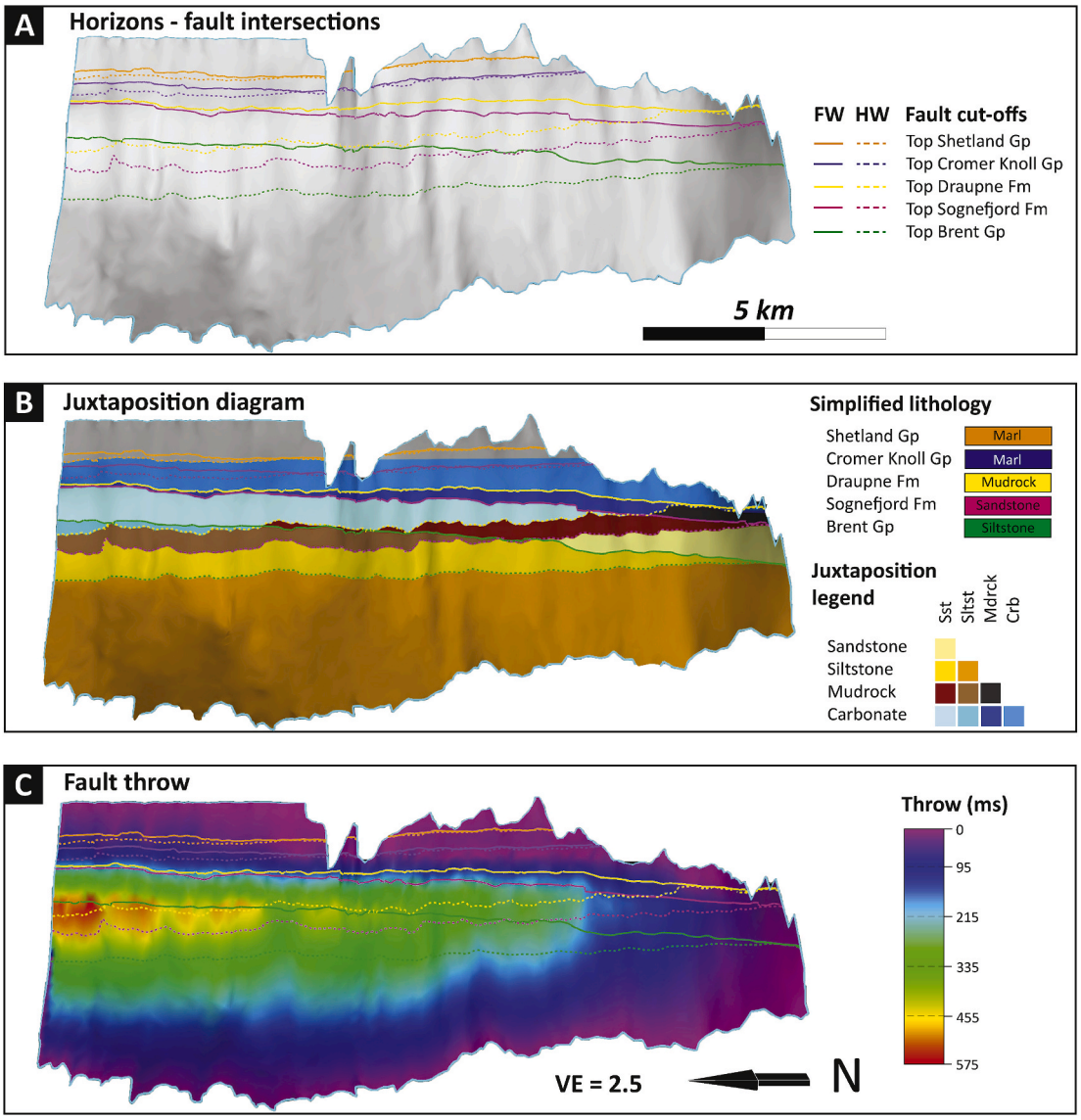

Fig. 10. Perspective images of an approx. 15 km long section of the main segment of the Vette Fault Zone (Vette 01) showing A) fault-horizon intersections (cut-offs), B) simplified lithological juxtaposition across the fault and C) fault throw distribution. Location of fault shown in Fig. 9B. Note the storage formation (here considered the interval between the top of the Brent Group and the Sognefjord Formation) is progressively juxtaposed with the Cromer Knoll Group towards the north where throw values are higher. Progressive thinning of the primary caprock (Draupne Formation) is also seen towards the north.

GN1101 seismic survey, and more probably occur north and south of the survey.

Seismic variance attribute maps (Fig. 5F and G) show a dense population of low-displacement faults parallel to, and in the immediate hanging wall of the ØFC. Localisation of these structures along the crest of the ØFC hanging wall rollover is apparent, which also coincides with the Beta closure. Here, these faults often have trace lengths of less than 1 km, show both synthetic and antithetic dip directions to the ØFC, spacing in the range of 100–300 m and maximum throws of 10–20 ms TWT. Moreover, these small faults appear to branch from a common origin at depth in the Permo-Triassic or Lower Jurassic successions, and mostly tip-out up-section in the upper-most Jurassic interval. A population of low-displacement subsidiary faults intersect the Permo-Triassic succession at depth (Fig. 2), but are poorly resolved by the GN1101 seismic survey.

Throw vs distance (T-d), throw vs depth (T-z) and Expansion Index (E.I.) plots for FW 01 N that is representative of the northwest-southeast striking second-order faults that intersect the Jurassic reservoir interval within the Alpha closure are shown in Fig. 9C. The FW 01 N fault cuts down section into the upper-most Permo-Triassic succession, but not through the basement (thin-skinned). At the point of maximum displacement, this fault shows an up-section increase in displacement throughout the Jurassic strata, consistent displacement within the Lower Cretaceous (slightly increasing up-section), followed by a displacement spike within the Upper Cretaceous Shetland Group and the Palaeocene–lower Eocene Rogaland Group (maximum of 60 ms TWT). Displacement dissipates to zero by the top of the Sele Formation (upper Palaeocene). T-d plots show some along-strike variation to this trend, notably 6 displacement minima that broadly correlate between all horizons. Hanging wall expansion is observed in the Upper Jurassic succession, and within the Late Cretaceous succession. No faults displace strata above the base Quaternary unconformity, although erosion has made the cessation of their displacement impossible to interpret precisely from the seismic data.

Fig. 12 shows hanging wall and footwall horizon-fault intersections (cut-offs), lithological cross-fault juxtaposition (for generalized lithologies) and computed throw values for FW 01 N. Typically, the majority of the Viking Group sandstones (perspective storage formation) are self-

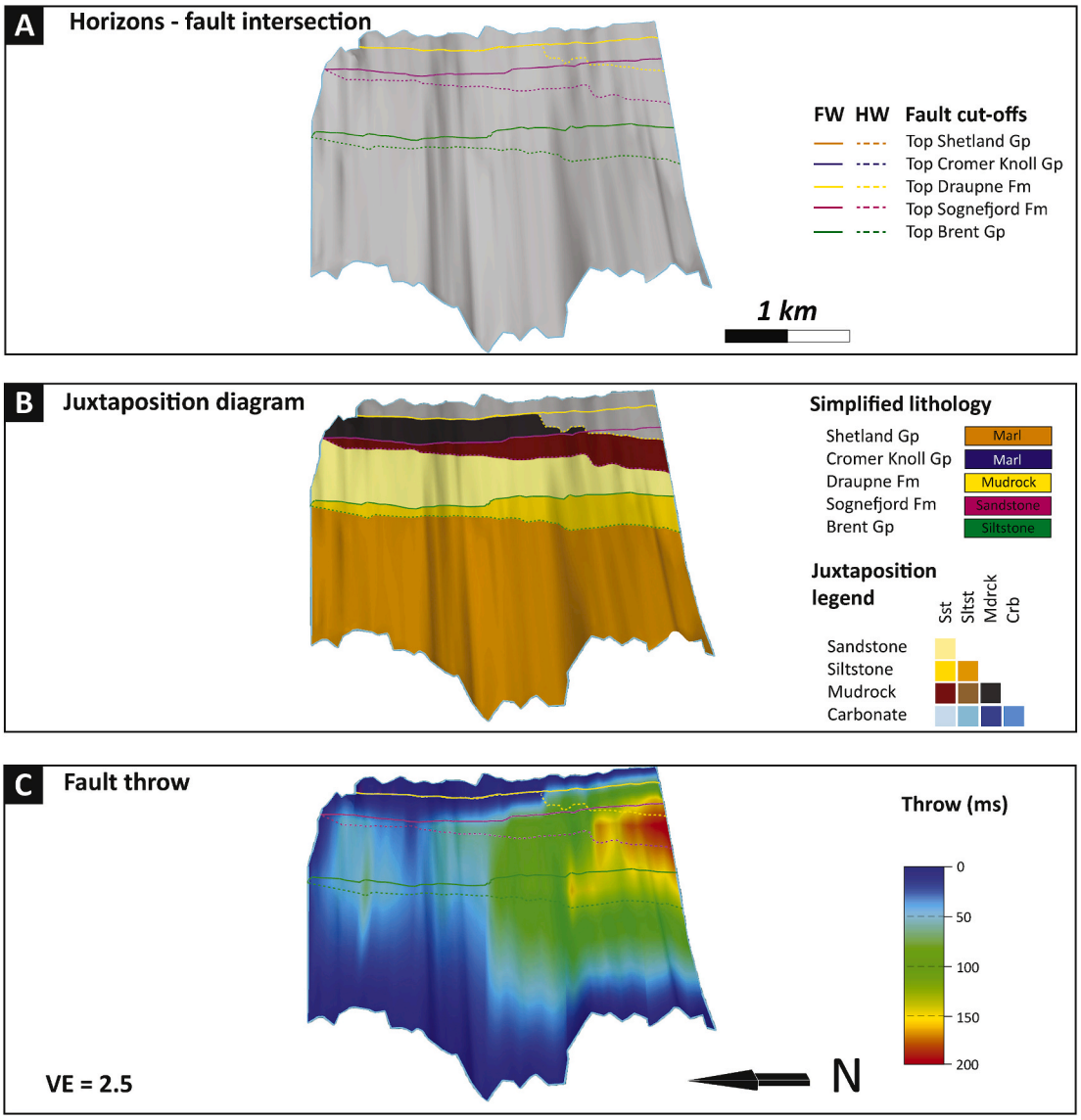

Fig. 11. Perspective images of an approx. 3 km long section of the Vette 02 segment that forms a relay zone with the Vette 01 segment. A) fault-horizon intersections (cut-offs), B) simplified lithological juxtaposition across the fault and C) fault throw distribution. Location of fault shown in Fig. 9B. Note, the storage formation is primarily self-juxtaposed across the fault.

juxtaposed across these faults (e.g., Fig. 12B). FW 01 N shows an asymmetric throw distribution (Figs. 9C and 12C), with less throw towards the northwest, where the fault becomes hard-linked with Vette 01. Throw values for the top Shetland Group dissipate to zero approx. 1.5 km southeast of the north-western extent of the fault. Rapid dissipation of the fault throw is also noted towards the southeast extent of the fault (approx. 6000 m distance in Fig. 9C).

The second-order faults that only displace Upper Jurassic and overlying strata initiated during the second phase of rifting (Late Jurassic–Early Cretaceous), where pre-existing Permo-Triassic and older basement structures were presumably not preferentially orientated (striking mostly north-south), an interpretation which agrees with previous workers (e.g., Færseth, 1996; Færseth & Ravnås, 1998; Tomasso et al., 2008; Phillips et al., 2019). Isolated pulses of activity are discernible by E.I. and T-z analyses (see Discussion). The asymmetric throw profile is credited to interactions with the Vette 01 segment to the northwest, and an overlapping subsidiary fault to the south (FW 01 S in Fig. 7). The rapid dissipation of throw in the top Shetland Group towards the north-western extent of the fault may be misleading as the fault was interpreted to tip-out further-down section. As such, higher resolution data may show that the fault persists here which would produce a smoother T-d taper.

The population of closely spaced, low-displacement faults affecting the culmination of the Beta closure are interpreted as crestal collapse faults. These faults form due to the gravitational instability of roll-over folds which form due to the listric or ramp-flat-ramp geometries on underlying faults (e.g. McClay and Ellis, 1987; McClay, 1990; McClay and Scott, 1991). While their north-south orientation conforms to an east-west extensional direction during the second phase of rifting as postulated by Whipp et al. (2014) and Reeve et al. (2015), the strikes of these structures are not envisaged to represent the regional in-situ stress field, but rather reflect the trend of the roll-over fold. The combination of small growth packages within the Draupne Formation (Fig. 2B) and the up-section extent of these faults suggests they were short lived; both initiating and terminating (for the most part) during the Late Jurassic.

4.5. *Structural closures*

Following the above structural description, and considering the Sognefjord and Draupne formations as prospective CO_2 storage and top

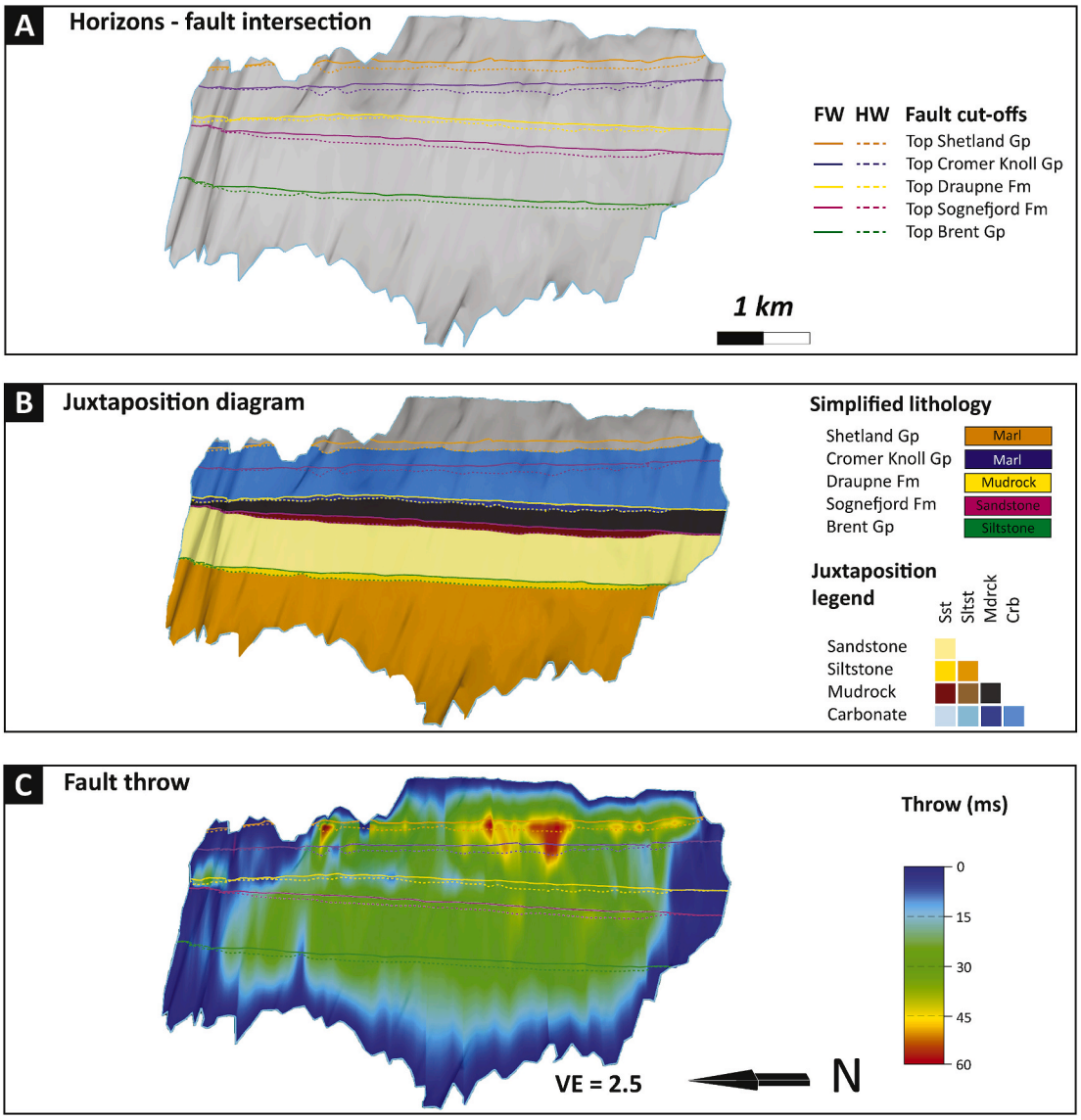

Fig. 12. Perspective images of the approx. 5 km long synthetic subsidiary fault (FW 01 N) that intersects the Alpha prospect showing A) fault–horizon intersections (cut-offs), B) simplified lithological juxtaposition across the fault and C) fault throw distribution. Location of fault shown in Fig. 9B. Note, the storage formation is primarily self-juxtaposed across the fault.

seal formations, respectively, two structural closures (Figs. 2 and 6D) previously defined by Statoil (2016), have been outlined at a higher resolution herein. The Alpha structure (Fig. 6D) is defined as a three-way closure in the footwall of, and against, the VFZ. Here, the Sognefjord Formation dips gently towards the east, north and south. In map view (Figs. 1B, 5 and 6), this closure is considered domal towards the northern extent of the GN1101 survey, with an elongated axis towards the NNW (interpreted using 2D regional seismic). The Alpha structure comprises an areal extent of 27.2 km^2, at the fill-to-spill point and proposed CO_2-formation water contact (Fig. 6D) at −1323 ms TWT depth. The culmination of the closure is situated at −1259 ms TWT (Fig. 2A). The spill point envisaged for Alpha to spill over to Beta is shown in Fig. 6D. At a shallower depth (100–150 ms TWT shallower than Alpha), the Beta structure (Fig. 6D) is also defined as a three-way closure where the Sognefjord Formation dips to the west, east and south but abuts the ØFC north and outside of the GN1101 seismic survey (Fig. 1B) where the complex undergoes a sharp change from a north-south to a northwest-southeast strike. The Beta structure comprises an areal extent of approximately 105.5 km^2 at the fill-to-spill point and proposed CO_2-formation water contact at −1175 ms TWT depth (Fig. 6D. The culmination of the closure is situated at −930 ms TWT (Fig. 2). In map view, the Beta closure (Fig. 6D) is characterised by a gentle sinusoidal geometry that is overall elongated NNW-SSE parallel to the ØFC. Deeper formations, e.g., the Jurassic Johansen and Cook formations (Bergmo et al., 2011; Bretan et al., 2011), and the Triassic Lunde Formation (Reinholdtsen et al., 2011) have also been proposed as potential CO_2 storage units. While the Johansen Formation may have a similar but smaller closure geometry as the Sognefjord Formation in the Alpha closure, the formation is not present in Beta (Sundal et al., 2016). The Triassic succession shows no significant Alpha closure, whereas the Beta expression of the closure is narrower than at the Sognefjord Formation level. Moreover, fracture zones and weathering profiles in the crystalline basement rocks (e.g., Riber et al., 2015, 2016) may also present potential CO_2 storage opportunity but are beyond the scope of this study.

4.6. Overburden

A time-thickness map (Fig. 13), in addition to horizon-fault intersections (Fig. 10A) show the primary caprock envisaged for

Smeaheia, the Draupne Formation, thins northwards along the VFZ and above the Alpha closure. Immediately adjacent to the VFZ, within the resolution of the data, the caprock may be completely absent to the north. In these thinned areas, the upper boundary of the formation truncates intra-formational reflectors. A slight thickening of the caprock is observed towards the centre of the study area between the Alpha and Beta prospects whilst the northern part of the Beta prospect again shows caprock thinning, but not as severe as for Alpha.

A population of low displacement faults is recognised (Figs. 5 and 14) intersecting, and generally confined to the sedimentary overburden (the Cretaceous Cromer Knoll Group and above) in the Smeaheia fault block. The faults exhibit somewhat chaotic orientations. A northwest-southeast direction dominates (Fig. 14), however this may be an artefact of uni-directional (inlines only) interpretation. Trace lengths are typically less than 1 km, while displacement is on the border of seismic resolution. Bifurcation up-section from within the Cromer Knoll Group is observed and fault populations are at a maximum within the Rogaland Group. These faults also intersect the Eocene to lower Miocene Hordaland Group to the west of the study area where these units are present (i.e., Wrona et al., 2017). Occasionally these low displacement faults intersect or branch from deeper tectonic faults and displace sediments all the way up to the base of the Quaternary interval.

The thin nature of the caprock on the north-western margin of the Alpha closure adjacent to the VFZ and in the northern part of the Beta closure is interpreted as the product of the Northern North Sea Unconformity Complex (Fyfe et al., 1981; Rawson and Riley, 1982; Kyrkjebø et al., 2004), i.e., the base Cretaceous unconformity (BCU) that divides syn-and post-rift in the North Sea. Results herein (Fig. 9) indicate vertical movements on the VFZ during deposition of the Draupne Formation (Late Jurassic to Early Cretaceous). The thinning of the caprock is interpreted as erosion due to footwall rebound (e.g., Wernicke and Axen, 1988). Given the diminished thickness of the Draupne Formation, the immediate overburden, i.e., the Cromer Knoll Group must act as a secondary caprock. Fair seal potential of the Cromer Knoll Group is a possibility given the argillaceous, fine-grained composition of the group, and its apparent capacity to seal the neighbouring Troll field in some locations (Bolle, 1992; Bretan et al., 2011; Osmond et al., 2020b, 2020c).

The population of low displacement, somewhat chaotically orientated faults are similar to polygonal faults described in many other mud dominated Cenozoic successions in the North Sea (e.g., Henriet et al., 1991; Stewart, 1996; Cartwright, 2004; Cartwright and Lonergan, 1996; Lonergan et al., 1998). Several mechanisms have been suggested for the formation of polygonal faults, e.g., basement reactivation, thermal subsidence, gravitational instability, overpressure build-up and volumetric contraction during compaction. Previous studies on these faults from the Horda Platform (Clausen et al., 1999; Wrona et al., 2017) used fault throw measurements to determine that these faults developed during the Eocene to early Oligocene, with possible reactivation during the late Oligocene to mid-Miocene.

While several of the aforementioned mechanisms proposed for polygonal faults are non-tectonic, the northwest-southeast organization, if a robust observation, suggests ambient stress fields acting on the area. Moreover, the occasional connectivity with deeper seated tectonic faults suggests minor Cenozoic reactivation of older faults played a role.

5. Discussion

The GN1101 seismic survey provides high resolution imagery of the Smeaheia fault block which is one of several rotated fault blocks that

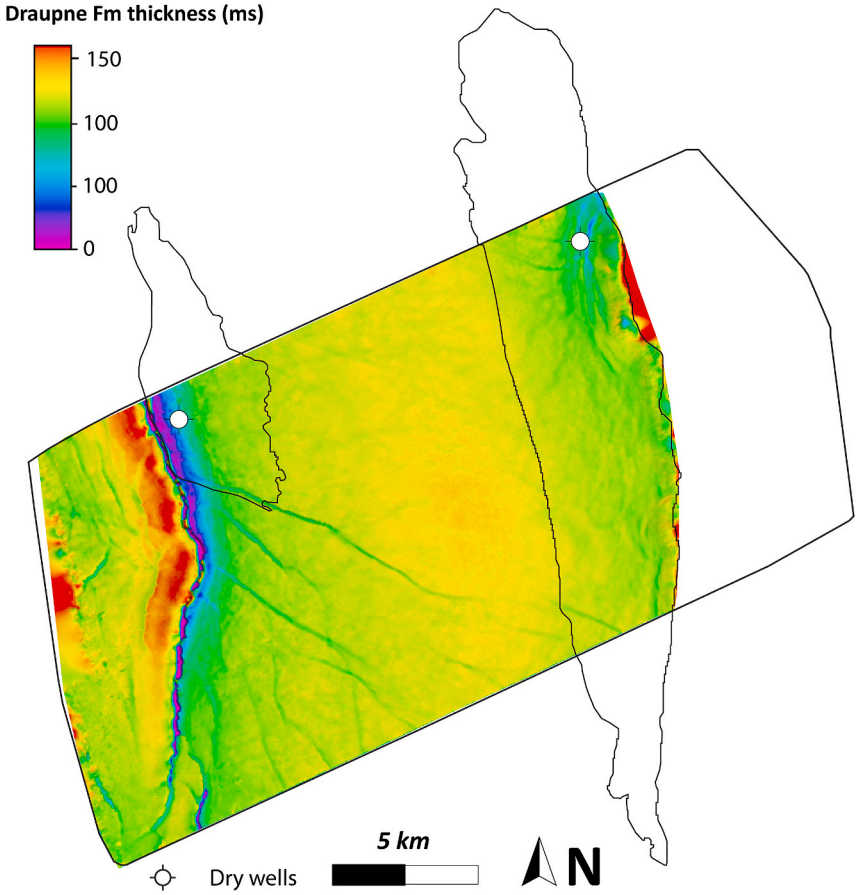

Fig. 13. Time-thickness variation map of the Draupne Formation from the GN1101 3D seismic survey. Note the formation is drastically thinner in the immediate footwall of the Vette Fault Zone. Outline of the Alpha and Beta prospect's CO_2-water contacts in fill-to-spill scenarios also shown in black.

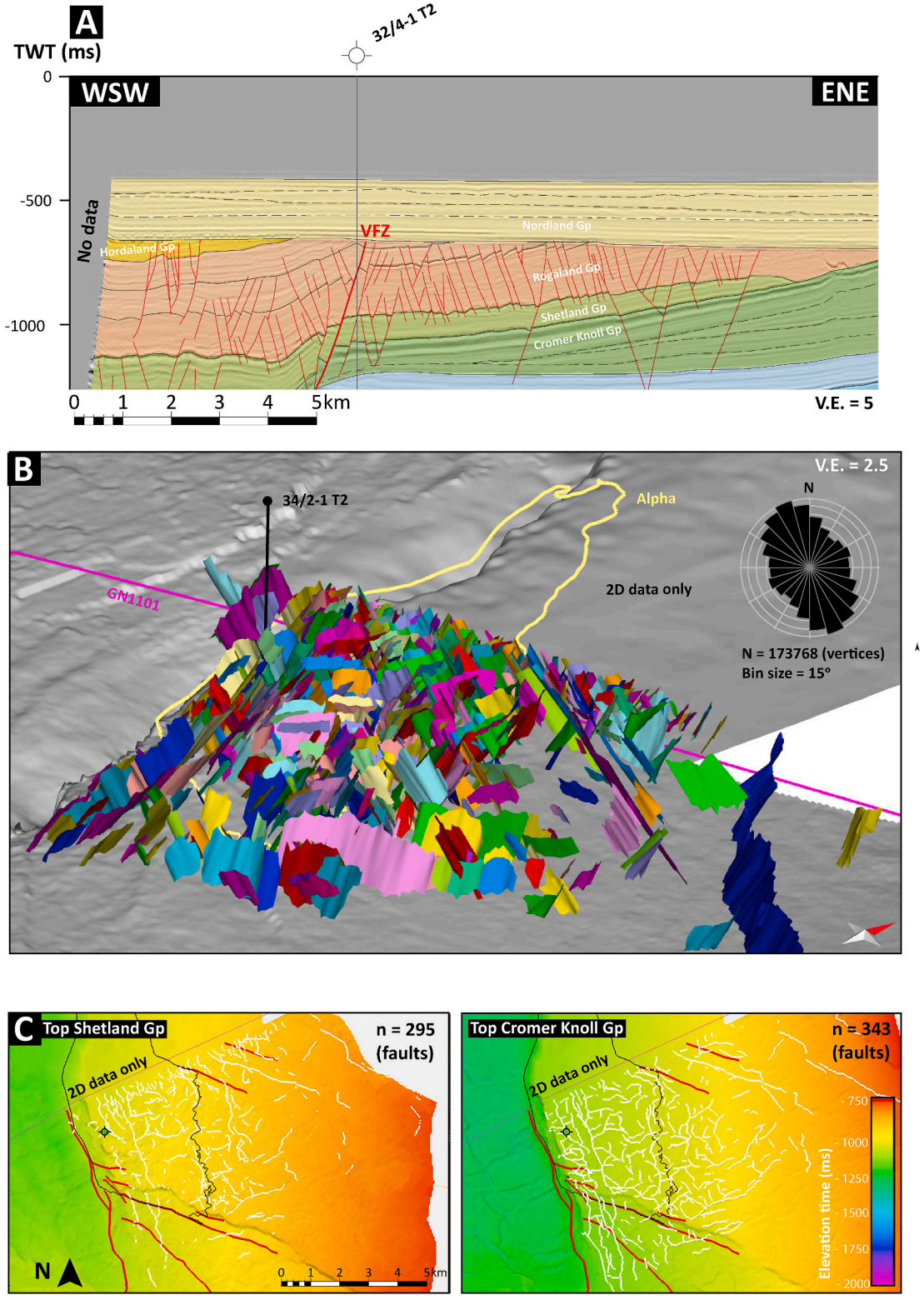

Fig. 14. A) Expanded view of section 1 shown in Fig. 2A highlighting overburden-confined, low displacement, closely spaced faulting (polygonal faults). A small number of faults affecting the overburden can be seen continuing down-section and intersecting the potential CO_2 reservoir (Jurassic Sognefjord Formation). B) Oblique 3D perspective view of polygonal faults affecting the Smeaheia overburden. Fault colours are arbitrary. The top of the Draupne Formation underlying the low displacement faults is shown in grey. The purple line represents the northern extent of the GN1101 survey, while the yellow line delineates the Alpha prospect's potential CO_2-water contacts in a fill-to-spill scenario. Vertical exaggeration (V.E.) is denoted in (A) and (B). C) Structure maps (ms TWT) showing fault-horizon intersection trace lines (white) for the top of the Shetland and Cromer Knoll groups. Tectonic faults that extend down-section into the Sognefjord Formation are shown in red, while the Alpha prospect is outlined in black. Fault interpretations are restricted to within the area of the Alpha closure only. (For interpretation of the references to colour in this figure legend, the reader is referred to the Web version of this article.)

comprise the northern Horda Platform, and more regionally, the eastern margin of the North Sea rift system (the ØFC, and the ØFC footwall horsts/grabens mark the eastern extent of the first and second rift phases, respectively). This localised study provides insight for the timing of rifting on the Horda Platform, especially during Rift Phase 2 (Jurassic-Cretaceous rifting) which previous workers have described as diachronous with strain localisation in the Viking Graben area, but eastwards migration of activity over a 30 My period (e.g., Bell et al., 2014). As such this section starts with a detailed discussion on the timing of first- and second-order fault activity in the Smeaheia fault block which contributes to regional understanding of how and when the Horda Platform developed. Secondly, fault orientations and interactions between first- and second-order faults provide insight into the directionality of stresses during the second phase of rifting in the Horda Platform. Finally, given that the Alpha and Beta closures are two fault-bound CO_2 prospects, the structural analysis herein serves to reduce important geological uncertainties including cross-fault juxtaposition of both the closure bounding faults and second-order faults that intersect the storage formation, caprock continuity, and connectivity between deep tectonic and shallow polygonal faults. The implications of these findings on CO_2 storage within the Smeaheia fault block are discussed below.

5.1. Fault evolution and timing

Synthesis of the T-d, T-z and E.I. diagrams (Fig. 9), in addition to recognition of growth wedges (Fig. 2) provide compelling evidence for fault timing and syn-kinematic sedimentation which have been summarised in Fig. 15. Comparison of fault timing derived herein with previous work (e.g., Bell et al., 2014; Whipp et al., 2014; Duffy et al., 2015) highlights the diachronous nature of the second phase of rifting in the northern North Sea.

Starting with the oldest imaged structures, considerable displacement of the basement-cover contact across Vette 01 and below (Fig. 9C), is consistent with upward propagation of basement lineaments, (e.g., Walsh et al., 2003). Moreover, mapping of the Vette 01 fault segment at depth (Fig. 4) reveals it is hard-linked with two separate basement structures (dual-rooted).

Displacement values within the Permo-Triassic and the Jurassic successions of the VFZ, are sizeable (up to 1000 ms TWT; approx. 1400), and are consistent with two rift events. E.I. plots (Fig. 9) confirm syn-kinematic sedimentation during both the Permo-Triassic and Upper Jurassic–Cretaceous packages. It should be noted, however, that erosion of the Draupne Formation in the hanging wall of Vette 01 may exaggerate Upper Jurassic values. Modest expansion of the Shetland Group indicates that the VFZ continued to accrue displacement later in this area (Late Cretaceous) than further west which corroborates previous work by Bell et al. (2014) and Phillips et al. (2019).

T-z and E.I. diagrams provide robust evidence of the timing of formation and breach of the VFZ relay zone. The faults that are involved in the relay, i.e., the southern-most part of Vette 01 and northern-most part of Vette 02 (Fig. 8) record displacement (Fig. 9A and B), but no expansion of the Permo-Triassic. Expansion of this interval in the hanging wall of Vette 01 (Fig. 9A) is only seen further north on the segment. Further, the displacement spike within the Jurassic, and the expansion of the Upper Jurassic to Lower Cretaceous packages indicate a single phase of rifting (Fig. 9). Vette 01 and 02 are therefore envisaged to have existed as separate non-linked faults during the Permo-Triassic rift phase, only becoming hard-linked during the later Jurassic–Cretaceous rift phase.

Up-section, the recognition of expansion of the Rogaland Group in the hanging wall of Vette 01 (Figs. 2 and 9) is novel and indicates a late phase of reactivation in the Palaeocene. Similar hanging wall expansions of the Svartalv and Troll fault systems (and associated second-order faults) to the west have been advocated by Whipp et al. (2014) which suggests this reactivation, while not recording high displacement, was distributed across at least a 50 km zone in the northern Horda Platform (Fig. 1B).

On the opposite side of the fault block, poor stratigraphic control across the ØFZ owing to Cenozoic uplift and erosion makes T-z and E.I. analyses impractical. Wedge geometries, however, are consistent with activity during the Permo-Triassic (Rift Phase 1), and in the Early Cretaceous (Rift Phase 2). No evidence of movement during deposition of the Jurassic has been observed, however, which is the main phase of fault activity further west in the northern North Sea (e.g., Badley et al., 1988; Underhill and Partington, 1993; Roberts et al., 1995; Coward et al., 2003; Cowie et al., 2005). This again corroborates the diachronous nature of Rift Phase 2 (e.g., Coward et al., 2003; Cowie et al., 2005; Bell et al., 2014). Missing stratigraphy due to uplift and erosion between the Lower Cretaceous and the Quaternary successions hinder interpretation of the ØFC's late-most activity history, and as such we cannot determine if the fault moved during the aforementioned Palaeocene reactivation.

Within the fault block, second-order faults (e.g., FW 01 N; Fig. 9C) show isolated Late Jurassic and Late Cretaceous pulses of activity which again reflects the late timing of this rift event on the eastern margin of the Horda Platform. These faults are thin skinned and did not exist during Rift Phase I. The aforementioned late pulse of reactivation during the Palaeocene–Early Eocene documented on Vette 01 is also seen on some intra-block second order faults (e.g. FW 01 N). This is a novel observation for the Smeaheia fault block.

Our analysis suggests cessation of faults that bound (first-order) and lie within (second-order) the Smeaheia fault block occurred sometime before deposition of the preserved portion of the Quaternary succession. This time for the end of major fault activity in the area is corroborated by previous studies (e.g., Bell et al., 2014) and as such seems to be generally true for the entire northern Horda Platform. Farther north, however, Bell et al. (2014) have suggested displacement continued to accrue locally on a northern segment of the ØFC until the Holocene. Moreover, present seismicity has been recorded in the Øygarden area (e.g., Olesen et al., 2013). The late-most extension on the northern Horda Platform has been credited to flexural bending associated with post-rift thermal subsidence focused in the North Viking Graben (Badley et al., 1984), and far-field stresses associated with rifting and final breakup in the North Atlantic (Bell et al., 2014; Phillips et al., 2019).

In summary, rift ages determined herein are generally consistent with previous works (e.g., Faerseth et al., 1995; Færseth, 1996; Ter Voorde et al., 2000; Davies et al., 2001; Coward et al., 2003; Cowie et al., 2005; Bell et al., 2014; Duffy et al., 2015). The Permo-Triassic rift event is recorded on the main northern segment of the VFZ (Vette 01) and on the ØFC, but without precise timing owing to diminishing seismic resolution and well control with depth. The results in Fig. 9, however, provide novel information regarding the timing of the later rift event, usually ascribed to the Late Jurassic to Early Cretaceous (e.g., Badley et al., 1988; Underhill and Partington, 1993; Duffy et al., 2015 and references therein). We determine the VFZ, while reactivated in the Late Jurassic, accrued the largest displacement during the Early Cretaceous (Ryazanian to Albian/Early Cenomanian), but remained active (in parts) throughout the Late Cretaceous and into the Palaeocene—Eocene. Further, there is a complete lack of evidence for any movement during the second phase of rifting on the ØFC before deposition of the Lower Cretaceous. Intra-block, second-order faults show isolated Late Jurassic and Late Cretaceous pulses of activity and again show evidence of reactivation in the Palaeocene—Eocene. These observations corroborate the diachronous migration of strain during Rift Phase 2, and suggest this phase of rifting lasted far longer than 30 Myr as previously suggested (e.g., Færseth, 1996; Bell et al., 2014; Whipp et al., 2014; Deng et al., 2017).

5.2. Stress orientation during rift phase 2

No consensus on the direction of extension during the second phase of rifting in the northern North Sea prevails. Several orientations have been postulated including east-west, northwest-southeast, and

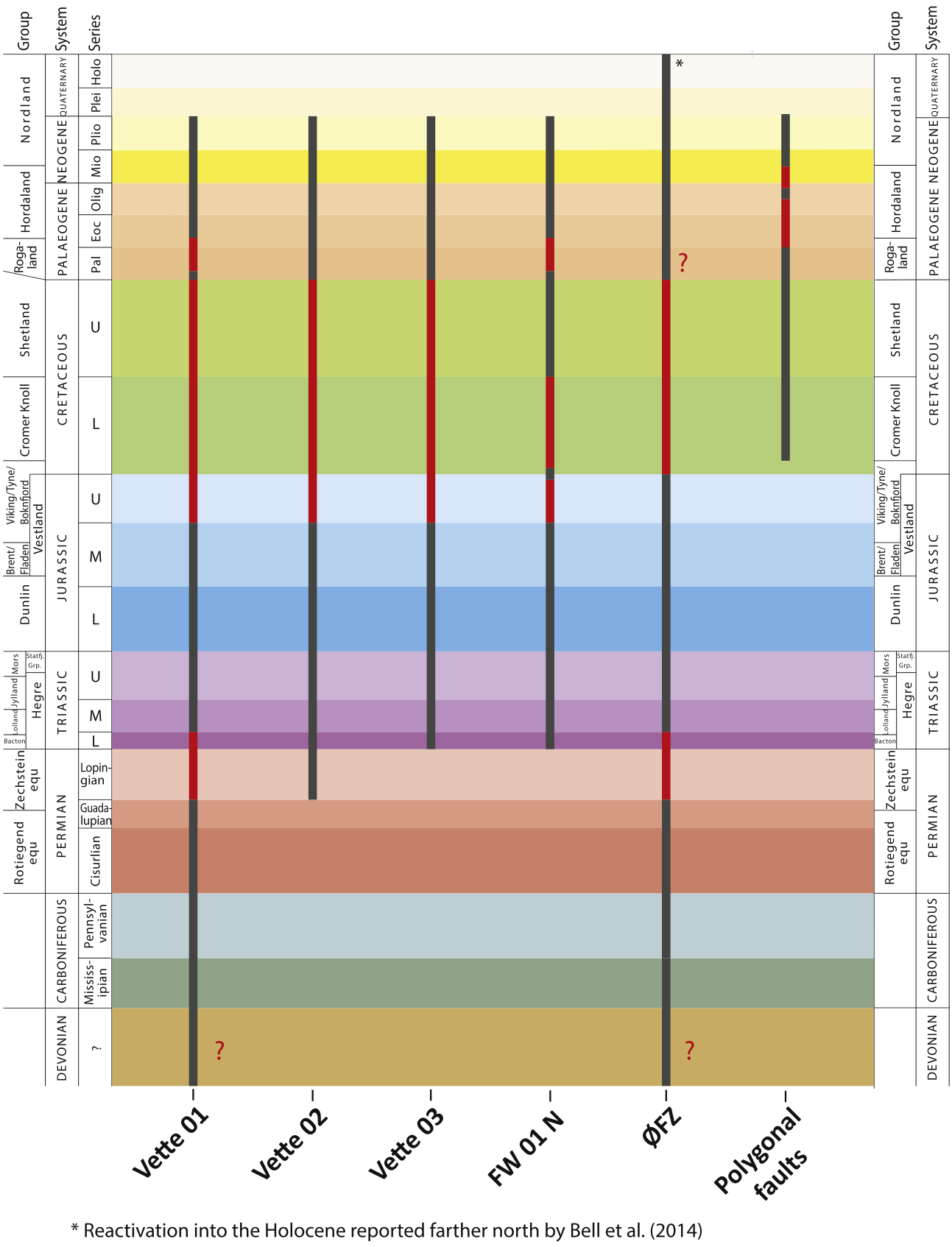

Fig. 15. Fault activity diagram showing stratigraphic successions intersected by the tectonic and non-tectonic faults within the GN1101 seismic survey. FW 01 N is representative of the population of northwest-southeast second-order faults, although some tip-out at shallower depths than depicted here. Grey bars indicate successions are simply displaced, whereas red bars indicate fault activity discerned from growth geometries, T-z and E.I. analyses herein. Polygonal fault ages are derived from Clausen et al. (1999) and Wrona et al. (2017). (For interpretation of the references to colour in this figure legend, the reader is referred to the Web version of this article.)

northeast-southwest (Badley et al., 1988; Roberts et al., 1990, 1993; Ziegler, 1990; Stewart et al., 1992; Bartholomew et al., 1993; Brun and Tron, 1993 Færseth, 1996; Doré et al., 1997; Faerseth and Ravnås, 1998; Duffy et al., 2015). Given the evidence for limited or very late reactivation of the VFZ (Phillips et al., 2019; Zhong and Escalona, 2020 and herein), we consider east-west extensional stresses to be very unlikely. Our study area, however, may not be representative of the larger Horda Platform. Northwest-southeast fault orientations of the second rift phase described herein (and by Phillips et al., 2019) are similar to that described by Deng et al. (2017) who credit a northeast-southwest extensional stress direction for creation of these subsidiary faults. This orientation suggests clockwise rotation of stresses from the Permo-Triassic rift event. Fault orientation does not, however, ubiquitously represent the direction of causal stresses. Phillips et al. (2019) argue that the northwest-southeast orientation of faulting is instead a result of local stress perturbations surrounding larger N–S striking faults as documented by Duffy et al. (2015), Reeve et al. (2015) and Whipp et al. (2014). We have documented that these northwest-southeast striking faults form a triangular region of defuse strain (branching towards the south) that coincides with decoupling between a deep-rooted basement fault and the VFZ towards the south of the study area. This region of diffuse strain likely accommodated differential movement on two adjacent basement structures (Fig. 4). As such, the orientation of these Late Jurassic–Early Cretaceous faults is likely influenced by local stress perturbations and cannot be used to accurately discern the orientation of horizontal stresses during rifting.

The observations herein that polygonal faults which intersect the sedimentary overburden (the Cretaceous Cromer Knoll Group and above) show a degree of northwest-southeast organisation, and that in some cases they are hard-linked with deeper tectonic faults, suggests

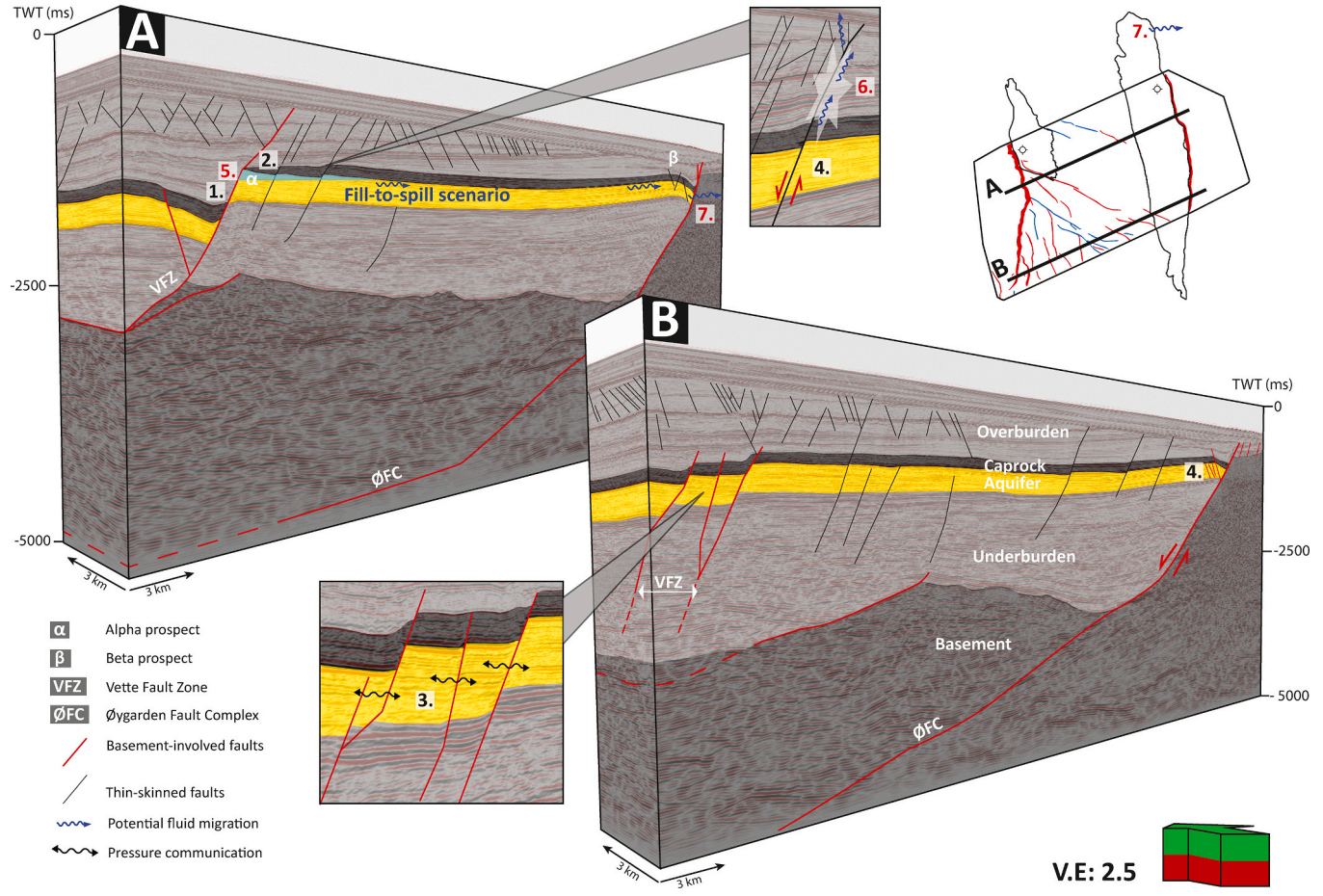

Fig. 16. Perspective view of two composite seismic lines intersecting the (A) north and the (B) south of the GN1101 seismic survey. Key geological controls informed by this study on injection of CO_2 into Jurassic Viking Group sandstones (yellow) are schematised and numbered 1–4 (black). 1) The perspective storage aquifer in the Alpha prospect is primarily juxtaposed against the Cretaceous overburden across the VFZ. 2) The Draupne Formation, i.e., the primary caprock is thin overlying the alpha prospect. The overburden, however will likely contribute as a secondary caprock, as it does in the neighbouring Troll East field. 3) Juxtaposition of the perspective storage aquifer across a relay zone in the VFZ provides a possible pressure communication pathway between the Smeaheia area and the Troll fields to the east. 4) Intra-block, second-order faults show predominant cross-fault juxtaposition of the primary storage formation. While these faults may present some baffling capacity to fluid flow on injection timescales, they are not expected to act as sealing faults. As such, the target formation is not considered compartmentalised. Further, observations herein inform additional uncertainties which require future maturation in order to reduce subsurface risk associated with CO_2 injection into the Smeaheia fault block. These observations are schematised and numbered 5–7 (red).5) While provisional cross-fault juxtaposition of Vette 01 provides qualitative analysis of fault seal, in-depth quantitative analysis of both fault seal and caprock integrity are required in order to fully de-risk the Alpha closure. The neighbouring Troll East field may provide a good analogue for fault and top seal calibration. 6) Several intra-block, second-order faults intersect both the proposed storage formation, caprock and overburden. Further, intra-formational polygonal faults in the overburden tend to abut against first- and second-order tectonic faults. This connectively has been recognised as a possible seal bypass system. Fault reactivation potential must be determined to understand how these faults will respond to injection-related pressure increases. As pressure depletion is feasible within the Smeaheia fault block, this should inform future modelling. 7) North of the GN1101 3D survey, 2D seismic lines (e.g., Appendix 3) reveal juxtaposition of the perspective storage aquifer against heterogeneous, fractured and weathered basement across the ØFC. This observation implies significant uncertainty in relation to storage formation integrity. (For interpretation of the references to colour in this figure legend, the reader is referred to the Web version of this article.)

they reflect the ambient stress field orientation during their formation (e.g., Maher et al., 2020). The northwest-southeast organisation documented herein, supports a maximum horizontal stress vector orientated northeast-southwest during the Eocene–middle Miocene. Clausen et al. (1999) concluded with the same orientation and postulated that the stresses on the Horda Platform were a consequence of several far field causal mechanisms, including ridge-push, doming of Fennoscandia and differential subsidence of the North Sea.

5.3. Integrity of CO_2 storage formations in the Smeaheia fault block

The structural analysis herein establishes the tectonic framework of the Smeaheia fault block. As such this work provides new information that effectively reduces geological uncertainty associated with injection and storage of CO_2 within the fault block while highlighting persistent geological uncertainties which merit further study. Key geological controls on CO_2 storage informed by this study are highlighted below and summarised schematically in Fig. 16.

5.3.1. New insights into CO_2 injection and storage

In order for successful CO_2 containment, the reservoir unit in the Alpha closure must be sealed against the VFZ by a juxtaposition or capillary (membrane) seal (e.g., Yielding et al., 1997, 1998). Juxtaposition analysis herein provides provisional qualitative assessment of fault seal. The potential CO_2-formation water contact at approximately −1320 ms TWT for a fill-to-spill Alpha closure scenario (Fig. 10) coincides with juxtaposition of the footwall storage formation with the hanging wall Cretaceous overburden (Cromer Knoll Group; Osmond et al., 2020b). The lithological composition of the Cromer Knoll Group, i.e., fine-grained, argillaceous, marine sediments with a varying content of calcareous material, at first approximation provides high potential for a suitable juxtaposition seal (after Færseth et al., 2007's qualitative juxtaposition method). Moreover, a preliminary model (Mulrooney et al., 2018a) utilising the Shale Gouge Ratio (SGR) method (Yielding et al., 1997) shows that for optimistic shale volume estimates for the Cromer Knoll Group (Vsh = 1), the VFZ is sealing. Considering this scenario, the observation herein that the Draupne Formation is very thin above the Alpha closure (Fig. 13) is also not problematic as the Cromer Knoll Group can contribute as a secondary caprock, as it does in the neighbouring Troll East field.

The cross-fault juxtaposition of the southern portion of Vette 01, and the additional faults that comprise the VFZ (Figs. 8 and 11) is not important for lateral seal of the Alpha closure (e.g., Fig. 5). These faults lie further south than the envisaged CO_2-formation water contact. The cross-fault juxtaposition of the VFZ relay does, however, inform pressure communication scenarios between the Smeaheia and Troll field fault blocks (e.g., Tusse fault block). Fault analysis herein reveals the Vette 01 (southern part), Vette 02 and Vette 03 segments have a large area of cross-fault self-juxtaposition of the storage formation (Figs. 8, 10C and 11C). This considerable self-juxtaposition likely presents pressure communication pathways along Viking Group sandstone-on-sandstone contacts. Limited pressure information is available from exploration wells, 32/4-1 T2 (Alpha) and 32/2–1 (Beta) which were drilled in 1996 and 2008, respectively. At time of testing, pressures in these wells were approximately hydrostatic. It can be expected, however, that the reservoir pressure in Smeaheia is sub-normal due to continued Troll field draw down since 1995. A regional investigation (Lauritsen et al., 2018) identified 6 such potential communication pathways related to relay ramp structures. Lauritsen et al. (2018) also identified the southernmost tip of the VFZ as a potential pressure communication pathway where the primary storage unit lacks any major structural barriers. While reservoir depletion can mitigate against injection-related fault reactivation (Mulrooney et al., 2018a, 2020), CO_2 storage volume can be negatively impacted (Statoil, 2016). With this in mind, work continues to address potential intra-fault block pressure communication (e.g., Riis, 2018; Lothe et al., 2019; Orsini et al., 2020).

Intra-block, second-order faults predominantly show cross-fault juxtaposition of the primary storage formation (Fig. 12). As such, the target formation is not considered compartmentalised, at least on a geological timescale. They may, however provide baffles to CO_2 flow during the course of injection. If baffling, these faults could influence target formation pressure which can in turn influence injection operations, e.g., the Snøhvit CO2 sequestration project (Chiaramonte et al., 2015). Given that the entire Alpha closure is not covered by the GN1101 seismic survey, expanding this study further north will be required to identify the areal extent of the storage formation intersected by these faults.

5.3.2. Informing future de-risking strategies

The cross-fault juxtaposition analysis herein provides a first approximation that the Vette 01 will act as a sealing fault for injected CO_2 into the Alpha closure. In order to fully de-risk the Alpha closure, however, an in-depth quantitative analysis of both fault seal and caprock integrity will be required, and can build on fault and horizon geometries presented herein. The neighbouring Tusse Fault Zone, which supports a ~250 m hydrocarbon column in the Troll East field (Spencer and Larsen, 1990; Bolle, 1992), provides a good analogue to the VFZ (Osmond et al., 2020c). In this case, the Tusse Fault Zone possesses a nearly-identical structural history and very similar cross-fault lithological juxtaposition relationships, in addition to an equally thinned Draupne Formation. Given the lack of information from the Smeaheia fault block, an in-depth fault and top seal analogy study of the Tusse Fault Zone is merited as the relationship between cross-fault pressure and lithological well data from Troll can be extrapolated to the VFZ (Osmond et al., 2020a,b,c). Challenges persist, however, given that the Cretaceous interval is rather carbonate-rich (Osmond et al., 2020b), which is problematic when relying on siliciclastic-based membrane seal algorithms (such as SGR) for fault seal prediction.

Fault mapping herein has identified several tectonic faults that intersect the reservoir, cut up-section through the caprock, and tip out within the overburden (Fig. 7). Moreover, some polygonal faults that intersect the overburden are hard-linked with deeper first- and second-order tectonic faults. Utilising the high resolution geomodel herein, future work should assess the reactivation potential of these faults with regard to injection related pressure or from naturally occurring earthquakes which is important to rule out a potential seal bypass system (e.g., Cartwright et al., 2007; Ogata et al., 2014). Moreover, this analysis should consider initially sub-hydrostatic storage formation pressures given that potential pressure communication pathways across the VFZ relay zone have been identified.

Polygonal faults (Fig. 5 D) mapped herein underlie pockmarks (grey circular impressions in Fig. 5A and B) that represent palaeo-fluid seepage on the seabed and within Quaternary sediments (Leon, 2019; Osmond et al., 2020a). There is a potential that these polygonal faults and deeper tectonic faults have previously delivered fluids to the free surface. Ostanin et al. (2013) have identified a current analogue to this scenario where the Snøhvit and Albatross gas fields in the southwest Barents Sea show leakage of thermogenic fluids from large surface pockmarks which link at depth to regional and shallow faults. Provisional investigations by Osmond et al. (2020a), however, show no direct evidence of a similar "plumbing system" in the Smeaheia fault block, but suggest palaeo-fluids are sourced from further west, i.e., the Tusse fault block. Current models (Goldsmith, 2000) suggest the target formation in the Smeaheia fault block was never charged by hydrocarbons. Nonetheless, the faults that are through-going and intersect the reservoir unit require further detailed investigation in order to determine reactivation potential under evolving reservoir pressure regimes (e.g., Mulrooney et al., 2020).

The geomodel herein shows that the Beta structure is intersected by numerous closely spaced, low-displacement faults that again show predominate cross-fault juxtaposition of the storage formation. As in the Alpha closure, the target formation is not considered

compartmentalised, but determining the influence of these numerous faults on injection pressures will require high-resolution quantitative fault seal analysis or pressure testing during field development.

Regional 2D lines (e.g., Appendix 3) north of the GN1101 3D seismic survey show that the Beta closure is a three-way closure with considerable juxtaposition against basement rocks that comprises the footwall block of the ØFC. The sealing capacity of this juxtaposition relationship is unknown. Onshore investigations of the Caledonian basement in western Norway (e.g., Norton, 1986; Fossen, 1992; Faerseth et al., 1995; Færseth, 1996; Wennberg, 1996; Fossen and Hurich, 2005; Vetti and Fossen, 2012; Gabrielsen and Braathen, 2014; Fossen et al., 2017; Torabi et al., 2019) reveal basement rocks are heterogeneous, intensely weathered and contain numerous fracture and shear zones. Weathering profiles have been shown to exhibit significant porosity/permeability (e.g., Gyllenhammar, 2019) whereas fracture and shear zones could potentially act as conduits for CO_2 to escape into the presumed Jurassic sediments in the immediate footwall of the ØFC (Bjerkeli, 2019), into overlying Quaternary sediments, or to the seafloor. According to Goldsmith (2000), a regionally high, northwest-southeast, lateral in-situ compressive stress throughout the onshore and offshore areas of mid to northern Norway may help to keep the ØFZ sealed, but the fault is close to an area of significant tectonic activity (Bungum et al., 1991; Gabrielsen, 1989) and therefore has the added risk that periodic earthquakes could compromise any demonstrable seals. Detailed onshore analogue studies may narrow this knowledge gap, but quantitative fault seal analysis of the Øygarden Fault Complex is beyond the scope of this study.

6. Conclusions

Creation and analysis of a geomodel derived from the GN1101 3D seismic survey and a regional 2D grid has informed the structural style and evolution of the Smeaheia fault block in the Horda Platform.

- The Vette Fault Zone (VFZ) and Øygarden Fault Complex (ØFC) are north-south striking basement involved faults which were active during both the Permo-Triassic and the Late Jurassic–Early Cretaceous phases of rifting. These first-order fault zones delineate the Smeaheia fault block.
- For the latter rift-phase, most displacement accrued in the Early Cretaceous, later than recorded on fault blocks to the west.
- Fault activity continued into the Late Cretaceous on the VFZ and ØFC.
- A late pulse of reactivation of the VFZ and the second-order faults occurred during the Palaeocene to Eocene.
- Northwest-southeast striking intra-block, second-order faults developed during two main pulses of activity, in the Late Jurassic and the Early Cretaceous, with minor reactivation in the Palaeocene – Eocene.
- Second-order faults define a triangular region of defuse strain (branching towards the south) that coincides with differential movement on two adjacent basement faults.
- The VFZ is hard-linked with two different basement structures (i.e., dual-rooted).
- The roll-over geometries expressed in the hanging walls of both the VFZ and the ØFC (Fig. 2) are attributed to listric and ramp-flat-ramp geometries of the respective faults.
- Linkage of two segments of the VFZ took place during the Late Jurassic–Early Cretaceous.
- A population of low-displacement polygonal faults intersect the Cromer Knoll, Rogaland and Hordaland groups and developed during the Eocene to middle Miocene. They are primarily strata-bound but are occasionally hard-linked with both first- and second-order tectonic faults.

Injection and storage of CO_2 within the subsurface of the Smeaheia fault block has been proposed with Jurassic Viking Group sandstones and the Draupne Formation being targeted as the primary storage formation and caprock, respectively. This structural analysis serves to reduce important geological uncertainties associated with injection and storage.

- The nature of juxtaposition across the Vette 01 fault is favourable for CO_2 containment within the Alpha structure. The storage formation (Viking Group sandstones), which is also the primary reservoir unit for the Troll fields, is primarily juxtaposed against the Cromer Knoll Group.
- Viking Group sandstones are predominantly self-juxtaposed across the VFZ relay zone. This relationship can promote pressure communication between the Smeaheia and Tusse fault blocks.
- The storage formation is also primarily self-juxtaposed across intra-block, second-order faults. These faults may act as baffles, but are not expected to act as intra-closure sealing faults.
- The primary caprock, the Draupne Formation is significantly eroded (i.e., Northern North Sea Unconformity Complex), and possibly absent above the north of the Alpha closure along the footwall of the VFZ. Highly argillaceous Cretaceous lithologies belonging to the Cromer Knoll Group overly the Draupne Formation and could also serve as the caprock where the Draupne Formation has been eroded, as it does in Troll East.
- North of the GN1101 3D seismic survey, the Beta structure is juxtaposed against basement rocks across the ØFC. The sealing capacity of this juxtaposition relationship is unknown.

Declaration of competing interest

The authors declare that they have no known competing financialinterestsor personal relationships that could have appeared to influence the work reported in this paper.

Acknowledgments

This publication has been produced with support from the NCCS Centre, performed under the Norwegian research program Centres for Environment-friendly Energy Research (FME). The authors acknowledge the following partners for their contributions: Aker Solutions, Ansaldo Energia, CoorsTek Membrane Sciences, EMGS, Equinor, Gassco, Krohne, Larvik Shipping, Lundin, Norcem, Norwegian Oil and Gas, Quad Geometrics, Total, Vår Energi, and the Research Council of Norway (257579/E20).The workflows herein were conducted in collaboration with the Northern Lights project (Equinor, Total and Shell). We gratefully acknowledge Schlumberger for the provision of academic licenses for the Petrel E&P Software Platform and Petroleum Experts for the provision of academic licenses for the Move Software Suite. Gassnova SF provided access to the GN1101 3D seismic survey. The authors wish to thank reviewers Kamaldeen Omosanya and James Van Tuyl for critically reading the manuscript.

Appendix A. Supplementary data

Supplementary data to this article can be found online at https://doi.org/10.1016/j.marpetgeo.2020.104598.

Appendix 1Fault attributes. Abbreviations: CK Gp = Cromer Knoll Group, Lwr = Lower, PT = Permo-Triassic, R1 = Rift Phase 1, R2 = Rift Phase 2, Rog Gp = Rogaland Group, BQU = Base Quaternary unconformity. *Synthetic faults dip in accordance to the dip of the Vette Fault Zone and the Øygarden Fault Complex, i.e., towards the west or southwest. Antithetic faults dip towards the east or northeast

Fault	Max throw (ms TWT)	Trace lenght (m)	Entire trace lenght imaged?	Up-section extent	Down-section extent	*Anthithetic/ Syntethic	Strike	Dip	Activity
Vette_01	554	16200	No	BQU	Basement	S	South	West	R1/R2
Vette_01_S_tipsplay	52	800	No	Lwr CK Gp	Brent/Dunlin Gp	A	North	East	R2
Vette_02	186	3800	No	Lwr CK Gp	PT	S	South	West	R1/R2
Vette_03	31	3900	Yes	Lwr CK/ Draupne Fm	PT	S	South	West	R2
HW_01	58	3120	No	Rog Gp	PT	S	South	West	R2
FW_01_N	31	7000	Yes	BQU	PT	S	Southeast	Southwest	R2
FW_01_S	32	5900	Yes	BQU	PT	S	Southeast	Southwest	R2
FW_02_N	42	4130	Yes	Draupne Fm	PT	S	Southeast	Southwest	R2
FW_02_S	13	2275	Yes	Draupne Fm	PT	S	Southeast	Southwest	R2
FW_03	38	7000	Yes	BQU	Brent/Dunlin Gp	A	Northwest	Northeast	R2
FW_04	27	5800	Yes	Draupne Fm	PT	S	South	West	R2
FW_05	32	3650	Yes	Draupne Fm/ Rog Gp	PT	A	North	East	R2
FW_06_N	15	2300	Yes	Draupne Fm	PT	S	SSE	WSW	R2
FW_06_S	15	2250	No	Draupne Fm	PT	S	SSE	WSW	R2
FW_07	21	1760	Yes	Draupne Fm	Brent/Dunlin Gp	S	Southeast	Southwest	R2
FW_08	28	2145	No	Draupne Fm	PT	S	Southeast	Southwest	R2
FW_09	18	3100	No	BQU	PT	S	Southeast	Southwest	R2
FW_10	10	2900	No	BQU	PT	S	Southeast	Southwest	R2
FW_10_splay	5	2750	Yes	Draupne Fm	Viking Gp ssts	S	Southeast	Southwest	R2
FW_11	23	3300	Yes	Lwr CK Gp	PT	S	Southeast	Southwest	R2
FW_11_splay	3	1200	No	Lwr CK Gp	PT	A	Northwest	Northeast	R2
FW_12	6	2900	No	CK Gp	PT	A	Northwest	Northeast	R2
FW_13	3	4000	No	Lwr CK Gp	PT	A	Northwest	Northeast	R2
FW_14	15	1600	No	Draupne Fm	PT	S	SSE	WSW	R2
FW_15	1	5400	No	CK Gp	Brent/Dunlin Gp	A	Northwest	Northeast	R2
FW_15_splay1	8	3000	No	Lwr CK Gp	PT	A	Northwest	Northeast	R2
FW_15_splay2	12	1820	No	CK Gp	Brent/Dunlin Gp	S	Southeast	Southwest	R2
FW_17_N	13	1850	No	BQU	Draupne Fm	A	Northwest	Northeast	R2
FW_17_C	5	2800	Yes	BQU	Viking Gp ssts	A	Northwest	Northeast	R2
FW_17_S	20	4800	Yes	BQU	Viking Gp ssts	S	Southeast	Southwest	R2
FW_18	26	5430	No	Shetland Gp	Basement	S	SSE	WSW	R2
Vette_breach	45	1220	Yes	Lwr CK Gp	PT/Viking Gp sst	S	Southeast	Southwest	R2
Vette_01_splay	36	730	Yes	Draupne Fm	PT	S	Southwest	Northwest	R2
Øygarden	2150	15000	No	BQU	Basement	S	South	West	R1/R2

Appendix 2Uninterrupted WSW-ENE trending seismic transects through the GN1101 3D survey. Interpretations are shown in Figure 2. Locations are shown in Figure 1B

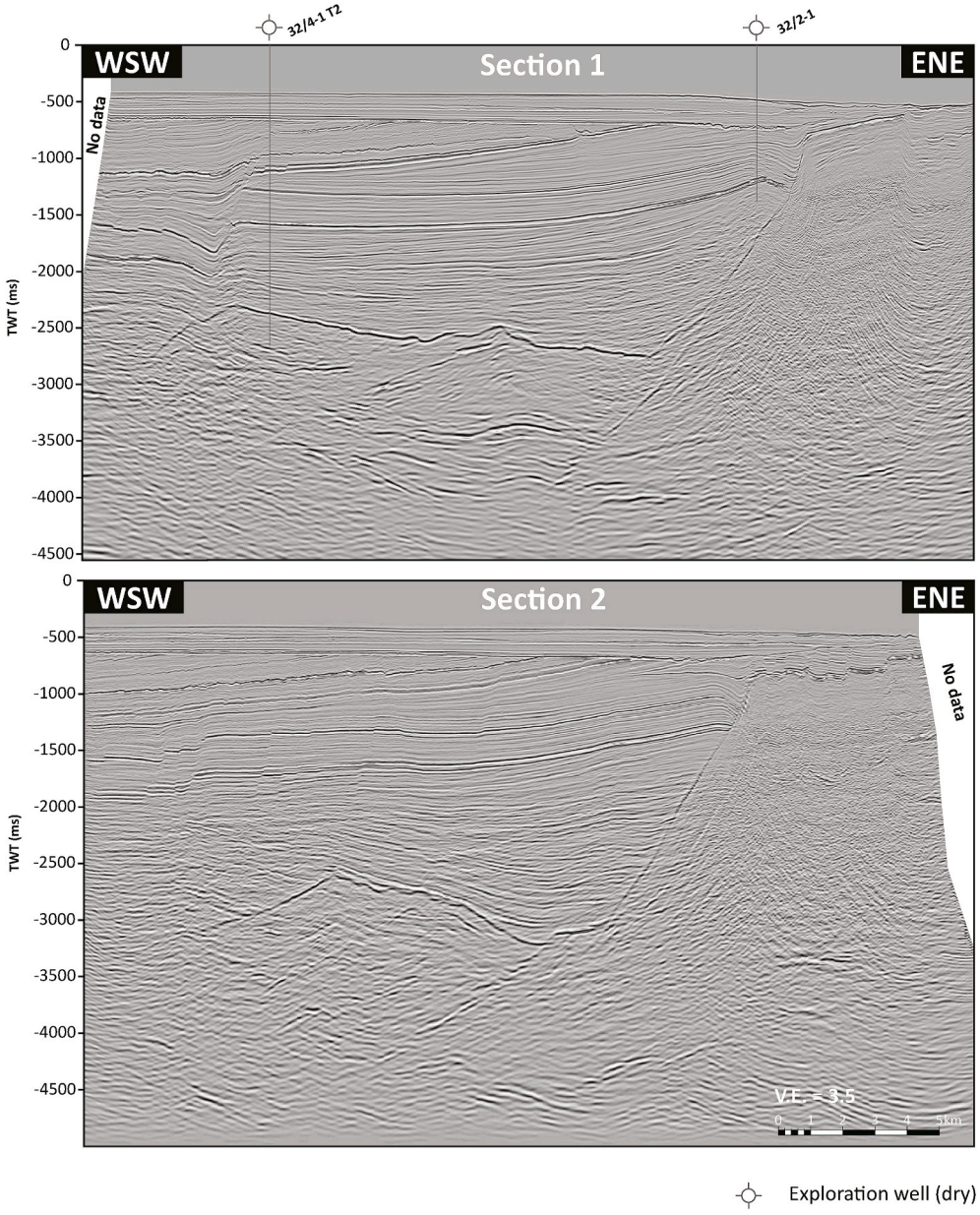

Appendix 3. Western part of 2D regional transect TE93-113 which transects the northern extremity of the Beta closure where the prospective storage formation is juxtaposed with basement rocks in the footwall of the ØFC. A) Interpreted, B) Uninterpreted. Location is shown in Figure 1B

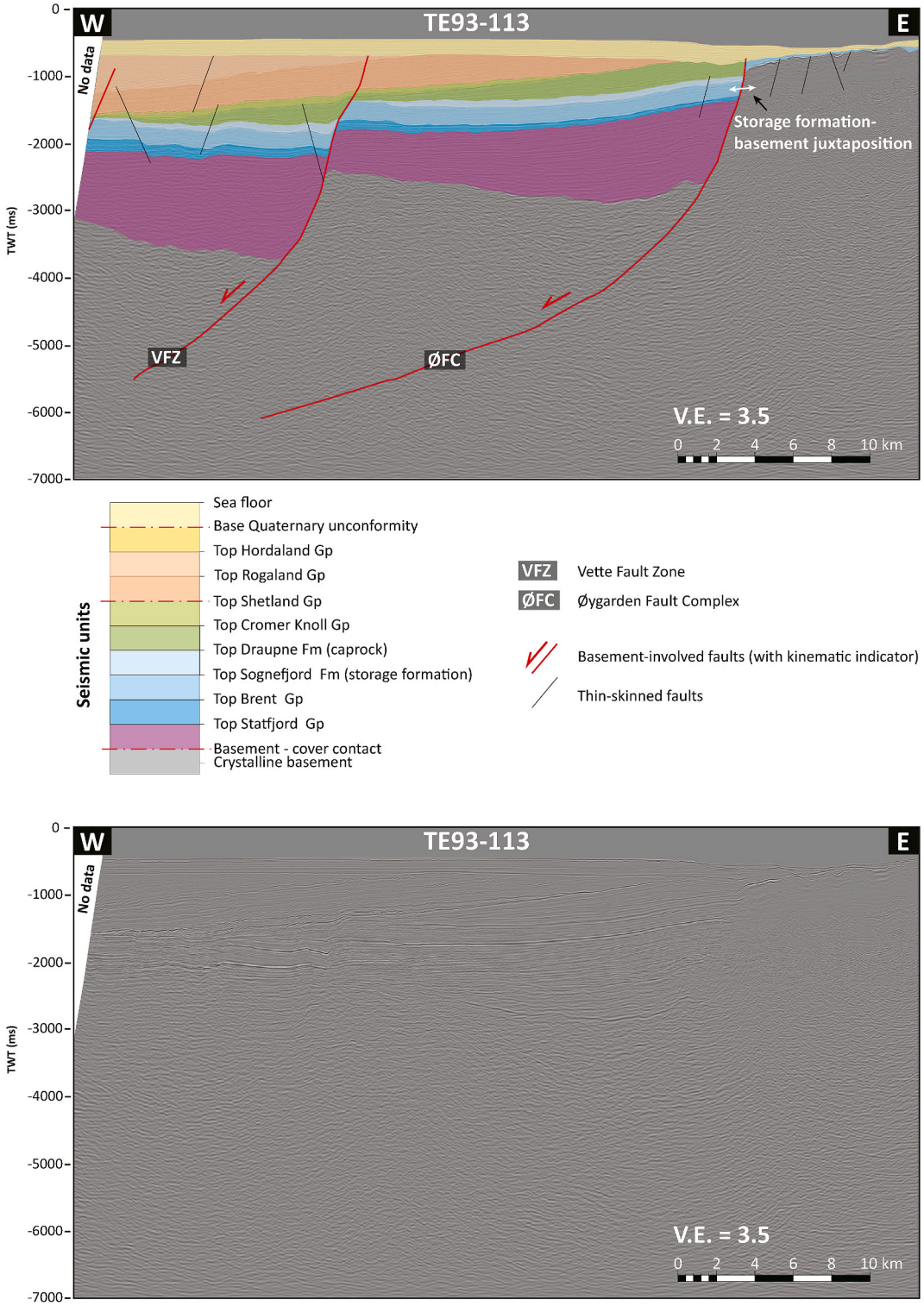

Appendix 4. Western part of 2D regional transect NNST84-05 which transects the GN1101 3D seismic survey and extends through the Tusse and Svartalv fault zones to the west. A) Interpreted, B) Uninterpreted. Location is shown in Figure 1B

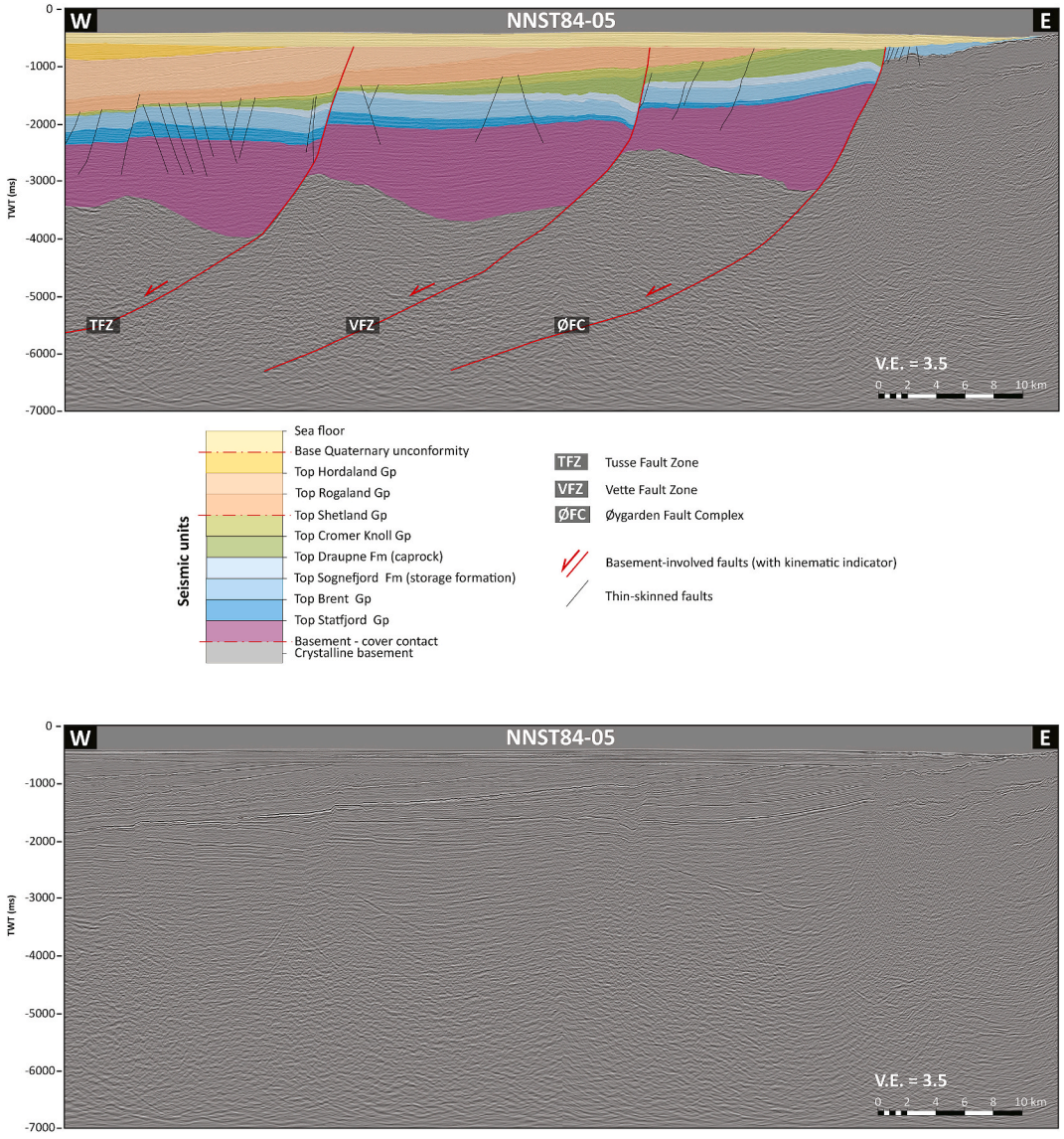

Appendix 5. . Western part of 2D regional transect GNSR-91 which transects the Horda Platform fault blocks to the south of the GN1101 3D seismic survey. A) Interpreted, B) Uninterpreted. Location is shown in Figure 1B.

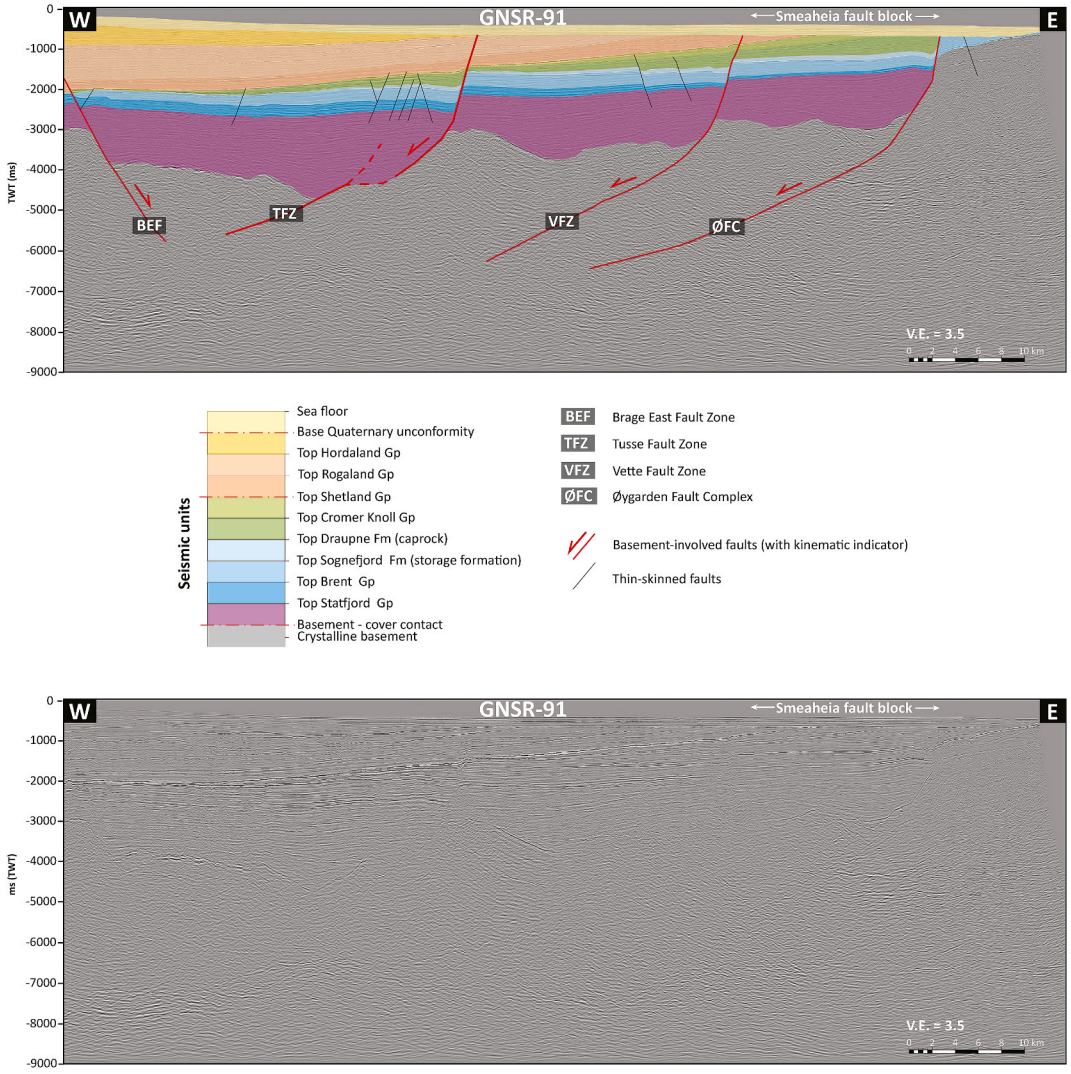

References

Allan, U.S., 1989. Model for hydrocarbon migration and entrapment within faulted structures. Am. Assoc. Pet. Geol. Bull. 73, 803–811.

Alves, T.M., 2012. Scale-relationships and geometry of normal faults reactivated during gravitational gliding of Albian rafts (Espírito Santo Basin, SE Brazil). Earth Planet. Sci. Lett. 331– 332, 80–96. https://doi.org/10.1016/j.epsl.2012.03.014.

Anell, I., Thybo, H., Rasmussen, E., 2012. A synthesis of Cenozoic sedimentation in the North Sea. Basin Res 24, 154–179. https://doi.org/10.1111/j.1365-2117.2011.00517.x.

Arts, R.J., Chadwick, A., Eiken, O., Thibeau, S., Nooner, S., 2008. Ten Years' Experience of Monitoring CO_2 Injection in the Utsira Sand at Sleipner, Offshore Norway. First Break 26.

Bachu, S., 2008. CO_2 storage in geological media: role, means, status and barriers to deployment. Prog. Energy Combust. Sci. 34, 254–273. https://doi.org/10.1016/j.pecs.2007.10.001.

Badley, M.E., Egeberg, T., Nipen, O., 1984. Development of rift basins illustrated by the structural evolution of the Oseberg feature, Block 30/6, offshore Norway. J. Geol. Soc. London. 141, 639–649. https://doi.org/10.1144/gsjgs.141.4.0639.

Badley, M.E., Price, J.D., Dahl, C.R., Agdestein, T., 1988. The structural evolution of the northern Viking Graben and its bearing upon extensional modes of basin formation. J. Geol. Soc. London. 145, 455–472. https://doi.org/10.1144/gsjgs.145.3.0455.

Bally, A.W., Bernoulli, D., Davis, G.A., Montadert, L., 1981. Listric normal faults: oceanologica acta. In: Proceedings of the 26th International Geological Congress. Geology of Continental Margins Colloque C3. Paris, July, pp. 87–101.

Bartholomew, I.D., Peters, J.M., Powell, C.M., 1993. Regional structural evolution of the North Sea: oblique slip and the reactivation of basement lineaments. In: Geological Society, London, Petroleum Geology Conference, pp. 1109–1122. https://doi.org/10.1144/0041109. Proceedings. Geological Society of London.

Baudon, C., Cartwright, J., 2008. The kinematics of reactivation of normal faults using high resolution throw mapping. J. Struct. Geol. 30, 1072–1084. https://doi.org/10.1016/j.jsg.2008.04.008.

Bell, R.E., Jackson, C.A.L., Whipp, P.S., Clements, B., 2014. Strain migration during multiphase extension: observations from the northern North Sea. Tectonics 33, 1936–1963. https://doi.org/10.1002/2014TC003551.

Benson, S.M., Cole, D.R., 2008. CO 2 sequestration in deep sedimentary formations. Elements 4, 325–331. https://doi.org/10.2113/gselements.4.5.325.

Bergmo, P.E.S., Grimstad, A.A., Lindeberg, E., 2011. Simultaneous CO_2 injection and water production to optimise aquifer storage capacity. Int. J. Greenh. Gas Control 5, 555–564. https://doi.org/10.1016/j.ijggc.2010.09.002.

Bertram, G.T., Milton, N.J., 1988. Reconstructing basin evolution from sedimentary thickness; the importance of palaeobathymetric control, with reference to the North Sea. Basin Res. 1, 247–257. https://doi.org/10.1111/j.1365-2117.1988.tb00020.x.

Bischke, R.E., 1994. Interpreting sedimentary growth structures from well log and seismic data (with examples). Am. Assoc. Petrol. Geol. Bull. 78, 873–892. https://doi.org/10.1306/a25fe3d3-171b-11d7-8645000102c1865d.

Bjerkeli, A., 2019. Tectonostratigraphy and Fault Analysis of the Øygarden Fault Complex Footwall, Northern Horda Platform, Northern North Sea. MSc Thesis, University of Oslo.

Blystad, P., Brekke, R.B., Færseth Larsen, B.T., Skogeid, J., Tørudbakken, B., 1995. Structural elements of the Norwegian continental shelf. Part 2: the Norwegian Sea region. Nor. Pet. Dir. Bull. 8.

Bolle, L., 1992. Troll Field: Norway's giant offshore gas field. In: Giant Oil and Gas Fields of the Decade 1978-1988. AAPG Special Volumes, pp. 447–458.

Braathen, A., Osmundsen, P.T., Gabrielsen, R.H., 2004. Dynamic development of fault rocks in a crustal-scale detachment: an example from western Norway. Tectonics 23. https://doi.org/10.1029/2003TC001558.

Braathen, A., Bælum, K., Maher Jr., H., Buckley, S.J., 2011. Growth of extensional faults and folds during deposition of an evaporite-dominated half-graben basin; the Carboniferous Billefjorden Trough. Svalbard. Nor. J. Geol. 91, 137–161.

Bretan, P., Yielding, G., Mathiassen, O.M., Thorsnes, T., 2011. Fault-seal analysis for CO_2 storage: an example from the Troll area, Norwegian Continental Shelf. Petrol. Geosci. 17, 181–192. https://doi.org/10.1144/1354-079310-025.

Brun, J.P., Tron, V., 1993. Development of the north viking graben: inferences from laboratory modelling. Sediment. Geol. 86, 31–51. https://doi.org/10.1016/0037-0738(93)90132-O.

Bungum, H., Alsaker, A., Kvamme, L.B., Hansen, R.A., 1991. Seismicity and seismotectonics of Norway and nearby continental shelf areas. J. Geophys. Res. 96, 2249–2265. https://doi.org/10.1029/90jb02010.

Busch, A., Amann-Hildenbrand, A., Bertier, P., Waschbuesch, M., Krooss, B.M., 2010. The significance of caprock sealing integrity for CO_2 storage. In: Society of Petroleum Engineers - SPE International Conference on CO_2 Capture, Storage, and Utilization 2010. Society of Petroleum Engineers, pp. 300–307. https://doi.org/10.2118/139588-ms.

Cartwright, J.A., 2004. Geological evidence for widespread faulting and fracturing of clay-rich sediments during initial consolidation. In: Advances in Geotechnical Engineering: the Skempton Conference, on vols. 29–31. Thomas Telford Publishing, London, UK, pp. 1243–1254. Proceedings of a Three Day Conference on Advances in Geotechnical Engineering, Organised by the Institution of Civil Engineers and Held at the Royal Geographical Society.

Cartwright, J.A., Lonergan, L., 1996. Volumetric contraction during the compaction of mudrocks: a mechanism for the development of regional-scale polygonal fault systems. Basin Res. 8, 183–193. https://doi.org/10.1046/j.1365-2117.1996.01536.x.

Cartwright, J.A., Mansfield, C.S., 1998. Lateral displacement variation and lateral tip geometry of normal faults in the Canyonlands National Park, Utah. J. Struct. Geol. 20, 3–19. https://doi.org/10.1016/S0191-8141(97)00079-5.

Cartwright, J., Bouroullec, R., James, D., Johnson, H., 1998. Polycyclic motion history of some Gulf Coast growth faults from high-resolution displacement analysis. Geology 26, 819–822. https://doi.org/10.1130/0091-7613(1998)026<0819:PMHOSG>2.3.CO;2.

Cartwright, J., Huuse, M., Aplin, A., 2007. Seal bypass systems. Am. Assoc. Petrol. Geol. Bull. 91, 1141–1166. https://doi.org/10.1306/04090705181.

Chadwick, R.A., Zweigel, P., Gregersen, U., Kirby, G.A., Holloway, S., Johannessen, P.N., 2004. Geological reservoir characterization of a CO_2 storage site: the utsira sand, sleipner, Northern North sea. Energy 29, 1371–1381. https://doi.org/10.1016/j.energy.2004.03.071.

Chadwick, R.A., Arts, R., Eiken, O., 2005. 4D seismic quantification of a growing CO_2 plume at Sleipner, North Sea. In: Petroleum Geology Conference, pp. 1385–1399. https://doi.org/10.1144/0061385. Proceedings. Geological Society of London.

Chiaramonte, L., White, J.A., Trainor-Guitton, W., 2015. Probabilistic geomechanical analysis of compartmentalization at the Snøhvit CO_2 sequestration project. J. Geophys. Res. Solid Earth 120, 1195–1209. https://doi.org/10.1002/2014JB011376.

Childs, C., Nicol, A., Walsh, J.J., Watterson, J., 2002. The growth and propagation of synsedimentary faults. J. Struct. Geol. 25, 633–648. https://doi.org/10.1016/S0191-8141(02)00054-8.

Christiansson, P., Faleide, J.I., Berge, A.M., 2000. Crustal structure in the northern North Sea: an integrated geophysical study. Geol. Soc. London, Spec. Publ. 167, 15–40. https://doi.org/10.1144/GSL.SP.2000.167.01.02.

Clausen, J.A., Gabrielsen, R.H., Reksnes, P.A., Nysæther, E., 1999. Development of intraformational (Oligocene-Miocene) faults in the northern North Sea: influence of remote stresses and doming of Fennoscandia. J. Struct. Geol. 21, 1457–1475. https://doi.org/10.1016/S0191-8141(99)00083-8.

Coward, M.P., Dewey, J.F., Hempton, M., Holroyd, J., 2003. Tectonic evolution. Millenn. Atlas pet. Geol. Cent. North. North sea. Geol. Soc. London 17, 33.

Cowie, P.A., Underhill, J.R., Behn, M.D., Lin, J., Gill, C.E., 2005. Spatio-temporal evolution of strain accumulation derived from multi-scale observations of Late Jurassic rifting in the northern North Sea: a critical test of models for lithospheric extension. Earth Planet Sci. Lett. 234, 401–419. https://doi.org/10.1016/j.epsl.2005.01.039.

Davies, R.J., Turner, J.D., Underhill, J.R., 2001. Sequential dip-slip fault movement during rifting: a new model for the evolution of the Jurassic trilete North sea rift system. Petrol. Geosci. 7, 371–388. https://doi.org/10.1144/petgeo.7.4.371.

Deegan, C.E., Scull, B.J., 1977. A proposed standard lithostratigraphic nomenclature for the Mesozoic of the central and northern North Sea. In: Mesozoic North, vol. 1. North Sea Symp, pp. 1–24.

Deng, C., Fossen, H., Gawthorpe, R.L., Rotevatn, A., Jackson, C.A.L., FazliKhani, H., 2017. Influence of fault reactivation during multiphase rifting: the Oseberg area, northern North Sea rift. Mar. Petrol. Geol. 86, 1252–1272. https://doi.org/10.1016/j.marpetgeo.2017.07.025.

Domínguez, R., 2007. Structural evolution of the penguins cluster, UK Northern North sea. Geol. Soc. London Spec. Publ. 292, 25–48. https://doi.org/10.1144/SP292.2.

Doré, A.G., Lundin, E.R., Fichler, C., Olesen, O., 1997. Patterns of basement structure and reactivation along the NE Atlantic margin. J. Geol. Soc. London. 154, 85–92. https://doi.org/10.1144/gsjgs.154.1.0085.

Doré, A.G., Lundin, E.R., Jensen, L.N., Birkeland, O., Eliassen, P.E., Fichler, C., 1999. Principal tectonic events in the evolution of the northwest European Atlantic margin. In: Petroleum Geology Conference, pp. 41–61. https://doi.org/10.1144/0050041. Proceedings. Geological Society of London.

Dreyer, T., Whitaker, M., Dexter, J., Flesche, H., Larsen, E., 2005. From spit system to tide-dominated delta: integrated reservoir model of the upper Jurassic Sognefjord formation on the Troll West Field. In: Petroleum Geology Conference, pp. 423–448. https://doi.org/10.1144/0060423. Proceedings. Geological Society of London.

Duffy, O.B., Bell, R.E., Jackson, C.A.L., Gawthorpe, R.L., Whipp, P.S., 2015. Fault growth and interactions in a multiphase rift fault network: Horda Platform, Norwegian North Sea. J. Struct. Geol. 80, 99–119. https://doi.org/10.1016/j.jsg.2015.08.015.

Dula, W.F., 1991. Geometric models of listric normal faults and rollover folds. Am. Assoc. Petrol. Geol. Bull. 75, 1609–1625. https://doi.org/10.1306/0c9b29b1-1710-11d7-8645000102c1865d.

Egermann, P., Lombard, J.M., Bretonnier, P., 2006. A fast and accurate method to measure threshold capillary pressure of caprocks under representative conditions. Int. Symp. Soc. Core Anal. Trondheim, Norw. 46, 1–14.

Eiken, O., Ringrose, P., Hermanrud, C., Nazarian, B., Torp, T.A., Høier, L., 2011. Lessons learned from 14 years of CCS operations: sleipner, in salah and Snøhvit. Energy Procedia 4, 5541–5548. https://doi.org/10.1016/j.egypro.2011.02.541.

32/2-1 End of well report, 2008. https://factpages.npd.no/pbl/wellbore_documents/2918_32_4_1_COMPLETION_REPORT_AND_COMPLETION_LOG.pdf.

E.U. Commission, 2018. Communication from the commission to the European parliament, the European Council, the Council, the European economic and social committee, the committee of the regions and the European investment bank. A Clean Planet all. A Eur. Strateg. long-term Vis. a prosperous. Mod. Compet. Clim. neutral Econ. Brussels 28.

Faerseth, R.B., Ravnås, R., 1998. Evolution of the Oseberg fault-block in context of the northern North Sea structural framework. Mar. Petrol. Geol. 15, 467–490. https://doi.org/10.1016/S0264-8172(97)00046-9.

Faerseth, R.B., Gabrielsen, R.H., Hurich, C.A., 1995. Influence of basement in structuring of the North Sea Basin, offshore southwest Norway. Nor. J. Geol. 75, 105–119.

Færseth, R.B., 1996. Interaction of permo-triassic and jurassic extensional fault-blocks during the development of the Northern North sea. J. Geol. Soc. London. 153, 931–944 https://doi.org/https://doi.org/10.1144/gsjgs.153.6.0931.

Færseth, R.B., Johnsen, E., Sperrevik, S., 2007. Methodology for risking fault seal capacity: implications of fault zone architecture. Am. Assoc. Petrol. Geol. Bull. 91, 1231–1246. https://doi.org/10.1306/03080706051.

Faleide, J.I., Kyrkjebø, R., Kjennerud, T., Gabrielsen, R.H., Jordt, H., Fanavoll, S., Bjerke, M.D., 2002. Tectonic impact on sedimentary processes during Cenozoic evolution of the northern North Sea and surrounding areas. Geol. Soc. London, Spec. Publ. 196, 235–269. https://doi.org/10.1144/GSL.SP.2002.196.01.14.

Fazlikhani, H., Fossen, H., Gawthorpe, R.L., Faleide, J.I., Bell, R.E., 2017. Basement structure and its influence on the structural configuration of the northern North Sea rift. Tectonics 36, 1151–1177. https://doi.org/10.1002/2017TC004514.

Ferrill, D.A., Stamatakos, J.A., Sims, D., 1999. Normal fault corrugation: implications for growth and seismicity of active normal faults. J. Struct. Geol. 21, 1027–1038. https://doi.org/10.1016/S0191-8141(99)00017-6.

Fisher, Q.J., Knipe, R.J., 1998. Fault sealing processes in siliciclastic sediments. Geol. Soc. Spec. Publ. 147, 117–134. https://doi.org/10.1144/GSL.SP.1998.147.01.08.

Fjeldskaar, W., Lindholm, C., Dehls, J.F., Fjeldskaar, I., 2000. Postglacial uplift, neotectonics and seismicity in Fennoscandia. Quat. Sci. Rev. 19, 1413–1422. https://doi.org/10.1016/S0277-3791(00)00070-6.

Forsberg, C.F., Planke, S., Tjelta, T.I., Svanø, G., Strout, J.M., Svensen, H., 2007. Formation of pockmarks in the Norwegian channel. In: Proceedings of the 6th International Offshore Site Investigation and Geotechnics Conference: Confronting New Challenges and Sharing Knowledge, OSIG 2007. Society of Underwater Technology, pp. 221–230.

Fossen, H., 1992. The role of extensional tectonics in the Caledonides of south Norway. J. Struct. Geol. 14, 1033–1046.

Fossen, H., Hurich, C.A., 2005. The hardangerfjord shear zone in SW Norway and the north sea: a large-scale low-angle shear zone in the caledonian crust. J. Geol. Soc. London. 162, 675–687. https://doi.org/10.1144/0016-764904-136.

Fossen, H., Mangerud, G., Hesthammer, J., Bugge, T., Gabrielsen, R.H., 1997. The bjorøy formation: a newly discovered occurrence of jurassic sediments in the Bergen Arc system. Nor. J. Geol. 77, 269–287.

Fossen, H., Khani, H.F., Faleide, J.I., Ksienzyk, A.K., Dunlap, W.J., 2017. Post-Caledonian extension in the West Norway-northern North Sea region: the role of structural inheritance. Geol. Soc. London, Spec. Publ. 439, 465–486. https://doi.org/10.1144/SP439.6.

Freeman, B., Klemperer, S.L., Hobbs, R.W., 1988. The deep structure of northern England and the Iapetus Suture zone from BIRPS deep seismic reflection profiles. J. -of Geol. Soc. London 145, 727–740. https://doi.org/10.1144/gsjgs.145.5.0727.

Frost, R.T.C., Fitch, F.J., Miller, J.A., 1981. The age and nature of the crystalline basement of the North Sea Basin. Pet. Geol. Cont. shelf northwest Eur. Proc. Second Conf. Pet. Geol. Cont. Shelf North-West Eur. 43–57.

Furre, A.K., Meneguolo, R., Ringrose, P., Kassold, S., 2019. Building confidence in CCS: from sleipner to the northern Lights project. First Break 37, 81–87. https://doi.org/10.3997/1365-2397.n0038.

Fyfe, J.A., Abbotts, I., Crosby, A., 1981. The subcrop of the mid-Mesozoic unconformity in the UK area. Pet. Geol. Cont. Shelf North-West Eur. Inst. Pet. London 1, 236–244.

Gabrielsen, R.H., 1989. Reactivation of faults on the Norwegian continental shelf and its implications for earthquake occurrence. In: Gregersen, S., Basham, P.W. (Eds.), Earthquakes at North-Atlantic Passive Margins: Neotectonics and Postglacial Rebound. Springer, pp. 67–90. https://doi.org/10.1007/978-94-009-2311-9_6.

Gabrielsen, R.H., Braathen, A., 2014. Models of fracture lineaments - joint swarms, fracture corridors and faults in crystalline rocks, and their genetic relations. Tectonophysics 628, 26–44. https://doi.org/10.1016/j.tecto.2014.04.022.

Gabrielsen, R.H., Kyrkjebo, R., Faleide, J.I., Fjeldskaar, W., Kjennerud, T., 2001. The Cretaceous post-rift basin configuration of the northern North Sea. Petrol. Geosci. 7, 137–154. https://doi.org/10.1144/petgeo.7.2.137.

Gabrielsen, R.H., Braathen, A., Dehls, J., Roberts, D., 2002. Tectonic lineaments of Norway. Nor. Geol. Tidsskr. 82, 153–174.

Gabrielsen, R.H., Nystuen, J.P., Jarsve, E.M., Lundmark, A.M., 2015. The Sub-Cambrian Peneplain in southern Norway: its geological significance and its implications for post-Caledonian faulting, uplift and denudation. J. Geol. Soc. London. 172, 777–791.

Gabrielsen, R.H., Olesen, O., Braathen, A., Faleide, J.I., Baranwal, V.C., Lindholm, C., 2019. The Listafjorden–Drangedal Fault Complex of the Agder–Telemark Lineament Zone, southern Norway. A structural analysis based on remote sensing and potential field data. GFF 141, 200–215. https://doi.org/10.1080/11035897.2019.1624978.

Gee, D.G., Fossen, H., Henriksen, N., Higgins, A.K., 2008. From the early paleozoic platforms of baltica and laurentia to the caledonide orogen of scandinavia and Greenland. Episodes 31, 44–51.

Gibbins, J., Chalmers, H., 2008. Carbon capture and storage. Energy Pol. 36, 4317–4322. https://doi.org/10.1016/j.enpol.2008.09.058.

Gibbs, A.D., 1987. Linked tectonics of the northern North Sea basins. Sediment. Basins Basin-Forming Mech. — Mem. 12, 163–171.

Glennie, K.W., 1995. Permian and triassic rifting in northwest Europe. Geol. Soc. London, Spec. Publ. 91, 1–5. https://doi.org/10.1144/GSL.SP.1995.091.01.01.

Goldsmith, P.J., 2000. Exploration Potential East of the Troll Field, Offshore Norway. Norwegian Petroleum Society Special Publications. Elsevier, pp. 65–97. https://doi.org/10.1016/S0928-8937(00)80010-7 after dry well 32/4-1.

Gradstein, F.M., Waters, C.N., Charnock, M., Munsterman, D., Hollerbach, M., Brunstad, H., Hammer, Ø., Vergara, L., 2016. Stratigraphic guide to the cromer knoll, shetland and chalk groups, north sea and Norwegian sea. Newsl. Stratigr. 49, 73–280. https://doi.org/10.1127/nos/2016/0071.

Gyllenhammar, C.F., 2019. Formation waters of the Norwegian Continental Shelf - where is the fresh water coming from?. In: G&G-Lecture. University of Oslo, 4rth February. Oslo.

Heeremans, M., Faleide, J.I., 2004. Late carboniferous-permian tectonics and magmatic activity in the skagerrak, kattegat and the north sea. Geol. Soc. Spec. Publ. 223, 157–176. https://doi.org/10.1144/GSL.SP.2004.223.01.07.

Helland-Hansen, W., Ashton, M., Lømo, L., Steel, R., 1992. Advance and retreat of the Brent delta: recent contributions to the depositional model. Geol. Soc. London, Spec. Publ. 61, 109–127. https://doi.org/10.1144/GSL.SP.1992.061.01.07.

Henriet, J.P., De Batist, M., Verschuren, M., 1991. Early fracturing of Palaeogene clays, southernmost North Sea: relevance to mechanisms of primary hydrocarbon migration. Gener. accumulation, Prod. Eur. Hydrocarb. 1, 217–227.

Holgate, N.E., Jackson, C.A.L., Hampson, G.J., Dreyer, T., 2013. Sedimentology and sequence stratigraphy of the Middle-Upper Jurassic Krossfjord and Fensfjord formations, Troll field, norther n north sea. Petrol. Geosci. 19, 237–258. https://doi.org/10.1144/petgeo2012-039.

Hongxing, G., Anderson, J.K., 2007. fault throw profile and kinematics of normal fault.-Conceptual models and geologic examples. Geol. J. China 13, 75–88 https://doi.org/https://doi.org/10.1016/j.jsg.2013.06.012.

Hospers, J., Ediriweera, K.K., 1991. Depth and configuration of the crystalline basement in the Viking Graben area, northern North Sea. J. Geol. Soc. London. 148, 261–265. https://doi.org/10.1144/gsjgs.148.2.0261.

Ingram, G.M., Urai, J.L., 1999. Top-seal leakage through faults and fractures: the role of mudrock properties. Geol. Soc. Spec. Publ. 158, 125–135. https://doi.org/10.1144/GSL.SP.1999.158.01.10.

Intergovernmental Panel on Climate Change Special Report, 2005. Carbon Dioxide Capture and Storage, IPCC Special Report.

Intergovernmental Panel on Climate Change Special Report, 2007. Mitigation of Climate Change Contribution of Working Group III to the IPCC Fourth Assessment Report.

Intergovernmental Panel on Climate Change Special Report, 2014. Intergovernmental Panel on Climate Change Special Report: Synthesis Report.

International Energy Agency, 2013. CO_2 Emissions from Fuel Combustion 2013. OECD Publishing, Paris. https://doi.org/10.1787/co2_fuel-2013-en.

Ivanova, A., Kashubin, A., Juhojuntti, N., Kummerow, J., Henninges, J., Juhlin, C., Lüth, S., Ivandic, M., 2012. Monitoring and volumetric estimation of injected CO 2 using 4D seismic, petrophysical data, core measurements and well logging: a case study at Ketzin, Germany. Geophys. Prospect. 60, 957–973. https://doi.org/10.1111/j.1365-2478.2012.01045.x.

Jackson, C.A.-L., Rotevatn, A., 2013. 3D seismic analysis of the structure and evolution of a salt-influenced normal fault zone: a test of competing fault growth models. J. Struct. Geol. 54, 215–234. https://doi.org/10.1016/j.jsg.2013.09.007.

Jackson, C.A.L., Gawthorpe, R.L., Sharp, I.R., 2006. Style and sequence of deformation during extensional fault-propagation folding: examples from the Hammam Faraun and El-Qaa fault blocks, Suez Rift, Egypt. J. Struct. Geol. 28, 519–535. https://doi.org/10.1016/j.jsg.2005.11.009.

Jackson, C.A.L., Barber, G.P., Martinsen, O.J., 2008. Submarine slope morphology as a control on the development of sand-rich turbidite depositional systems: 3D seismic analysis of the Kyrre Fm (Upper Cretaceous), Måløy Slope, offshore Norway. Mar. Petrol. Geol. 25, 663–680. https://doi.org/10.1016/j.marpetgeo.2007.12.007.

Jordt, H., Faleide, J.I., Bjørlykke, K., Ibrahim, M.T., 1995. Cenozoic sequence stratigraphy of the central and northern North Sea Basin: tectonic development, sediment distribution and provenance areas. Mar. Petrol. Geol. 12, 845–879. https://doi.org/10.1016/0264-8172(95)98852-V.

Jordt, H., Thyberg, B.I., Nøttvedt, A., 2000. Cenozoic evolution of the central and northern North Sea with focus on differential vertical movements of the basin floor and surrounding clastic source areas. Geol. Soc. London, Spec. Publ. 167, 219–243. https://doi.org/10.1144/GSL.SP.2000.167.01.09.

Kaldi, J., Daniel, R., Tenthorey, E., Michae, K., Schacht, U., Nicol, A., Underschultz, J., Backe, G., 2013. Containment of CO_2 in CCS: role of caprocks and faults. Energy Procedia 37, 5403–5410. https://doi.org/10.1016/j.egypro.2013.06.458.

Kaufmann, R., Gasda, S.E., Elenius, M., Skurtveit, E., Choi, J.C., Braathen, A., Mulrooney, M., Sundal, A., Wangen, M., 2018. Large-scale CO_2-injection in Smeaheia-FME SUCCESS Synthesis Report, vol. 8.

Knipe, R.J., Fisher, Q.J., Jones, G., Clennell, M.R., Farmer, A.B., Harrison, A., Kidd, B., Mcallister, E., Porter, J.R., White, E.A., 1997. Fault seal analysis: successful methodologies, application and future directions. Norwegian Petroleum Society Special Publications. Elsevier, pp. 15–38. https://doi.org/10.1016/S0928-8937(97)80004-5.

Knipe, R.J., Jones, G., Fisher, Q.J., 1998. Faulting, fault sealing and fluid flow in hydrocarbon reservoirs: an introduction. Geol. Soc. London, Spec. Publ. 147, 117–134. https://doi.org/10.1144/GSL.SP.1998.147.01.01.

Koson, S., Chenrai, P., Choowong, M., 2014. Seismic attributes and their applications in seismic geomorphology. Bull. Earth Sci. Thail. 6, 1–9.

Kyrkjebø, R., Gabrielsen, R.H., Faleide, J.I., 2004. Unconformities related to the Jurassic-Cretaceous synrift-post-rift transition of the northern North Sea. J. Geol. Soc. London. 161, 1–17. https://doi.org/10.1144/0016-764903-051.

Lauritsen, H., Kassold, S., Meneguolo, R., Furre, A., 2018. Assessing potential influence of nearby hydrocarbon production on CO_2 storage at Smeaheia. 5th CO_2 Geol. Storage Work. 2018-Novem 1–5. https://doi.org/10.3997/2214-4609.201802970.

Lee, J.J., Bruhn, R.L., 1996. Structural anisotropy of normal fault surfaces. J. Struct. Geol. 18, 1043–1058. https://doi.org/10.1016/0191-8141(96)00022-3.

Leon, E.H., 2019. Distribution and Spatial Statistics of Pockmarks over the Storage Area for Smeaheia CO_2: Evaluation of Quaternary Sediments as a Secondary Seal. MSc Thesis, University of Oslo, Department of Geosciences.

Lepercq, J.-Y., Gaulier, J.-M., 1996. Two-stage rifting in the north viking graben area (North Sea): inferences from a new three-dimensional subsidence analysis. Mar. Petrol. Geol. 13, 129–148. https://doi.org/10.1016/0264-8172(95)00031-3.

Lervik, K.S., 2006. Triassic lithostratigraphy of the Northern North Sea basin. Nor. J. Geol. 86, 93–115.

Lervik, K.S., Spencer, A.M., Warrington, G., 1989. Outline of Triassic stratigraphy and structure in the central and northern North Sea. In: Correlation in Hydrocarbon Exploration. Proc. Conference. Springer, Bergen, pp. 173–189. https://doi.org/10.1007/978-94-009-1149-9_14.

Lohr, T., Krawczyk, C.M., Oncken, O., Tanner, D.C., 2008. Evolution of a fault surface from 3D attribute analysis and displacement measurements. J. Struct. Geol. 30, 690–700. https://doi.org/10.1016/j.jsg.2008.02.009.

Lonergan, L., Cartwright, J., Jolly, R., 1998. The geometry of polygonal fault systems in Tertiary mudrocks of the North Sea. J. Struct. Geol. 20, 529–548. https://doi.org/10.1016/S0191-8141(97)00113-2.

Lothe, A.E., Bergmo, P.E., Grimstad, A.-A., 2019. Storage resources for future European CCS deployment; A roadmap for a Horda CO_2 storage hub, offshore Norway. SINTEF Academic Press. Proceedings of the 10th Trondheim Conference on CO_2 Capture (TCCS-10), Transport and Storage.

Lumley, D., 2010. 4D seismic monitoring of CO 2 sequestration. Lead. Edge 29, 150–155.

Maerten, L., Gillespie, P., Pollard, D.D., 2002. Effects of local stress perturbation on secondary fault development. J. Struct. Geol. 24, 145–153. https://doi.org/10.1016/S0191-8141(01)00054-2.

Maher, H.D., Braathen, A., 2011. Løvehovden fault and Billefjorden rift basin segmentation and development, Spitsbergen, Norway. Geol. Mag. 148, 154–170. https://doi.org/10.1017/S0016756810000567.

Maher, H., Senger, K., Ogata, K., Braathen, A., Mulrooney, M., Smyrak-Sikora, A., Osmundson, P.T., 2020. Mesozoic Regional Stress Field Evolution in Svalbard. Tectonics e2018TC005461. https://doi.org/10.1130/abs/2016am-281384.

Matthews, D.H., Cheadle, M.J., 1986. Deep reflections from the caledonides and variscides west of britain and comparison with the himalayas. Reflect. Seismol. A Glob. Perspect. 13, 5–19. https://doi.org/10.1029/GD013p0005.

Mazzini, A., Svensen, H.H., Planke, S., Forsberg, C.F., Tjelta, T.I., 2016. Pockmarks and methanogenic carbonates above the giant Troll gas field in the Norwegian North Sea. Mar. Geol. 373, 26–38. https://doi.org/10.1016/j.margeo.2015.12.012.

Mazzini, A., Svensen, H.H., Forsberg, C.F., Linge, H., Lauritzen, S.-E., Haflidason, H., Hammer, Ø., Planke, S., Tjelta, T.I., 2017. A climatic trigger for the giant Troll pockmark field in the northern North Sea. Earth Planet Sci. Lett. 464, 24–34. https://doi.org/10.1016/j.epsl.2017.02.014.

McClay, K.R., 1990. Extensional fault systems in sedimentary basins: a review of analogue model studies. Mar. Petrol. Geol. 7, 206–233. https://doi.org/10.1016/0264-8172(90)90001-W.

McClay, K.R., Ellis, P.G., 1987. Geometries of extensional fault systems developed in model experiments. Geology 15, 341–344. https://doi.org/10.1130/0091-7613(1987)15<341.

McClay, K.R., Scott, A.D., 1991. Experimental models of hangingwall deformation in ramp-flat listric extensional fault systems. Tectonophysics 188, 85–96. https://doi.org/10.1016/0040-1951(91)90316-K.

Mulrooney, M.J., Leutscher, J., Braathen, A., 2017. A 3D structural analysis of the Goliat field, Barents Sea, Norway. Mar. Petrol. Geol. 86, 192–212. https://doi.org/10.1016/j.marpetgeo.2017.05.038.

Mulrooney, M.J., Osmond, J., Skurtveit, E., Wu, L., Braathen, A., 2018a. Smeaheia, a potential Northern North Sea CO_2 storage site: structural description and de-risking strategies. In: 5th CO_2 Geological Storage Workshop. https://doi.org/10.3997/2214-4609.201802957. Utrecht.

Mulrooney, M.J., Osmond, J.L., Skurtveit, E., Braathen, A., 2020. Fault stability of seismic-scale normal faults: implications for CO_2 storage on the northern Horda Platform. In: Nordic Geological Winter Meeting, January 8th-10th. Oslo.

Nadin, P.A., Kusznir, N.J., Toth, J., 1995. Transient regional uplift in the early Tertiary of the northern North Sea and the development of the Iceland plume. J. Geol. Soc. 152, 953–958. https://doi.org/10.1144/GSL.JGS.1995.152.01.12.

Nadin, P.A., Kusznir, N.J., Cheadle, M.J., 1997. Early tertiary plume uplift of the north sea and faeroe-shetland basins. Earth Planet Sci. Lett. 148, 109–127. https://doi.org/10.1016/s0012-821x(97)00035-6.

Norton, M.G., 1986. Late Caledonide Extension in western Norway: a response to extreme crustal thickening. Tectonics 5, 195–204. https://doi.org/10.1029/TC005i002p00195.

Nøttvedt, A., Gabrielsen, R.H., Steel, R.J., 1995. Tectonostratigraphy and sedimentary architecture of rift basins, with reference to the northern North Sea. Mar. Petrol. Geol. 12, 881–901. https://doi.org/10.1016/0264-8172(95)98853-W.

Nøttvedt, A., Johannessen, E.P., Surlyk, F., 2008. The mesozoic of western Scandinavia and East Greenland. Episodes 31, 59–65. https://doi.org/10.18814/epiiugs/2008/v31i1/009.

Odinsen, T., Christiansson, P., Gabrielsen, R.H., Faleide, J.I., Berge, A.M., 2000a. The geometries and deep structure of the northern North Sea rift system. Geol. Soc. London, Spec. Publ. 167, 41–57. https://doi.org/10.1144/GSL.SP.2000.167.01.03.

Odinsen, T., Reemst, P., Van Der Beek, P., Faleide, J.I., Gabrielsen, R.H., 2000b. Permo-Triassic and Jurassic extension in the northern North Sea: results from tectonostratigraphic forward modelling. Geol. Soc. London, Spec. Publ. 167, 83–103. https://doi.org/10.1144/GSL.SP.2000.167.01.05.

Ogata, K., Senger, K., Braathen, A., Tveranger, J., 2014. Fracture corridors as seal-bypass systems in siliciclastic reservoir-cap rock successions: field-based insights from the Jurassic Entrada Formation (SE Utah, USA). J. Struct. Geol. 66, 162–187. https://doi.org/10.1016/j.jsg.2014.05.005.

Olesen, O., Bungum, H., Dehls, J., Lindholm, C.D., Pascal, C., Roberts, D., 2013. Neotectonics, seismicity and contemporary stress field in Norway–mechanisms and implications. Quat. Geol. Norw. 13, 145–174.

Omosanya, K.O., Alves, T.M., 2014. Mass-transport deposits controlling fault propagation, reactivation and structural decoupling on continental margins (Espírito Santo Basin, SE Brazil). Tectonophysics 628, 158–171. https://doi.org/10.1016/j.tecto.2014.04.045.

Orsini, P., Ponting, D., Stone, D., Nazarian, B., 2020. An Assessment of the CO_2 fate at Smeaheia, a potential large-scale storage site in Norway.Conference. Proceedings, 82nd EAGE Annual Conference & Exhibition, December 6th-8th, Amsterdam, 2020, 1–5. https://doi.org/10.3997/2214-4609.202011099.

Osagiede, E.E., Rotevatn, A., Gawthorpe, R., Kristensen, T.B., Jackson, C.A.-L., Marsh, N., 2020. Pre-existing intra-basement shear zones influence growth and geometry of non-colinear normal faults, western Utsira High–Heimdal Terrace, North Sea. J. Struct. Geol. 130 https://doi.org/10.1016/j.jsg.2019.103908, 103908.

Osagiede, E.E., Duffy, O.B., Jackson, C.A.L., Wrona, T., 2014. Quantifying the growth history of seismically imaged normal faults. J. Struct. Geol. 66, 382–399. https://doi.org/10.1016/j.jsg.2014.05.021.

Osmond, J.L., Leon, E.H., Mulrooney, M.J., Braathen, A., 2020a. Quaternary pockmark distributions informed by 3D seismic interpretation above the Horda Platform, northern North Sea. In: Nordic Geological Winter Meeting, January 8th-10th. Oslo.

Osmond, J.L., Mulrooney, M.J., Skurtveit, E., Braathen, A., 2020b. Analogous juxtaposition of mixed lithologies against a siliciclastic hydrocarbon reservoir and proposed CO_2storage formation in the Norwegian North Sea. AAPG Search and Discovery Article 80721, 1–3.

Osmond, J.L., Mulrooney, M.J., Skurtveit, E., Braathen, A., 2020c. Distribution of faulted mesozoic and tertiary seals for CCS in the Horda platform, Northern North sea, conference. Proceedings. 82nd EAGE Annual Conference & Exhibition, December 6th-8th, Amsterdam, 2020, 1–5. https://doi.org/10.3997/2214-4609.202012027.

Osmundsen, P.T., Andersen, T.B., 2001. The middle Devonian basins of western Norway: sedimentary response to large-scale transtensional tectonics? Tectonophysics 332, 51–68. https://doi.org/10.1016/S0040-1951(00)00249-3.

Osmundsen, P.T., Bakke, B., Svendby, A.K., Andersen, T.B., 2000. Architecture of the middle Devonian Kvamshesten group, Western Norway: sedimentary response to deformation above a ramp-flat extensional fault. Geol. Soc. Spec. Publ. 180, 503–535. https://doi.org/10.1144/GSL.SP.2000.180.01.27.

Ostanin, I., Anka, Z., di Primio, R., Bernal, A., 2013. Hydrocarbon plumbing systems above the Snøhvit gas field: structural control and implications for thermogenic methane leakage in the Hammerfest Basin, SW Barents Sea. Mar. Petrol. Geol. 43, 127–146. https://doi.org/10.1016/j.marpetgeo.2013.02.012.

Ottesen, D., Batchelor, C.L., Dowdeswell, J.A., Løseth, H., 2018. Morphology and pattern of quaternary sedimentation in the north Sea basin (52–62°N). Mar. Petrol. Geol. 98, 836–859. https://doi.org/10.1016/j.marpetgeo.2018.08.022.

Peacock, D.C.P., Xing, Z., 1994. Field examples and numerical modelling of oversteps and bends along normal faults in cross-section. Tectonophysics 234, 147–167.

Phillips, T.B., Fazlikhani, H., Gawthorpe, R.L., Fossen, H., Jackson, C.A.L., Bell, R.E., Faleide, J.I., Rotevatn, A., 2019. The influence of structural inheritance and multiphase extension on rift development, the Northern North sea. Tectonics 38, 4099–4126. https://doi.org/10.1029/2019TC005756.

Pigott, J.D., Kang, M.H., Han, H.C., 2013. First order seismic attributes for clastic seismic facies interpretation: examples from the East China Sea. J. Asian Earth Sci. 66, 34–54. https://doi.org/10.1016/j.jseaes.2012.11.043.

PL 205 Licence Group Well, 1997. 32/4-1-T2 Final Well Report. https://factpages.npd.no/pbl/wellbore_documents/2918_32_4_1_COMPLETION_REPORT_AND_COMPLETION_LOG.pdf.

Pochat, S., Castelltort, S., Choblet, G., Van Den Driessche, J., 2009. High-resolution record of tectonic and sedimentary processes in growth strata. Mar. Petrol. Geol. 26, 1350–1364. https://doi.org/10.1016/j.marpetgeo.2009.06.001.

Ramberg, I.B., Gabrielsen, R.H., Larsen, B.T., Solli, A., 1977. Analysis of fracture patterns in southern Norway. Geol. Min. 56, 295–310.

Ravnås, R., Bondevik, K., 1997. Architecture and controls on Bathonian-Kimmeridgian shallow-marine synrift wedges of the Oseberg-Brage area, northern North Sea. Basin Res. 9, 197–226. https://doi.org/10.1046/j.1365-2117.1997.00041.x.

Ravnås, R., Steel, R.J., 1997. Contrasting styles of Late Jurassic syn-rift turbidite sedimentation: a comparative study of the Magnus and Oseberg areas, northern North Sea. Mar. Petrol. Geol. 14, 417–449. https://doi.org/10.1016/S0264-8172(97)00010-X.

Ravnås, R., Steel, R.J., 1998. Architecture of marine rift-basin successions. Am. Assoc. Petrol. Geol. Bull. 82, 110–146. https://doi.org/10.1306/1d9bc3a9-172d-11d7-8645000102c1865d.

Ravnås, R., Nøttvedt, A., Steel, R.J., Windelstad, J., 2000. syn-rift sedimentary architectures in the northern North sea. Geol. Soc. London, Spec. Publ. 167, 133–177. https://doi.org/10.1144/GSL.SP.2000.167.01.07.

Rawson, P.F., Riley, L.A., 1982. Latest jurassic-early cretaceous events and the "late cimmerian unconformity" in north sea area. Am. Assoc. Petrol. Geol. Bull. 66, 2628–2648. https://doi.org/10.1306/03b5ac87-16d1-11d7-8645000102c1865d.

Reeve, M.T., Bell, R.E., Duffy, O.B., Jackson, C.A.-L., Sansom, E., 2015. The growth of non-colinear normal fault systems; What can we learn from 3D seismic reflection data? J. Struct. Geol. 70, 141–155. https://doi.org/10.1016/j.jsg.2014.11.007.

Reinholdtsen, A.J., RezaeiDoust, A.R., Strand, S., Austad, T., 2011. Why such a small low salinity EOR - potential from the Snorre formation?. In: 16th European Symposium on Improved Oil Recovery 2011. European Association of Geoscientists & Engineers, pp. 748–757. https://doi.org/10.3997/2214-4609.201404796.

Riber, L., Dypvik, H., Sørlie, R., 2015. Altered basement rocks on the utsira high and its surroundings, Norwegian North Sea. Nor. J. Geol. 95, 57–89. https://doi.org/10.17850/njg95-1-04.

Riber, L., Dypvik, H., Sørlie, R., Ferrell Jr., R.E., 2016. Clay minerals in deeply buried paleoregolith profiles, Norwegian North Sea. Clay Clay Miner. 64, 588–607. https://doi.org/10.1346/CCMN.2016.064036.

Riis, F., 2018. Norway CCS Demonstration Project: evaluation of Jurassic reservoirs for safe CO_2 injection and storage. In: Fifth CO2 Geological Storage Workshop. https://doi.org/10.3997/2214-4609.201802954. Utrecht.

Roberts, A.M., Price, J.D., Olsen, T.S., 1990. Late Jurassic half-graben control on the siting and structure of hydrocarbon accumulations: UK/Norwegian Central Graben. Geol. Soc. London, Spec. Publ. 55, 229–257. https://doi.org/10.1144/GSL.SP.1990.055.01.11.

Roberts, A.M., Yielding, G., Kusznir, N.J., Walker, I., Dorn-Lopez, D., 1993. Mesozoic extension in the North Sea: constraints from flexural backstripping, forward modelling and fault populations. In: Geological Society, London, Petroleum Geology Conference Series. Geological Society of London, pp. 1123–1136. https://doi.org/10.1144/0041123.

Roberts, A.M., Yielding, G., Kusznir, N.J., Walker, I.M., Dorn- Lopez, D., 1995. Quantitative analysis of triassic extension in the northern viking graben. J. Geol. Soc. 152, 15–26. https://doi.org/10.1144/gsjgs.152.1.0015.

Roelofse, C., Alves, T.M., Gafeira, J., Omosanya, K.O., 2019. An integrated geological and GIS-based method to assess caprock risk in mature basins proposed for carbon capture and storage. Int. J. Greenh. Gas Control 80, 103–122. https://doi.org/10.1016/j.ijggc.2018.11.007.

Rokoengen, K., Sørensen, S., 1990. Late Jurassic sedimentary bedrock north of Utsira, offshore western Norway. Nor. Geol. Tidsskr. 70, 61–63.

Rundberg, Y., Olaussen, S., Gradstein, F., 1995. Incision of Oligocene strata; evidence for northern North Sea Miocene uplift and key to the formation of the Utsira sands. Geonytt Abstr 22, 62.

Sharp, I.R., Gawthorpe, R.L., Underhill, J.R., Gupta, S., 2000. Fault-propagation folding in extensional settings: examples of structural style and synrift sedimentary response from the Suez rift, Sinai, Egypt. Bull. Geol. Soc. Am. 112, 1877–1899. https://doi.org/10.1130/0016-7606(2000)112<1877:FPFIES>2.0.CO;2.

Shelton, J.W., 1984. Listric normal faults: an illustrated summary. Am. Assoc. Petrol. Geol. Bull. 68, 801–815. https://doi.org/10.1306/ad461426-16f7-11d7-8645000102c1865d.

Sigmond, E.M.O., 1985. The mandal—ustaoset line, A newly discovered major fault zone in south Norway. In: The Deep Proterozoic Crust in the North Atlantic Provinces. Springer, pp. 323–331. https://doi.org/10.1007/978-94-009-5450-2_19.

Skurtveit, E., Aker, E., Soldal, M., Angeli, M., Wang, Z., 2012. Experimental investigation of CO_2 breakthrough and flow mechanisms in shale. Petrol. Geosci. 18, 3–15. https://doi.org/10.1144/1354-079311-016.

Spencer, A.M., Larsen, V.B., 1990. Fault traps in the northern North sea. Geol. Soc. Spec. Publ. 55, 281–298. https://doi.org/10.1144/GSL.SP.1990.055.01.13.

Statoil, 2016. Feasibility Study. Planning and Design of a CO_2 Storage Facility on the Norwegian Continental Shelf. OED 15/1785. Document A - Underground Report Smeahei (Internal report - available on request only).

Steel, R.J., 1993. Triassic–Jurassic megasequence stratigraphy in the Northern North Sea: rift to post-rift evolution. In: Geological Society, London, Petroleum Geology Conference Series. Geological Society of London, pp. 299–315. https://doi.org/10.1144/0040299.

Stewart, S.A., 1996. Tertiary extensional fault systems on the western margin of the North Sea Basin. Petrol. Geosci. 2, 167–176. https://doi.org/10.1144/petgeo.2.2.167.

Stewart, I.J., Rattey, R.P., Vann, I.R., 1992. Structural style and the habitat of hydrocarbons in the North Sea. Norwegian Petroleum Society Special Publications. Elsevier, pp. 197–220. https://doi.org/10.1016/B978-0-444-88607-1.50018-8.

Sturt, B.A., Braathen, A., 2001. Deformation and metamorphism of Devonian rocks in the outer Solund area, western Norway: implication for models of Devonian deformation. Int. J. Earth Sci. 90, 270–286. https://doi.org/10.1007/s005310000131.

Sundal, A., Nystuen, J.P., Rørvik, K.L., Dypvik, H., Aagaard, P., 2016. The lower Jurassic Johansen Formation, Northern North sea – depositional model and reservoir characterization for CO_2 storage. Mar. Petrol. Geol. 77, 1376–1401. https://doi.org/10.1016/j.marpetgeo.2016.01.021.

Tearpock, D.J., Bischke, R.E., 2002. Applied Subsurface Geological Mapping : with Structural Methods, second ed. Pearson Education.

Ter Voorde, M., Færseth, R.B., Gabrielsen, R.H., Cloetingh, S.A.P.L., 2000. Repeated lithosphere extension in the northern Viking Graben: a coupled or a decoupled rheology? Geol. Soc. Spec. Publ. 167, 59–81. https://doi.org/10.1144/GSL.SP.2000.167.01.04.

Thorsen, C.E., 1963. Age of growth faulting in the southern Louisiana. Trans. Gulf Coast Assoc. Geol. Soc. 13, 103–110.

Tomasso, M., Underhill, J.R., Hodgkinson, R.A., Young, M.J., 2008. Structural styles and depositional architecture in the triassic of the ninian and alwyn north fields: implications for basin development and prospectivity in the northern North sea. Mar. Petrol. Geol. 25, 588–605. https://doi.org/10.1016/j.marpetgeo.2007.11.007.

Torabi, A., Ellingsen, T.S.S., Johannessen, M.U., Alaei, B., Rotevatn, A., Chiarella, D., 2019. Fault zone architecture and its scaling laws: where does the damage zone start and stop? Geol. Soc. London, Spec. Publ. 496, 2018–2151. https://doi.org/10.1144/sp496-2018-151.

Torp, T.A., Gale, J., 2004. Demonstrating storage of CO_2 in geological reservoirs: the Sleipner and SACS projects. In: Proceedings of the 6th International Conference on Greenhouse Gas Control Technologies. Elsevier, pp. 1361–1369. https://doi.org/10.1016/j.energy.2004.03.104.

Torsvik, T.H., Carlos, D., Mosar, J., Cocks, L.R.M., Malme, T., 2002. Global reconstructions and north atlantic paleogeography 440 ma to recent. In: BATLAS–Mid Norw. Plate Reconstr. Atlas with Glob. Atl. Perspect. Geol. Surv. Norway, Trondheim, pp. 18–39.

Tvedt, A.B.M., Rotevatn, A., Jackson, C.A.L., Fossen, H., Gawthorpe, R.L., 2013. Growth of normal faults in multilayer sequences: a 3D seismic case study from the Egersund Basin, Norwegian North Sea. J. Struct. Geol. 55, 1–20. https://doi.org/10.1016/j.jsg.2013.08.002.

Underhill, J.R., Partington, M.A., 1993. Jurassic thermal doming and deflation in the North Sea: implications of the sequence stratigraphic evidence. In: Geological Society, London, Petroleum Geology Conference Series. Geological Society of London, pp. 337–345.

Vetti, V.V., Fossen, H., 2012. Origin of contrasting Devonian supradetachment basin types in the Scandinavian Caledonides. Geology 40, 571–574. https://doi.org/10.1130/G32512.1.

Walsh, J.J., Bailey, W.R., Childs, C., Nicol, A., Bonson, C.G., 2003. Formation of segmented normal faults: a 3-D perspective. J. Struct. Geol. 25, 1251–1262. https://doi.org/10.1016/S0191-8141(02)00161-X.

Wennberg, O.P., 1996. Superimposed fabrics due to reversal of shear sense: an example from the Bergen Arc Shear Zone, western Norway. J. Struct. Geol. 18, 871–879. https://doi.org/10.1016/0191-8141(96)00014-4.

Wernicke, B., Axen, G.J., 1988. On the role of isostasy in the evolution of normal fault systems. Geology 16, 848–851. https://doi.org/10.1130/0091-7613(1988)016<0848:OTROII>2.3.CO;2.

Whipp, P.S., Jackson, C.A.-L., Gawthorpe, R.L., Dreyer, T., Quinn, D., 2014. Normal fault array evolution above a reactivated rift fabric; a subsurface example from the northern Horda Platform, Norwegian North Sea. Basin Res. 26, 523–549. https://doi.org/10.1111/bre.12050.

Williams, G., Vann, I., 1987. The geometry of listric normal faults and deformation in their hangingwalls. J. Struct. Geol. 9, 789–795. https://doi.org/10.1016/0191-8141(87)90080-0.

Wrona, T., Magee, C., Jackson, C.A.L., Huuse, M., Taylor, K.G., 2017. Kinematics of polygonal fault systems: observations from the northern north sea. Front. Earth Sci. 5, 101. https://doi.org/10.3389/feart.2017.00101.

Wrona, T., Pan, I., Gawthorpe, R.L., Fossen, H., 2018. Seismic facies analysis using machine learning. Geophysics 83, 83–95. https://doi.org/10.1190/geo2017-0595.1.

Xiao, Hongbin, Suppe, J., 1992. Origin of rollover. Am. Assoc. Petrol. Geol. Bull. 76, 509–529. https://doi.org/10.1306/bdff8858-1718-11d7-8645000102c1865d.

Yielding, G., Freeman, B., Needham, D.T., 1997. Quantitative fault seal prediction. Am. Assoc. Petrol. Geol. Bull. 81, 897–917. https://doi.org/10.1306/522b498d-1727-11d7-8645000102c1865d.

Ze, T., Alves, T.M., 2019. Impacts of data sampling on the interpretation of normal fault propagation and segment linkage. Tectonophysics 762, 79–96.

Zhong, X., Escalona, A., 2020. Evidence of rift segmentation and controls of Middle to Late Jurassic synrift deposition in the Ryggsteinen ridge area, northern North Sea. AAPG (Am. Assoc. Pet. Geol.) Bull. 104 (7), 1531–1565. https://doi.org/10.1306/03172018173.

Ziegler, P.A., 1975. Geologic evolution of north sea and its tectonic framework. Am. Assoc. Petrol. Geol. Bull. 59, 1073–1097. https://doi.org/10.1306/83d91f2e-16c7-11d7-8645000102c1865d.

Ziegler, P.A., 1982. Triassic rifts and facies patterns in western and central Europe. Geol. Rundsch. 71, 747–772. https://doi.org/10.1007/BF01821101.

Ziegler, P.A., 1990. Permo-triassic development of pangea. Geol. Atlas west. Cent. Eur. Shell Int. Pet. Maatsch. BV, Hague 68–90.